Fakultät für Medizin

In vitro and in vivo characterization of T-cell receptors specifically recognizing human melanoma neoantigens identified by immunopeptidomics and in-silico predictions

Gaia Lupoli

Vollständiger Abdruck der von der Fakultät für Medizin der Technischen Universität München zur Erlangung des akademischen Grades einer

Doktorin der Naturwissenschaften (Dr. rer. nat.)

genehmigten Dissertation.

Vorsitz: Prof. Dr. Carsten Schmidt-Weber

Prüfer*innen der Dissertation:

1. Prof. Dr. Angela Krackhardt

2. Prof. Dr. Ulrike Protzer

Die Dissertation wurde am 09.05.2022 bei der Technischen Universität München eingereicht und durch die Fakultät für Medizin am 11.10.2022 angenommen.

Table of contents

Summary 8
Zusammenfassung 10
Introduction 12
1.1 Immunotherapy of Cancer 12
1.2 A new era for Cancer Immunotherapy 13
1.2.1 Immune checkpoint inhibitors 13
1.2.2 Adoptive T cell therapy: TIL and engineered T-cell transfer 14
1.2.3 Targets of TCR-T therapy 18
1.2.4 Identification of neoantigens 20
Purpose statement 24
Material 25
1.3 Technical Equipment 25
1.4 Consumables 26
1.5 Primary human material from patient Mel15 27
1.6 Vectors 27
1.7 Cell lines 28
1.8 Reagents and Chemicals 29
1.9 Kits 31
1.10 Media and Buffers 32
1.11 Recombinant cytokines 32
1.12 Peptides 33
1.13 Antibodies 35
1.14 Multimers 35
1.15 Primers 36
1.16 Software and web-based tools 38
1.17 Mouse model 39
Methods 40
1.18 Cell culture methods 40
1.18.1 Primary human material 40
1.18.2 Cell lines 41
1.18.3 Isolation of PBMCs from whole peripheral blood 41
1.18.4 PBMC-derived T cell recall responses assessed with accelerated co-culture dendritic cell assay (acDC) 41

1.18.5 Cloning of neoantigen-reactive T cell lines 43
1.18.6 Magnetic separation of $CD8^+$ T cell sub-population 43
1.18.7 In vitro activation of isolated $CD8^+$ T cells 43
1.18.8 TCR in vitro functional characterization 44
1.18.9 Detection of TIL recall responses and expansion of neoantigen-specific T cells 46
1.19 In silico methods 47
1.19.1 In silico prediction of mutated peptide antigens and HLA binding affinity 47
1.19.2 Immunopeptidomic 2018: mutation calling in non-coding regions of tumor genomes 48
1.20 Molecular biology methods 49
1.20.1 Nucleic acid extraction from PBMCs and histology slides 49
1.20.2 Reverse transcription PCR 49
1.20.3 TCR-β sequencing 50
1.20.4 Whole exome sequencing (WES) 50
1.20.5 RNA sequencing (RNA-seq) 50
1.20.6 Identification of TCR alpha and beta chains with repertoire PCR 50
1.20.7 Cloning of identified native TCR chains 51
1.20.8 Optimization of TCR sequences 51
1.20.9 Cloning of minigenes and tandem minigenes 51
1.20.10 Digestion with restriction enzymes and ligation of PCR products 51
1.20.11 PCR for amplification and cloning of constructs of interest 52
1.20.12 Purification of DNA plasmids 53
1.21 Immunological assays and sorting 53
1.21.1 IFN-γ ELISpot assay 53
1.21.2 IFN-γ ELISA assay 54
1.21.3 Preparation of peptide pools for acDC assay 54
1.21.4 Sorting of $CD137^+$ activated T cells 56
1.22 Retroviral gene transfer for T cell engineering and generation of target cells 56
1.22.1 Production of retroviral vectors 56
1.22.2 Generation of effector and target cells 56
1.23 Flow cytometry methods 57

1.23.1 Assessment of $CD8^+$ T cell subset isolation 57
1.23.2 Assessment of reporter gene expression 58
1.23.3 Staining of transduced TCRs on T cells 58
1.23.4 Multimer staining of transduced TCRs on T cells 58
1.23.5 Intracellular TCR staining 58
1.23.6 Quantification of TCR mediated multi-cytokine secretion 59
1.23.7 Flow cytometry of mouse organs and tumors to assess TCR-T biodistribution 59
1.24 Synthetic peptides 59
1.25 In vivo study 60
1.26 Statistics 61
Results 62
1.27 Clinical course of Mel15 62
1.28 In-silico predictions complement MS-based neoantigen identification 62
1.29 $KIF2C^{P13L}$ stimulated T cells show an activation phenotype 64
1.30 Screening of T-cell clones for reactivity to $KIF2C^{P13L}$ neoantigen 65
1.31 TCR-β repertoire analyses in tumor samples and peripheral blood 66
1.32 Transduction and functionality assessment of native-chain transduced $CD8^+$ T cells 69
1.33 Expression of optimized TCR constructs 71
1.33.1 Detection of transgenic codon optimized TCRs through murine constant chain 71
1.33.2 Detection of transgenic codon optimized TCRs through multimer staining 72
1.33.3 Flow cytometry intracellular staining of transgenic TCRs 74
1.34 In-depth characterization of immune responses against three neoantigens 75
1.35 Neoantigen-specific TCR show antigen-dependent binding and cross reactivity patterns ... 80
1.36 Assessing target cell cytolysis potential of TCR-transgenic T cells 82
1.36.1 Europium-release assay 82
1.36.2 Real-Time Quantitative Cell Analysis (xCELLigence) 83
1.37 Assessing TCR-mediated tumor rejection in an in-vivo immunocompromised xenogenic mouse model 86
1.38 Immunogenicity assessment of mutated peptide ligands from Immunopeptidomics 2018 pipeline 90
Discussion 92
1.39 Neoantigens 92
1.39.1 Neoantigen candidate selection and quality assessment 92
1.39.2 Immunoediting 94

1.39.3 KIF2C^{P13L} eluded MS-guided peptide screening 94
1.39.4 Optimized immunopeptidomic pipeline 2018 95
1.40 TCRs 96
1.40.1 Comparison of the seven neoantigen-specific TCRs 96
1.40.2 Functional discrepancies of neoantigen-specific TCRs in vitro and in vivo 97
1.40.3 TCR-β deep sequencing and "orphan" receptors 98
Conclusion and future aspects 99
References 100
Appendix 112
1.41 TCR sequences: native chains and optimized constructs 112
1.41.1 Native chains 112
1.41.2 Codon optimized and murinized TCR constructs 113
1.42 Affinity ranking of Mel15 predicted nonamers for HLA-A03:01 and B27:05 114
1.43 Peptides identified with Immunopeptidomics 2018 120
1.44 Abbreviations 122
Acknowledgements 126

Parts of this thesis have already been published:

"Functional analysis of peripheral and intratumoral neoantigen-specific TCRs identified in a patient with melanoma"

Eva Bräunlein, Gaia Lupoli, Franziska Füchsl, Esam T. Abualrous, Niklas de Andrade Krätzig, Dario Gosmann, Lukas Wietbrock, Sebastian Lange, Thomas Engleitner, Huan Lan, Stefan Audehm, Manuel Effenberger, Melanie Boxberg, Katja Steiger, Yinshui Chang, Kai Yu, Cigdem Atay, Florian Bassermann, Wilko Weichert, Dirk H. Busch, Roland Rad, Christian Freund, Iris Antes, Angela M. Krackhardt

doi: 10.1136/jitc-2021-002754

Summary

State-of-the-art: Since the advent of immune checkpoint inhibitors (ICI) and their demonstrated success in the treatment of various types of cancer, research focus shifted to T-lymphocytes and respective targets. Correlation between response to ICI with high mutational burden in malignant melanoma and non-small-cell lung cancer initially and urothelial and head and neck cancers after, gave further impetus to the investigation of neoantigens. However, not all cancer types with comparably high mutational load respond to ICI treatment, in fact other tumor-intrinsic, microenvironmental, and host-related biomarker factors have also been linked to response. Therefore, identification and characterization as well as understanding the role of neoantigens are of particular interest for generation of new personalized immunotherapies, such as vaccination and cellular therapies.

Defined features of tumors may therefore be predictive for an increased likelihood of a T-cell response to be generated. Several studies report neoantigen-specific T-cell reactivity in patients responding to checkpoint blockade, nevertheless, identification of circulating T cells recognizing specific neoepitopes is rarely possible.

Methods: In this research project, many research groups joined their expertise in order to identify neoantigens and specific T-cell receptors (TCRs), as well as to define their quality and functional features.

Base of this work was the successful identification of two neoantigens, in a patient with metastatic malignant melanoma treated with Ipilimumab (patient Mel15) using immunopeptidomics. Thus, these neoantigens were identified as mutated peptide ligands naturally presented on the tumor surface by immunoprecipitation and subsequent mass spectrometry (MS) analysis. This was made possible by coupling MS to a custom database containing the amino acid translation of all missense mutations found on the exome of the same patient (Bassani-Sternberg et al., 2016). Following this publication five autologous TCRs, specific for two of these neoantigens, were identified by Dr. Bräunlein in the research laboratory of Prof. Krackhardt. By using the same whole exome sequencing database as starting point, on which a more stringent mutation calling was performed, mutated peptides were predicted and tested in small-scale for immunogenicity.

TCR-β deep sequencing carried out on Mel15 samples (tumors, lymph nodes and blood) collected throughout patient's clinical history, provided detailed insights on the distribution of neoantigen specific clonotypes, as well as on other orphan beta chains, and their relative abundance.

Results: Tumor neoantigen KIF2C^{P13L} was identified in conjunction with two specific TCRs. A total of three neoantigens and seven TCRs was characterized in vitro and in vivo in collaboration with Dr. Bräunlein and Dario Gosmann, showing substantial differences in functionality and frequency. TCRs

with comparably lower functional avidity and cytokine release potential provided at least equal anti-tumor immune responses in vivo. Exploration of the TCR-β repertoire in blood and in different tumor-related tissues over three years offered insights on the high frequency and particular long-term persistence of lower-avidity TCRs.

Conclusion: The MS-based pipeline and in silico predictions for the identification of tumor neoantigens complement each other. Functional characterization of neoantigen-specific TCRs revealed that qualitative differences need to be investigated as they may play an important role in the development of novel immunotherapies including adoptive T-cell therapy strategies.

Zusammenfassung

Stand der Technik: Seit dem Aufkommen von Immun-Checkpoint-Inhibitoren (ICI) und ihrem nachgewiesenen Erfolg bei der Behandlung verschiedener Krebsarten hat sich der Forschungsschwerpunkt auf T-Lymphozyten und entsprechende Targets verlagert. Die Korrelation zwischen dem Ansprechen auf ICI mit hoher Mutationslast bei malignem Melanom, nicht-kleinzelligem Lungenkrebs und Urothel- und Kopf-Hals-Karzinomen, gab der Untersuchung von Neoantigenen weitere Impulse. Allerdings sprechen nicht alle Krebsarten mit einer vergleichbar hohen Mutationslast auf die ICI-Behandlung an, tatsächlich wurden auch andere tumorintrinsische, Mikroumgebungs- und wirtsbezogene Biomarkerfaktoren mit dem Ansprechen in Verbindung gebracht. Daher sind die Identifizierung und Charakterisierung sowie das Verständnis der Rolle von Neoantigenen von besonderem Interesse für die Entwicklung neuer personalisierter Immuntherapien wie Impfungen und Zelltherapien.

Definierte Merkmale von Tumoren können daher für eine erhöhte Wahrscheinlichkeit einer zu erzeugenden T-Zell-Antwort vorhersagbar sein. Mehrere Studien berichten von einer Neoantigen-spezifischen T-Zell-Reaktivität bei Patienten, die auf eine Checkpoint-Blockade ansprechen, dennoch ist die Identifizierung von zirkulierenden T-Zellen, die spezifische Neoepitope erkennen, selten möglich.

Methoden: In diesem Forschungsprojekt haben viele Forschungsgruppen ihre Expertise gebündelt, um verschiedene Strategien zu erforschen, um Neoantigene und spezifische T-Zell-Rezeptoren (TCRs) zu identifizieren sowie ihre Qualität und funktionalen Merkmale zu definieren.

Grundlage dieser Arbeit war die erfolgreiche Identifizierung von zwei Neoantigenen bei einem Patienten mit metastasiertem malignem Melanom, der mit Ipilimumab (Patient Mel15) unter Verwendung von Immunpeptidomik behandelt wurde. Somit wurden diese Neoantigene durch Immunpräzipitation und anschließende Massenspektrometrie (MS)-Analyse als mutierte Peptidliganden identifiziert, die natürlicherweise auf der Tumoroberfläche präsentiert werden. Dies wurde durch die Kopplung von MS an eine benutzerdefinierte Datenbank ermöglicht, die die Aminosäuretranslation aller Missense-Mutationen enthält, die im Exom desselben Patienten gefunden wurden (Bassani-Sternberg et al., 2016). Im Anschluss an diese Veröffentlichung wurden von Dr. Bräunlein im Forschungslabor von Prof. Krackhardt fünf autologe TCRs identifiziert, die für zwei dieser Neoantigene spezifisch sind. Unter Verwendung derselben Datenbank für die gesamte Exomsequenzierung als Ausgangspunkt, auf der ein strengeres Mutations-Calling durchgeführt wurde, wurden mutierte Peptide vorhergesagt und in kleinem Maßstab auf Immunogenität getestet. Als Ergebnis wurden im Rahmen dieser Diplomarbeit ein drittes Neoantigen und zwei spezifische TCRs identifiziert.

Die TCR-β-Tiefensequenzierung, die an Mel15-Proben (Tumoren, Lymphknoten und Blut) durchgeführt wurde, die während der gesamten Krankengeschichte des Patienten gesammelt wurden, lieferte detaillierte Einblicke in die Verteilung neoantigenspezifischer Klonotypen sowie in andere Orphan-Beta-Ketten und deren relative Häufigkeit.

Ergebnisse: Das Tumor-Neoantigen KIF2C^{P13L} wurde in Verbindung mit zwei spezifischen TCRs identifiziert. Insgesamt drei Neoantigene und sieben TCRs wurden in vitro und in vivo in Zusammenarbeit mit Dr. Bräunlein und Dario Gosmann charakterisiert und zeigten erhebliche Unterschiede in Funktionalität und Häufigkeit. TCRs mit vergleichsweise geringerer funktioneller Avidität und Zytokin-Freisetzungspotential lieferten in vivo mindestens gleiche Anti-Tumor-Immunantworten. Die Untersuchung des TCR-β-Repertoires im Blut und in verschiedenen tumorbezogenen Geweben über drei Jahre bot Einblicke in die hohe Häufigkeit und insbesondere die langfristige Persistenz von TCRs mit geringerer Avidität.

Schlussfolgerung: Die MS-basierte Pipeline und In-silico-Vorhersagen zur Identifizierung von Tumor-Neoantigenen ergänzen sich gegenseitig. Die funktionelle Charakterisierung neoantigenspezifischer TCRs zeigte, dass qualitative Unterschiede untersucht werden müssen, da sie eine wichtige Rolle bei der Entwicklung neuartiger Immuntherapien einschließlich adoptiver T-Zell-Therapiestrategien spielen könnten.

Introduction

1.1 Immunotherapy of Cancer

Immunotherapy is a field of medicine aiming at improving the immune system's natural ability to fight cancer, by activating or boosting mechanisms that are hindered during disease progression. The advent of immunotherapy led to a paradigm shift in the treatment of cancer, where the immune system and not the tumor itself represents the target.

The concept that the immune system is capable of recognizing and attacking cancerous cells traces back to the 19th century, when William B. Coley observed that some patients with cancer experienced spontaneous remission after developing erysipelas. Coley started injecting mixtures of live and inactivated *Streptococcus Pyogenes* and *Serratia Marcescens* into patients' tumors achieving sustained complete remission in several cancer types , such as, sarcoma, lymphoma, and testicular carcinoma (Coley, 1910, 1991).

The procedure foreseeing intratumor injection of attenuated bacteria to treat cancer reemerged in 1976 during a trial for testing the use of tuberculosis vaccine Bacille Calmette-Guérin (BCG) to prevent relapse of non-muscle invasive bladder cancer (Morales, Eidinger, & Bruce, 1976). BCG therapy was effective and continues to be used at present.

A more modern idea of immunotherapy as strategy for cancer treatment formed when Thomas and Burnet presented the theory of "cancer immunosurveillance" in 1957. They postulated that lymphocytes patrol the organism to annihilate somatic cells transformed by spontaneous mutations (Burnet, 1957; L. Thomas, 1982). Due to lack of data proving the existence of tumor-specific antigens and the technical inability to keep and manipulate lymphocytes in laboratory cultures, further progress in this area were delayed of some years.

When T-cell growth factor interleukin-2 (IL-2) was identified in 1976 (D. Morgan, Ruscetti, & Gallo, 1976), it allowed scientists to keep T cells in in vitro culture for the first time. Steven A. Rosenberg showed how administration of high doses of IL-2 can effectively enhance T-cell production in patients with established metastatic cancers (Steven A. Rosenberg et al., 1985). IL-2 was approved in 1992 by the US Food and Drug Administration (FDA) as an immunotherapeutic agent for the treatment of metastatic kidney cancer and metastatic melanoma in 1998. Before IL-2, the very first approved immunotherapy for cancer was recombinant interferon-α (IFN-α), approved in 1986 for the treatment of hairy cell leukemia, however this treatment was subsequently dismissed because of IFN-α short therapeutic duration (Ahmed & Rai, 2003).

Another approach pioneered by Rosenberg for the treatment of malignant melanoma, resulting from IL-2 discovery and possibility to culture primary T cells in vitro (Gillis & Smith, 1977; D. Morgan et al.,

1976), relies on the isolation of T infiltrating lymphocytes (TILs) from tumor biopsy, expansion and reinjection together with high doses of the cytokine (Steven A. Rosenberg et al., 1988).

1.2 A new era for Cancer Immunotherapy

The importance of T cells and efficacy of immunotherapy became even clearer with the advent of immune checkpoint inhibitors and CAR-T cells, which were acknowledged as "Breakthrough of the Year 2013" by the journal Science (Couzin-Frankel, 2013). Further recognition came from the Nobel prize for physiology or medicine 2018 awarded for the discovery of cytotoxic T-lymphocyte-associated protein (CTLA-4) to James P. Allison and programmed cell death protein 1 / programmed cell death protein ligand 1 (PD-1 / PD-L1) to Tasuku Honjo (Freeman et al., 2000; Ishida, Agata, Shibahara, & Honjo, 1992; Leach, Krummel, & Allison, 1996). These molecules, called immune checkpoints, play a central role in the induction and maintenance of immune tolerance and act as "breaks" of the immune system and in particular of T cells. In physiological conditions it is in fact essential to modulate or extinguish immune cell activity once the inflammation is cleared, however this safety mechanism is "exploited" by tumors to escape immune surveillance.

1.2.1 Immune checkpoint inhibitors

Immune checkpoints maintain appropriate physiological immune responses and protect healthy tissues from immune attack. The two most studied and most common checkpoint inhibitors promote blockade of PD-1/PD-L1 axis and inhibition of CTLA-4 molecule.

PD-1 is expressed on the surface of activated T cells and by binding to its ligand PD-L1, plays a role in tolerance maintenance and inflammation resolution (Bardhan, Anagnostou, & Boussiotis, 2016; Ishida et al., 1992; Nishimura, 2001). Another immune checkpoint, CTLA-4, is a co-inhibitory molecule that regulates the extent of T-cell activation (Brunet et al., 1987; Waterhouse et al., 1995). Interactions between CTLA-4 and its ligands CD80 and CD86, inhibit T-cell activity. Tumors cells express immune checkpoint ligands creating an immunosuppressive environment and promoting tumor progression (Munn & Bronte, 2017). By blocking the interaction between PD-1 and PD-L1 and CTLA-4 and its ligands, with monoclonal antibodies, T cells remain active and can recognize and lyse tumor cells (Pardoll, 2012).

Clinical impact of PD-1/PD-L1 and CTLA-4 blockade strategies has grown over the past few years. Six PD-1 or PD-L1 inhibitors and one CTLA-4 inhibitor have been approved to treat various cancers (see Table 1).

Table 1. List of FDA approved checkpoint inhibitors adapted from (Riley, June, Langer, & Mitchell, 2019)

Therapy	Type	Approved Cancers	Year of first approval	Ref.
Ipilimumab	CTLA-4 mAb	Melanoma	2011	(Hodi et al., 2010)
Cemiplimab	PD-1 mAb	Cutaneous squamous cell carcinoma, basal cell carcinoma, non-small-cell lung cancer	2018	(Migden et al., 2020)
Pembrolizumab	PD-1 mAb	Melanoma, non-small-cell lung cancer, Hodgkin lymphoma, advanced gastric cancer, microsatellite instability-high cancer, head and neck cancer and advanced urothelial bladder cancer	2014	(Ribas & Wolchok, 2018)
Nivolumab	PD-1 mAb	Melanoma, bladder cancer, classical Hodgkin lymphoma, colorectal cancer, hepatocellular cancer, non-small-cell lung cancer, kidney cancer, squamous cell carcinoma of the head and neck and urothelial cancer	2014	
Atezolizumab	PD-L1 mAb	Urothelial cancer and non-small-cell lung cancer	2014	
Avelumab	PD-L1 mAb	Merkel cell carcinoma and urothelial cancer	2017	
Durvalumab	PD-L1 mAb	Urothelial cancer and non-small-cell lung cancer	2017	

The efficacy of immune checkpoint inhibitors is established (Topalian, Drake, & Pardoll, 2015; Topalian et al., 2019) however, their use in the clinics is often associated with immune-related adverse events from mild to severe caused by the immune system hyper- and autoreactivity (Bajwa et al., 2019; June, Warshauer, & Bluestone, 2017). Moreover, some patients are non-responsive or develop resistance towards these medicaments (Restifo, Smyth, & Snyder, 2016). Responsiveness depends in fact on several factors, such as, composition, abundance and location of tumor-infiltrating cells, expression of checkpoint molecules by cancer cells and lymphocytes, and mutational load (Danaher et al., 2018; Rizvi et al., 2015; Snyder et al., 2014; Van Allen et al., 2015). Besides, there are many other immune checkpoints and different possible mechanisms of immunosuppression present in the tumor microenvironment which are under investigation.

In this regard, several approaches are currently investigated: strategies to inhibit innate immune suppression and modulate metabolism within the tumor microenvironment for T-cell exhaustion prevention, personalized cellular therapies, vaccines, adjuvants, and combinations with cytotoxic therapy (Murciano-Goroff, Warner, & Wolchok, 2020).

1.2.2 Adoptive T cell therapy: TIL and engineered T-cell transfer

Adoptive cell therapy is a type of immunotherapy in which T cells are administered to a patient to help the body fight cancer and it is currently represented by two general approaches: Tumor Infiltrating Lymphocyte (TIL) transfer and engineered T cell adoptive transfer. In the former approach, TILs are derived from surgical excision of tumor, while for the second approach, T cells from peripheral blood are genetically modified to express specific antigen receptors.

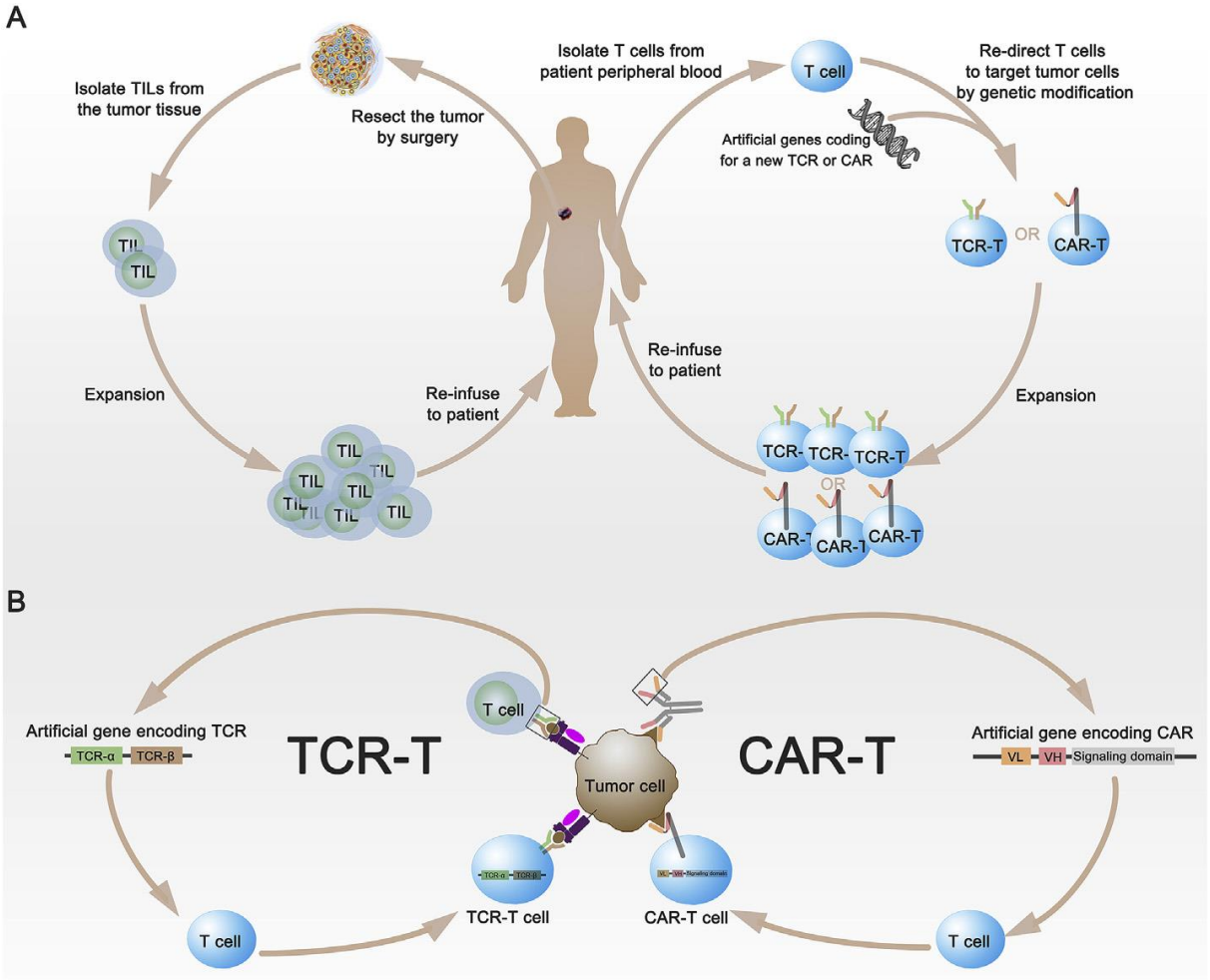

Figure 1. Illustration from (Jiang et al., 2019) A) The universal procedure of adoptive T-cell transfer. B) The different binding pattern of TCR-T and CAR-T. Reprinted from: vol 462:23-32, Jiang X. et al. *Adoptive CD8⁺ T cell therapy against cancer: Challenges and opportunities*, Copyright (2021), with permission from Elsevier.

1.2.2.1 TIL Transfer

The first approach was mastered by Rosenberg and colleagues in several clinical trials for the treatment of metastatic melanoma (Dudley, 2002; S. A. Rosenberg et al., 2011, 1994). In one of the first studies, reinjection of TILs and administration of high doses of IL-2 led to tumor regression in 34% of patients treated between 1987 and 1992 (n = 86) (S. A. Rosenberg et al., 1994).

This first unselected approach further evolved into selective enrichment of tumor-reactive lymphocytes within extracted TILs. Therefore, tumor DNA is sequenced to identify mutations and predict potential tumor-specific antigens. TILs are then co-cultured with autologous dendritic cells engineered to express potential tumor-specific antigens, and assayed for antigen recognition. Reactive TILs are selected, further expanded and reinjected in patients. This was done in cases of colorectal cancer, bile duct cancer, and breast cancer (E. Tran et al., 2014; Eric Tran et al., 2016; Zacharakis et al., 2018).

Despite encouraging results of TIL therapy for the treatment of different cancers, this approach presents some limitations, such as availability of an operable tumor, the possibility to grow TILs in culture and to detect tumor-specific reactivity. In fact, TILs often do not grow ex vivo or exhibit an exhausted phenotype (Baitsch et al., 2011; Gros et al., 2014). Detection of tumor-specific effector function can be often hindered by a lack of suitable tumor targets. In those cases where TILs can be successfully grown but do not exhibit in vitro effector function, injection of minimally cultured TILs with unknown specificity is still a possibility (Parkhurst et al., 2011).

For cases where malignant tissue cannot be surgical resected or TILs cannot be grown, engineered antigen-specific lymphocytes may represent a valid alternative (Cohen et al., 2005; Engels et al., 2005; Hughes et al., 2005; Johnson et al., 2006; R. A. Morgan et al., 2006; Roszkowski et al., 2005; Y. Zhao et al., 2005)

1.2.2.2 Engineered T-cell adoptive transfer: from CARs to TCRs

Adoptive transfer of engineered T cells has recently gained attention thanks to clinical successes of Chimeric Antigen Receptor (CAR)-T cell therapy of leukemia and lymphoma and its expedited FDA approval (US Food and Drug Administration Approved Products-KYMRIAH (Tisagenlecleucel), 2017) ("FDA Approves Second CAR T-cell Therapy," 2018). The infusion of gene-modified T cells endows or reinvigorates the immune system with effector activities which could be naturally present or not. Furthermore, it offers the possibility to transfer specific subsets of lymphocytes (γ/δ T cells, invariant natural killer T cells, regulatory T cells) or functionally different subsets such as central memory, effector memory, tissue-resident memory T cells (Busch, Fräβle, Sommermeyer, Buchholz, & Riddell, 2016). For adoptive T-cell transfer therapy, T cells are collected from patient blood or from a matched donor (Yang, Jacoby, & Fry, 2015) and are then genetically engineered to express receptors, CARs or TCRs, specific for antigens present on tumor cells. These engineered T cells are then re-administered to the same patient. Upon injection, engineered T cells recognize the targeted antigen on tumor cells and induce cell death. Many patients achieved remission and prolonged survival from CAR-T cell therapy, but the long-term effects remain under investigation (Benjamin & Yiping, 2018; Vairy, Lopes Garcia, Teira, & Bittencourt, 2018). The first target of the first two approved CAR-T cell therapies (**Table 2**) was CD19, a molecule expressed on B cell leukemias and lymphomas as well as on most parts of normal B cell lineage. Treatment with anti-CD19 CARs leads therefore to clearance of malignant B cells and aplasia of healthy B cells as side effect.

Table 2. List of FDA approved CAR-T cell treatments

Therapy	Target	Approved cancers	Year of approval	Reference
Tisagenlecleucel (Kymriah, CTL019)	CD19	B cell acute lymphocytic leukemia and non-Hodgkin lymphoma	2017	NCT03123939 (Maude et al., 2018)

Therapy	Target	Approved cancers	Year of approval	Reference
Axicabtagene ciloleucel (Yescarta, KET-C10)	CD19	Large B cell lymphoma	2017	NCT02348216 (Locke et al., 2019)
Brexucabtagene autoleucel (Tecartus, KTE-X19)	CD19	Mantel cell lymphoma	2020	NCT02601313 (M. Wang et al., 2020)
Lisocabtagene maraleucel (Breyanzi, JCAR017)	CD19	Non-Hodgkin lymphomas	2021	NCT02631044 (Abramson et al., 2020; Ogasawara et al., 2021)
Idecabtagene vicleucel (Abecma, bb2121)	BCMA	Multiple myeloma	2021	NCT03361748 (Munshi et al., 2021)

A CAR has an extracellular domain composed by antibody variable light and heavy chains fused together as a single chain, which can recognize proteins on the surface of cancer cells and transmits the signal to the intracellular domain for the activation of T cell effector functions (Gross, Waks, & Eshhar, 1989; Irving & Weiss, 1991; Kuwana et al., 1987). CAR antigen recognition is major histocompatibility complex (MHC) independent, therefore the target of choice has to be naturally present on the cell surface and be specific to the tissue/lineage to be eliminated. Because of these requirements, finding an antigen, which is solely expressed by cancer cells, presents quite a challenge. For some targets, such as CD19, the issue of complete B-cell lineage depletion, upon treatment of leukemia with CAR-T cells, can be overcome with immunoglobulin replacement therapy, however for many other surface ligands this is not the case (Sadelain, Brentjens, & Rivière, 2013). On the other hand, CARs can also recognize carbohydrate and glycolipid antigens, a peculiarity which is being explored in most recent clinical trials (Mezzanzanica et al., n.d.; Rossig, Kailayangiri, Jamitzky, & Altvater, 2018).

A TCR is a protein complex naturally present of the surface of lymphocytes for the recognition of antigens in the form of peptides bound to the MHC complex. A TCR consists of two protein chains, which are defined as alpha and beta in ~ 95% of T cell repertoire or gamma and delta in the remaining fraction. Each chain is consisting of two extracellular domains: variable (V) region and a constant (C) region. The constant region protrudes from the cell membrane, anchored through a transmembrane region, followed by a short cytoplasmic tail. The variable region is on top of the constant chains and binds to the peptide presented by the MHC complex (pMHC) (Allison, McIntyre, & Bloch, 1982; Kappler et al., 1983).

The variable domain of both α- and β-chain have three hypervariable complementarity-determining regions (CDRs). CDR3 is responsible for recognition of processed antigens.

The generation of TCR diversity arises from genetic recombination of genomic loci in individual T cells through a mechanism called “somatic V(D)J recombination”. This recombination process is unique to T lymphocytes during the early stages of their development in the thymus and confers particular antigen specificity to the TCRs (Born, Yague, Palmer, Kappler, & Marrack, 1985; Ferrier et al., 1990).

The MHC class I is expressed on the surface of all nucleated cells and presents cytosolic peptides, mostly self-peptides deriving from physiological protein turnover or defective proteins processed by the

proteasome. Any protein can enter this pathway of processing and presentation, including viral proteins resulting from infection and aberrant proteins deriving from a cancerous transformation process. In humans, human histocompatibility complex (HLA) -A, -B and -C correspond to MHC class I and are present in two copies in each individual. Accordingly, each person possesses a combination of up to six different alleles, which are extremely polymorphic within the population, making essentially each individual unique (Nakamura, Shirouzu, Nakata, Yoshimura, & Ushigome, 2019). Besides, different allotypes accommodate different peptides (8-11 amino acid long), depending on position and chemistry of the amino acids in the MHC cleft and of the presented peptide (Burrows, Rossjohn, & McCluskey, 2006; Matsumura, Fremont, Peterson, & Wilson, 1992).

As mentioned, TCRs are characterized by an MHC-restricted antigen recognition, which refers to the ability of a T cell to recognize a foreign peptide only when bound to a self MHC molecule. This feature is conferred during T-cell development in the thymus and is achieved through two different steps. In the first step, called "positive selection", T cell precursors not binding to MHC or not interacting strongly enough will face death due to lack of survival signal. In the second phase, "negative selection", self-peptides from all tissues of the body are presented to T cells by medullary thymic epithelial cells. T cell precursors possessing a TCR highly affine to any self-antigen receive an apoptotic signal that leads to death. This process is at the basis of "central tolerance" formation and prevents the formation of self-reactive T cells that are capable of inducing autoimmune diseases in the host (Klein, Kyewski, Allen, & Hogquist, 2014).

In the context of cancer disease and cancer immunotherapy with adoptive transfer of TCR-transgenic T cells, MHC restriction and TCR affinity play a central role. Recognition of peptides deriving from cytoplasmatic proteins broadens the spectrum of possible antigens of choice for TCR-based therapy, which represents a big advantage in comparison to CAR-therapy. On the other hand, TCRs are MHC-allele restricted and this limits the therapy to certain HLA alleles and in some cases to the single patient, depending on the chosen target. This leads into the field of personalized medicine, extremely appealing and challenging at the same time (Steven A Rosenberg & Restifo, 2015).

1.2.3 Targets of TCR-T therapy

With regard to the spectrum of potential antigens of TCR-based therapy, there are some more considerations to be done. First of all, cancer cells might present different antigens on their surface, which are traditionally categorized in: tumor associated (TAAs) and tumor specific antigens (TSAs). The line between these two categories is often blurred and should be dismissed in favor of a modern classification based on molecular structure and source of antigens, nonetheless scientists still refer to these two classes. With the term TAAs are indicated self-antigens present at physiological levels in one or more tissues and over-expressed in the tumor, triggering an immune response. An example is the

enzyme tyrosinase, which is required for melanin production and is extremely abundant in melanoma cells (Haen & Löffler, 2020).

Stand-alone categories of tumor antigens are: carcinoembryonic (CEAs), cancer-testis (CTAs) and viral antigens. CEAs are displayed in the early stages of embryonic development and disappear by the time the immune system is fully developed and self-tolerance is established. CTAs are antigens expressed primarily in the germ cells of the testes and by cancer cells aberrantly. Targeting of these antigens by T cells is made possible by the fact that testes are an "immunological sanctuary" and are ignored by the immune system (Jassim et al., 1989). Example antigens of this type are MAGEA1, NY-ESO-1 (Jäger et al., 1998; Traversari et al., 1992). Oncoviruses represent another source of tumor antigens, as viral proteins are implicated in oncogenesis, exposed on the surface of cancer cells and recognized by the immune cells (Renkvist, Castelli, Robbins, & Parmiani, 2001).

When the choice falls on targeting TAAs, it must be considered that identification of receptors specific to these antigens is problematic, as T-cell clones targeting them are subjected to central tolerance mechanisms potentially leading to survival of low-avidity T cells only (T. N. Schumacher & Schreiber, 2015).

However, in some cases, TCRs with intermediate affinity can be isolated from autologous repertoires, as in the case of antigen MART1, where a defined TCR was found within the TILs of a patient who responded to TIL therapy. Autologous T cells engineered with this TCR were administered to other 15 patients who experienced therapeutic responses (R. A. Morgan et al., 2006).

Nowadays, several clinical trials are ongoing for the investigation of TCR-T cell transfer efficacy in liquid and solid tumors (**Table 3**), targeting previously listed classes of antigens as well as neoantigens.

Table 3. Clinical Trials with TCR-T cells (L. Zhao & Cao, 2019; Q. Zhao et al., 2021 and ClinicalTrials.gov).

Target	Disease	Phase	NCT number
HA-1	Relapsed or refractory acute leukemia after donor stem cell	I	NCT03326921
WT-1	Myelodysplastic syndromes and acute myeloid leukemia patients	I/II	NCT 02550535
WT-1	Acute myeloid leukemia	I/II	NCT 02770820
CMV	Hematological malignancies and CMV infection	I	NCT 02988258
MAGE	Solid and hematological malignancies; Metastatic renal cancer and melanoma; Head and neck squamous cell carcinoma; non-small cell lung cancer; hepatocellular carcinoma	- I/II I I	NCT 03391791 NCT 01273181 NCT 03247309 NCT 03441100
Gp100	Metastatic melanoma; Malignant melanoma	II II	NCT 00923195 NCT 02889861
MART-1	Skin metastatic melanoma	I	NCT 00091104
HPV-16 E6	HPV^+ NHSCC or cervical cancer; HPV-associated cancer	I I/II	NCT 03578406 NCT 02280811
NY-ESO-1	Ovarian, fallopian tube or primary peritoneal cancer; advanced NSCLC; Sarcoma	I I I	NCT 03691376 NCT 03029273 NCT 03462316

		I	NCT 02650986
HBV	Hepatocellular	I	NCT 02719782
		I	NCT 02686372
P53	Metastatic cancer that over-expresses p53	II	NCT 00393029
CEA	Metastatic cancer	I	NCT 00923806
HPV E7	Human papillomavirus-associated cancers	I/II	NCT 02858310
SL9	HIV	I	NCT 00991224
TGFbII	Metastatic colorectal cancer	I/II	NCT 03431311
MCPyV	Metastatic or unresectable Merkel cell cancer	I/II	NCT 03747484
TRAIL	Metastatic renal cancer	I	NCT 00923390
PRAME	AML/MDS; metastatic uveal melanoma	I/II	NCT 02743611
	refractory cancer; solid tumors	I	NCT 03686124
		I/II	NCT 03503968
EBV	Recurrent or metastatic NPC	II	NCT 03648697
KRAS	KRAS G12V$^+$ tumor;	I/II	NCT 03190941
	KRAS G12D$^+$ tumor	I/II	NCT 03745326
Personalized neoantigens	Malignant epithelial neoplasms; solid tumors	I	NCT 04520711
		I	NCT 03970382

With TSAs the community normally refers to antigens, which result from somatic mutations causing or acquired during carcinogenesis or from modification on transcriptional or post-translational level. These epitopes are "new" and foreign to the immune system and are therefore defined as "neoantigens". This last aspect allows high affinity TCRs to be present in autologous repertoires, as tumor onset and mutation acquisition take place after T cell clone depletion in the thymus (T. N. Schumacher & Schreiber, 2015).

Nonetheless, neoantigens, pose an unprecedented challenge to developing antigen-specific immunotherapies. Occurrence of random somatic mutations overlapping in more than one patient is infrequent. However, combined with HLA restriction, most neoantigens are highly patient specific. Immunotherapies aiming at raising an antigen-specific immune response to such "private" neoantigens must therefore be customized for each individual patient, creating substantial practical and regulatory hurdles (Klebanoff et al., 2016).

To circumvent this problem scientists research for recurrent mutations in driver oncogenes that result in peptides binding to frequent HLA allotypes in the human population, such as peptides resulting from mutations in KRAS oncogene, which are currently being tested in clinical trials (Klebanoff & Wolchok, 2018; Eric Tran et al., 2016) (**Table 3**).

1.2.4 Identification of neoantigens

Due to "private" nature of neoantigens, potential immunogenic mutations can be identified only through mutanome analysis by next generation sequencing on tumor nucleic acids. This is generally done through whole genome sequencing (WGS) or whole exome genome sequencing (WES) of tumor and normal tissue derived DNA. Normal and tumor reads are then aligned to human reference genome for the identification of somatic variants using variant-calling algorithms. Somatic mutations include single nucleotide variants (SNVs), gene fusions and insertion or deletion variants (indels) (Xu, 2018). It is

worth mentioning that many different variant callers have been developed and that significant discrepancies were reported in detected variants from the same raw sequencing data (Hwang, Kim, Lee, & Marcotte, 2015; O'Rawe et al., 2013). Besides, tumor heterogeneity presents the additional obstacle of biasing clonal over sub-clonal mutation detection (Jurtz & Olsen, 2019), however neoantigens originating from clonal mutations might represent the ideal targets for T cells (N. McGranahan et al., 2016a).

RNA sequencing can as well be performed and provides information about gene expression and other types of variants deriving from RNA editing (alternative splicing, gene fusions and post-transcriptional modifications) (Rathe et al., 2019; Smart et al., 2018). RNA-seq is mostly used in combination with WES to detect variants exceeding a certain expression threshold, to detect missed variants or broaden the landscape of possible mutations. Despite the many advantages that RNA-seq might bring, mutation calling and filtering are still very challenging. Alignment of reads is made complex by alternative splicing, RNA editing, random errors introduced during reverse transcription and PCR and can lead to high false positive rate results. Tumor heterogeneity and heterozygosis complicate the picture even further (Smith et al., 2019).

Once somatic mutations are identified, a reference protein sequence database with genomic information derived from patients' next-gene-sequencing (NGS) data is established and different approaches can be pursued to identify neoantigens. Typically, two methods are adopted to narrow down the list of potential candidates: liquid chromatography-tandem mass spectrometry (LC-MS/MS)-based immunopeptidomics or in silico prediction and prioritization (Ton N. Schumacher & Schreiber, 2015). In MS-based immunopeptidomics, HLA complexes are immunoprecipitated from surgically resected tumor specimens and peptide ligands are eluted. Peptides are then analyzed with MS and the amino acid sequence is identified by matching spectra with a reference protein sequence database with genomic information derived from patient's NGS data (Bassani-Sternberg et al., 2016). Depending on mutations included in the database, it is possible to detect peptides deriving from SNVs, indels, intron retention etc. Advantages of this approach are: direct identification of naturally presented HLA binding peptides, narrowing of number of neoantigen candidates, identification of post-translational modified peptides and non-canonical neoantigens, identification of minimal epitopes (Smith et al., 2019). However, what MS can detect still represents the "tip of the iceberg" of the whole immunopeptidome. It has in fact limited sensitivity, it is biased toward detecting the more abundant peptides, it relies on defined chemical properties of the peptides (efficient ionization and fragmentation), it depends on HLA expression of tumor cells and necessitates high amount of tumor tissue (Bassani-Sternberg & Coukos, 2016).

In silico predictions are built on the idea of foreseeing whether putative peptides are likely to be presented on the surface of cancer cells and be possibly immunogenic. There are prediction algorithms designed to predict peptide processing (e.g. SYFPEITHI, NetChop) or transport (e.g., NetCTL),

however most efforts are concentrated on development of neural networks for binding affinity prediction between a peptide and the groove of patient-specific HLA allotypes (e.g. NetMHC, MHCflurry, EDGE etc.) (De Mattos-Arruda et al., 2020; Richters et al., 2019). These algorithm are the most used for neoantigen prediction and led to the identification of first neoantigens using WES (Robbins et al., 2013; N. H. Segal et al., 2008; Van Rooij et al., 2013). Other algorithms are continuously developed to analyze peptides from a more structural perspective and to determine whether a mutated amino acid either is likely orientated toward the TCR or reduces the affinity of the epitope for the HLA molecule itself.

Predictions allow the user to narrow down the number of neoantigens candidates and identify minimal epitopes, however their quality depends on accuracy of prediction algorithms, which relies on experimental data and is therefore lower for less frequent HLA clonotypes (Garcia-Garijo, Fajardo, & Gros, 2019; Richters et al., 2019).

Other strategies to narrow down a list of potential neoantigens include experimental measuring of peptide affinity, by for example comparing affinities of mutated peptides (mut p) with its wild-type (wt) counterpart (Kalaora et al., 2016; Zhang et al., 2019). Mutated peptides can be also directly tested by cloning coding minigenes in tandem, transduce them in antigen presenting cells and run an immunogenicity assessment assay with patient-derived T cells (Gros et al., 2016a; Eric Tran et al., 2015).

Immunogenicity assessment is carried out on patient-derived TILs or PBMCs or in some cases on HLA-matched healthy-donor derived PBMCs. Assays for immunogenicity assessment comprise ELISpot, ELISA or flow cytometry following T cell stimulation performed with different modalities and protocols (Cafri et al., 2019; Cohen et al., 2015; Gros et al., 2016a; N. McGranahan et al., 2016b)..

Due to correlation of immune checkpoint blockade success with tumor somatic mutational load across various disease entities (Chan et al., 2019; Rizvi et al., 2015; Samstein et al., 2019; Snyder et al., 2014), investigating the role of neoantigens in tumor recognition and rejection by T cells gained in popularity, especially in the treatment of melanoma (Gros et al., 2016a; Gubin et al., 2014; Rooney, Shukla, Wu, Getz, & Hacohen, 2015; Strønen et al., 2016). Despite this, recent reports show how mutational burden is only part of the story, as tumors with comparable mutation numbers exhibit a variable immune response (Rooney et al., 2015) and predicted neoantigen load does not correlate with T-cell infiltration in melanoma (Spranger et al., 2016). Intratumor heterogeneity, depending by the distribution of clonal versus sub-clonal mutations (Nicholas McGranahan & Swanton, 2017; Spranger et al., 2016), may influence immune response (McDonald et al., 2019; Mcgranahan et al., 2016; Reuben et al., 2017; Rosenthal et al., 2019). In other words, clonal neoantigen burden appears to correlate with an improved response to checkpoint inhibitors across a wide range of tumor types (Mcgranahan et al., 2016; Miao et al., 2018; Wolf et al., 2019).

Despite the countless number of reports, studies and emerging clinical trials on the topic, there is still much to learn about neoantigens' sources, ability to be presented and trigger the immune system, as well as, about T-cell relevant features in the fight against cancer. In this sense, we contributed with an unprecedented in-depth characterization and comparison of neoantigen specific TCRs identified from a melanoma patient treated with immune checkpoint inhibitors. This case study helped broadening current knowledge about TCR functionality, with potential implications for future personalized immunotherapies targeting neoantigens.

Purpose statement

This dissertation is based on previously published work (Bassani-Sternberg et al., 2016), where it was shown that cancer neoantigens can be identified from fresh tumor samples through exome sequencing and MS analyses.

Goals of the present work were: identification of neoantigens potentially missed by MS analysis, discovery of autologous TCRs recognizing these neoantigens and comparison of the neoantigens and TCR functionalities.

In melanoma patient Mel15, mutation calling on exome sequencing had shown a particularly high number of missense mutations, however only eight mutated peptides were found with MS, two of them being validated neoantigens (Bassani-Sternberg et al., 2016). The awareness MS shortcomings, in terms of sensitivity and chemical attributes of detected peptides, prompted the research of an alternative method. The question was whether it was possible to identify previously known neoantigens and additional ones by predicting the binding affinity between putative mutated peptides and the patient's HLA allotypes with a state-of-the-art algorithm.

Subsequently to the identification and validation of in silico predicted neoantigens, scope of this dissertation was to isolate neoantigen reactive T-cell clones from the circulating repertoire of the patient and obtain the TCR sequence.

Final aim of the project was to acquire knowledge about neoantigens qualities and TCR features, which are relevant for adoptive transfer of TCR-transgenic T cells in the clinical setting. Differences between neoantigens and wt counterparts in terms of measured binding affinity and chemical properties were investigated by our cooperation partners (respectively Prof. Dr. Freund and Prof. Dr. Antes) in order to pinpoint hallmarks of immunogenicity (E. Bräunlein et al., 2021).

On the TCR front, the goal was to compare all receptors isolated from patient Mel15 and evaluate their performance by taking several functional parameters into account, both in vitro and in vivo.

Gained knowledge will help in the prioritization of features important for the antigens to be targeted as well as for the receptors recognizing them and guide the choice of TCR candidates to be further tested in clinical trials.

Material

1.3 Technical Equipment

Table 4. Technical Equipment

Device	Company
Analytical balance SI-64	Denver Instrument / Sartorius AG, Göttingen, Germany
APOLLO Liquid nitrogen vacuum container	Cryotherm, Kirchen/Sieg, Germany
Autoclave Systec V95	Systec GmbH, Linden, Germany
BD™ LSR II	BD Biosciences, Franklin Lakes, USA
BioDocAnalyze Gel documentation system	Biometra GmbH, Göttingen, Germany
Biometra Mitsubishi P95 Printer	Biometra GmbH, Göttingen, Germany
BIOSAFE MD sample container	Cryotherm, Kirchen/Sieg, Germany
Centrifuge 5417R	Eppendorf AG, Hamburg, Germany
Centrifuge 5417R	Eppendorf AG, Hamburg, Germany
Centrifuge 5810R	Eppendorf AG, Hamburg, Germany
Centrifuge with vortex 7-0040	neoLab Migge GmbH, Heidelberg, Germany
Centrifuge with vortex 7-0040	neoLab Migge GmbH, Heidelberg, Germany
Compact M Horizontal Gel Electrophoresis Apparatus	Biometra GmbH, Göttingen, Germany
Digital microtiter shaker MTS 2/4	IKA®-Werke GmbH & CO. KG, Staufen, Germany
Dynal MPC™-L Magnetic Particle Concentrator	Invitrogen Dynal AS, Oslo, Norway
DynaMag™-2 Magnet	Invitrogen Dynal AS, Oslo, Norway
EcoVac Vacuum Pump	schuett-biotec GmbH, Göttingen, Germany
Electrophoresis Apparatus i-Mupid	Cosmo Bio Co., LTD, Tokyo, Japan
Fume cupboard 2-453	Köttermann GmbH & Co KG, Uetze/Hänigsen, Germany
Gene Pulser Xcell™ Electroporation System	Bio-Rad Laboratories GmbH, München, Germany
Growth chamber WTC	BINDER GmbH, Tuttlingen, Germany
HERAfreeze™ BASIC -86°C Freezer	Thermo Fisher scientific, Waltham, USA
ImmunoSpot S6 Ultra-V Analyzer	CTL - Europe GmbH, Bonn, Germany
Incubator BBD 6220	Heraeus Holding GmbH, Hanau, Germany
Incubator CB 150	BINDER GmbH, Tuttlingen, Germany
Innova 4000 Incubator Shaker	New Brunswick Scientific, Edison, USA
Irradiation chamber Cs137 Type Ob 29/902-1	Buchler GmbH, Braunschweig, Germany
Laminar flow HERAsafe KS 15	Heraeus Holding GmbH, Hanau, Germany
LS6000 sample container	tec-lab GmbH, Taunusstein, Germany
MACS MultiStand	Miltenyi Biotec GmbH, Bergisch Gladbach, Germany
MACSmix Tube Rotator	Miltenyi Biotec GmbH, Bergisch Gladbach, Germany
Magnetic stirrer RH basic 2	IKA®-Werke GmbH & CO. KG, Staufen, Germay
Microscope Axiovert 40 C	Carl Zeiss AG, Feldbach, Schweiz
MidiMACS Separator	Miltenyi Biotec GmbH, Bergisch Gladbach, Germany
Minishaker MS2	IKA®-Werke GmbH & CO. KG, Staufen, Germay
Multichannel pipets	Eppendorf AG, Hamburg, Germany
Multifuge 3 S-R	Heraeus Holding GmbH, Hanau, Germany
Multifuge 3s	Heraeus Holding GmbH, Hanau, Germany

NALGENE Cryo 1°C Freezing Container	Thermo Fisher scientific, Waltham, USA
NanoDrop Spectrophotometer ND1000	PeqLab / VWR International GmbH, Darmstadt, Germany
Neubauer improved counting chamber	Karl Hecht GmbH & Co KG, Sondheim/Röhn, Deutschland
OctoMACS Separator	Miltenyi Biotec GmbH, Bergisch Gladbach, Germany
Pipets	Eppendorf AG, Hamburg, Germany
Pipette controller	INTEGRA Biosciences GmbH, Biebertal, Germany
Precision balance 440	KERN & SOHN GmbH, Balingen, Germany
Premium -20°C Freezer	Liebherr-International Deutschland GmbH, Biberach an der Riβ, Germany
Refrigerator Profi line	Liebherr-International Deutschland GmbH, Biberach an der Riβ, Germany
Rotina 420R	Andreas Hettich GmbH & Co.KG, Tuttlingen, Germany
StepOnePlus™ Real-Time PCR System	Fisher Scientific GmbH, Schwerte, Germany
SunriseTM absorbance reader	Tecan Group Ltd., Männedorf, Switzerland
TGradient	Biometra GmbH, Göttingen, Germany
Thermomixer Compact	Eppendorf AG, Hamburg, Germany
Titramax 1000 shaker	Heidolph Instruments GmbH & Co.KG, Schwabach, Germany
TProfessional Thermocycler	Biometra GmbH, Göttingen, Germany
UV Transilluminator	Biometra GmbH, Göttingen, Germany
VICTOR2™ Fluorometer	Perkin Elmer, Waltham, Massachusetts, USA
Vortex Mixer 7-2020	neoLab Migge GmbH, Heidelberg, Germany
Vortexer Reax top	Heidolph Instruments GmbH & Co.KG, Schwabach, Germany
Vortex-Genie 2	Scientific Industries, Inc., New York, USA
VWR Power Source 300V	VWR International GmbH, Darmstadt, Germany
Waterbath	Memmert GmbH + Co. KG, Schwabach, Germany
xCELLigence RTCA MP	ACEA Biosciences Inc., San Diego, CA 92121 USA
Ziegra Ice machine	ZIEGRA Eismaschinen GmbH, Isernhagen, Germany
AID Classic ELR08 ELISpot Reader System	AID GmbH, Strassberg, Deutschland

1.4 Consumables

Table 5. Consumables

Consumable	Company
Cell culture flask (T25, T75, T175)	Greiner Bio-One GmbH, Frickenhausen, Germany
Cell scraper	TPP Techno Plastic Products AG, Trasadingen, Schweiz
Cell strainer 70 and 100µm	BD Biosciences, Franklin Lakes, USA
CyroPure tubes	Sarstedt AG & Co., Nümbrecht, Germany
Nunc-Immuno™ MicroWell™ 96 well solid plates	Merck KGaA, Darmstadt, Germany
E-Plate 96 culture plate for Xcelligence System	OMNI Life Science, Basel, Switzerland
Falcons (15ml, 50 ml)	BD Biosciences, Franklin Lakes, USA
Filcon 30 µm filter	Syntec International, Dublin, Ireland
Filters 0.22 and 0.45µm	Merck KGaA, Darmstadt, Germany
Gene Pulser® Electroporation Cuvettes 0.4 cm gap	Bio-Rad Laboratories GmbH, München, Germany
Gloves Dermatril P	KCL GmbH, Eichenzell, Germany
LD/LS columns	Miltenyi Biotec GmbH, Bergisch Gladbach, Germany
MAHAS4510 MultiScreen-HA 0.45 µm ELIspot plate	Merck KGaA, Darmstadt, Germany
MicroAmp Fast Optical 96well Reaction Plate with Barcode	Thermo Fisher scientific, Waltham, USA

Microtubes (1.2 ml)	Alpha Laboratories, Hampshire, UK
neoScrew Micro tubes 1.5ml brown	neoLab Migge GmbH, Heidelberg, Germany
Nitrile gloves	Abena A/Sm Aabenraa, Denmark
Non-tissue culture treated plates (6-/24-well)	BD Biosciences, Franklin Lakes, USA
Nunc™ Cell culture flask (80cm2)	Thermo Fisher scientific, Waltham, USA
Parafilm M® laboratory film	Pechiney Plastic Packaging, Chicago, USA
PCR reaction tubes (0.5 ml)	VWR International GmbH, Darmstadt, Germany
Pipet tips (10/20/300/1250 µl)	Sarstedt AG & Co., Nümbrecht, Germany
QIAshredder Homogenizer	QIAGEN GmbH, Hilden, Germany
RT-qPCR seal	4titude Ltd., Surrey, UK
Reaction tubes (1.5, 2 ml)	Sarstedt AG & Co., Nümbrecht, Germany
Screw Cap Micro Tubes	Sarstedt AG & Co., Nümbrecht, Germany
Sealing foil (ELISA)	Alpha Laboratories, Hampshire, UK
Serological Pipets (5 ml, 10 ml, 25 ml, 50 ml)	Sarstedt AG & Co., Nümbrecht, Germany
Stericup/Steritop 0.22 µm filters	Merck KGaA, Darmstadt, Germany
Syringe filters (0.2, 0.45 µm)	TPP Techno Plastic Products AG, Trasadingen, Schweiz
Tissue culture-treated plates (48-well)	BD Biosciences, Franklin Lakes, USA
Tissue culture-treated plates (6-/12-/24-well, round/flat bottom 96-well)	TPP Techno Plastic Products AG, Trasadingen, Schweiz

1.5 Primary human material from patient Mel15

Table 6. Mel15 primary samples

Material	Alias	Source	Storage
Blood	PBMCs	Klinikum Rechts der Isar	Frozen in N2
Lung metastasis	TILs	Klinikum Rechts der Isar	Frozen in N2
Intestinal metastasis	MInt	Klinikum Rechts der Isar	FFPE
Lung metastasis	MLung	Klinikum Rechts der Isar	FFPE
Draining lymph nodes (MInt)	MInt-LN1/LN2	Klinikum Rechts der Isar	FFPE
Draining lymph node (MLung)	MLung-LN	Klinikum Rechts der Isar	FFPE
Primary tumor	P		FFPE

1.6 Vectors

Table 7. DNA vector plasmids

Vector	Characteristics	Resistance	Source
pMP71-P2A-eGFP	pMP71GPRE retroviral vector with P2A element upstream of GFP; insertion of additional SalI cutting site	Ampicillin	Richard Klar and Martina Rami
pMP71-T2A-iRFP	pMP71GPRE retroviral vector with T2A element upstream of iRFP	Ampicillin	Henrique Bianchi
pMP71-P2A-dsRed	pMP71GPRE with P2A element upstream of dsRed	Ampicillin	Richard Klar
pMP71-TCR KIF2C-PBC1-alpha_chain-iRFP	pMP71GPRE retroviral vector with TCR KIF2C-PBC1 native alpha chain	Ampicillin	Gaia Lupoli
pMP71-TCR KIF2C-PBC1-beta_chain-eGFP	pMP71GPRE retroviral vector with TCR KIF2C-PBC1 native beta chain	Ampicillin	Gaia Lupoli
pMP71-TCR KIF2C-PBC2-alpha_chain-iRFP	pMP71GPRE retroviral vector with TCR KIF2C-PBC2 native alpha chain	Ampicillin	Gaia Lupoli
pMP71-TCR KIF2C-PBC2-beta_chain-eGFP	pMP71GPREretroviral vector with TCR KIF2C-PBC2 native beta chain	Ampicillin	Gaia Lupoli
pUC57-KIF2C minigene mut	Cloning vector containing minigene coding for KIF2C^{P13L} and dsRed	Ampicillin	Gaia Lupoli

Vector	Characteristics	Resistance	Source
pUC57-KIF2C minigene wt	Cloning vector containing minigene coding for KIF2C^{WT} and dsRed	Ampicillin	Gaia Lupoli
pMP71-KIF2C minigene mut	pMP71GPRE retroviral vector containing minigene coding for KIF2C^{P13L} and dsRed	Ampicillin	Gaia Lupoli
pMP71-KIF2C minigene wt	pMP71GPRE retroviral vector containing minigene coding for KIF2C^{WT} and dsRed	Ampicillin	Gaia Lupoli
pMP71-SYTL4 minigene mut	pMP71GPRE retroviral vector containing minigene coding for SYTL4^{S363F} and dsRed	Ampicillin	Eva Bräunlein
pMP71-SYTL4 minigene wt	pMP71GPRE retroviral vector containing minigene coding for SYTL4^{WT} and dsRed	Ampicillin	Eva Bräunlein
pMP71-NCAPG2 minigene mut	pMP71GPRE retroviral vector containing minigene coding for NCAPG2^{P333L} and dsRed	Ampicillin	Eva Bräunlein
pMP71-NCAPG2 minigene wt	pMP71GPRE retroviral vector containing minigene coding for NCAPG2^{WT} and dsRed	Ampicillin	Eva Bräunlein
pUC57-TCR NCAPG2-PBC1om.c	Cloning vector containing optimized and murinized TCR construct	Ampicillin	BioCat
pUC57-TCR KIF2C-PBC1om.c	Cloning vector containing optimized and murinized TCR construct	Ampicillin	BioCat
pUC57-TCR KIF2C-PBC2om.c	Cloning vector containing optimized and murinized TCR construct	Ampicillin	BioCat
pUC57-TCR SYTL4-TIL1om.c	Cloning vector containing optimized and murinized TCR construct	Ampicillin	BioCat
pUC57-TCR SYTL4-TIL2om.c	Cloning vector containing optimized and murinized TCR construct	Ampicillin	BioCat
pUC57-TCR SYTL4-PBC1om.c	Cloning vector containing optimized and murinized TCR construct	Ampicillin	BioCat
pUC57-TCR SYTL4-PBC2om.c	Cloning vector containing optimized and murinized TCR construct	Ampicillin	BioCat
pUC57-HLA-A03_B27	Cloning vector containing sequences coding for HLA-A03:01 and B27:05	Ampicillin	BioCat
#316	pMP71GPRE retroviral vector containing tandem minigenes coding for SYTL4^{S363F}, NCAPG2^{P333L}, KIF2C^{P13L} and dsRed	Ampicillin	Gaia Lupoli
#317	pMP71GPRE retroviral vector containing tandem minigenes coding for SYTL4^{WT}, NCAPG2^{WT}, KIF2C^{WT} and dsRed	Ampicillin	Gaia Lupoli
pMP71-TCR NCAPG2-PBC1om.c	pMP71GPRE retroviral vector containing optimized and murinized TCR construct	Ampicillin	Yinshui Chang
pMP71-TCR KIF2C-PBC1om.c	pMP71GPRE retroviral vector containing optimized and murinized TCR construct	Ampicillin	Gaia Lupoli
pMP71-TCR KIF2C-PBC2om.c	pMP71GPRE retroviral vector containing optimized and murinized TCR construct	Ampicillin	Gaia Lupoli
pMP71-TCR SYTL4-TIL1om.c	pMP71GPRE retroviral vector containing optimized and murinized TCR construct	Ampicillin	Yinshui Chang
pMP71-TCR SYTL4-TIL2om.c	pMP71GPRE retroviral vector containing optimized and murinized TCR construct	Ampicillin	Yinshui Chang
pMP71-TCR SYTL4-PBC1om.c	pMP71GPRE retroviral vector containing optimized and murinized TCR construct	Ampicillin	Yinshui Chang
pMP71-TCR SYTL4-PBC2om.c	pMP71GPRE retroviral vector containing optimized and murinized TCR construct	Ampicillin	Yinshui Chang

1.7 Cell lines

Table 8. Cell lines

Cell lines	Characteristics	Source/Origin
RD114	HEK 293-based packaging cell line	BioVec Pharma Inc., Québec, Canada
T2	T-cell leukemia/B-cell hybridoma; TAP-deficient	ATCC, Manassas, USA

Cell lines	Characteristics	Source/Origin
A2058	human metastatic melanoma cell line; HLA-A03:01	Sigma-Aldrich Chemie GmbH, Munich Germany
U698M	B cell lymphoma cell line; HLA-A03:01 and B27:05	Leibniz Institute, DSMZ-German Collection of Microorganisms and Cell Cultures GmbH, Braunschweig, Germany
MDST8	human colon carcinoma cell line; HLA-B27:05	Sigma-Aldrich Chemie GmbH, Munich Germany

Table 9. Cell lines produced by retroviral transduction

Cell lines	Characteristics	Source
T2-A3	T2, transduced with HLA-A*03:01-P2A-eGFP	Richard Klar, Martina Rami, Stefan Audehm
T2-B27	T2, transduced with HLA-B*27:05-P2A-dsRed	Richard Klar
A2058$^{MUT/WT}$	A2058, transduced with tandem minigene construct (#316; #317)	Gaia Lupoli
MDST8 $^{MUT/WT}$	MDST8, transduced with tandem minigene construct (#316; #317)	Gaia Lupoli
U698M $^{MUT/WT}$	U698M, transduced with tandem minigene construct (#316; #317)	Gaia Lupoli

Table 10. Lymphoblastoid cell lines (LCLs)

LCL	Name	HLA-A	HLA-B	HLA-C	Source
LCL-1	HOM2	03:01	27:05:00	01:02	Steve Marsh
LCL-2	SWEIG007	29:02:00	40:02:00	02:02	Steve Marsh
LCL-3	AMALA	02:17	15:01	03:03	Steve Marsh
LCL-4	OZB	02:09/03:01	35:01/38:01	04:01/12:03	Steve Marsh
LCL-5	RSH	68:02/30:01	42:01:00	17:01	Steve Marsh
LCL-6	KLO	02:08	50:01/08:01	07/06:02	Steve Marsh
LCL-7	LWAGS	33:01:00	14:02	08:02	Steve Marsh
LCL-8	MaOe	02:01	07:02/15:01	30:4/12:03	Eva Bräunlein
LCL-9	BM21	01:01	41:01:00	17:01	Steve Marsh
Mel 15 LCL		03:01/68:01	27:05/35:03		Eva Bräunlein and Gaia Lupoli

1.8 Reagents and Chemicals

Table 11. Reagents and chemicals

Reagent/Chemical	Company
1-Bromo-3-chloropropane	Sigma-Aldrich Chemie GmbH, Taufkirchen, Germany
6x loading buffer	Thermo Fisher scientific, Waltham, USA
7-Aminoactinomycin D (7-AAD)	Sigma-Aldrich Chemie GmbH, Taufkirchen, Germany
AccuCheck COUNTING BEADS	Thermo Fisher scientific, Waltham, USA
Acetic acid ($C_2H_4O_2$)	Merck KGaA, Darmstadt, Germany
AEC Substrate Set	BD Biosciences, Franklin Lakes, USA
Agarose NEEO Ultra-Qualität	Carl Roth GmbH + Co. KG, Karlsruhe, Germany
AIM V™	Thermo Fisher scientific, Waltham, USA
Ammonium Chloride Potassium (ACK)	Thermo Fisher scientific, Waltham, USA
Ampicillin	Sigma-Aldrich Chemie GmbH, Taufkirchen, Germany
Anti-APC microbeads	Miltenyi Biotec GmbH, Bergisch Gladbach, Germany

Reagent/Chemical	Company
Bovine Serum Albumine (BSA)	Sigma-Aldrich Chemie GmbH, Taufkirchen, Germany
Cyclosporin A	Klinikum rechts der Isar der Technischen Universität, München, Germany
DELFIA BATDA Reagent	Perkin Elmer, Rodgau, Germany
DELFIA Europium Solution	Perkin Elmer, Rodgau, Germany
DEPC H_2O	Thermo Fisher scientific, Waltham, USA
Dimethyl sulfoxide (DMSO)	Sigma-Aldrich Chemie GmbH, Taufkirchen, Germany
Dimethylformamide (DMF)	Sigma-Aldrich Chemie GmbH, Taufkirchen, Germany
DNA ladder (100 bp, 1 kbp)	PeqLab / VWR International GmbH, Darmstadt, Germany
dNTP (2 /10 mM each)	Thermo Fisher scientific, Waltham, USA
Dulbecco's Modified Eagle Medium (DMEM)	Thermo Fisher scientific, Waltham, USA
Ethanol	Merck KGaA, Darmstadt, Germany
Ethidium bromide solution	Sigma-Aldrich Chemie GmbH, Taufkirchen, Germany
Fetal calf serum (FCS)	Thermo Fisher scientific, Waltham, USA
Ficoll	Biochrom GmbH, Berlin, Germany
Gentamycin	Biochrom GmbH, Berlin, Germany
HEPES	Thermo Fisher scientific, Waltham, USA
Human serum (HS)	Technische Universität München, Germany
Hydrogen Peroxide Solution	Sigma-Aldrich Chemie GmbH, Taufkirchen, Germany
Ionomycin	Merck KGaA, Darmstadt, Germany
Isopropanol	Merck KGaA, Darmstadt, Germany
L-Glutamine	Thermo Fisher scientific, Waltham, USA
Milk powder	Sigma-Aldrich Chemie GmbH, Taufkirchen, Germany
Non-essential amio acids (NEAA)	Thermo Fisher scientific, Waltham, USA
Opti-MEM® I	Thermo Fisher scientific, Waltham, USA
Paraformaldehyde (PFA)	Sigma-Aldrich Chemie GmbH, Taufkirchen, Germany
PBS (Gibco)	Thermo Fisher scientific, Waltham, USA
PBS powder without Ca^{2+}, Mg^{2+}	Merck KGaA, Darmstadt, Germany
Penicilline/Streptomycin	Thermo Fisher scientific, Waltham, USA
Phorbol 12-myristate 13-acetate (PMA)	Sigma-Aldrich Chemie GmbH, Taufkirchen, Germany
Propidium Iodide (PI)	Sigma-Aldrich Chemie GmbH, Taufkirchen, Germany
Prostaglandine E_2 (PGE_2)	Sigma-Aldrich Chemie GmbH, Taufkirchen, Germany
Protamine Sulfate	MP Biomedicals GmbH, Illkirch, France
RetroNectin	Takara Bio Inc., Japan
RPMI-1640	Thermo Fisher scientific, Waltham, USA
RPMI-1640 (no phenol red)	Thermo Fisher scientific, Waltham, USA
S.O.C. medium	New England Biolabs Inc., Ipswich, USA
Sodium acetate ($C_2H_3NaO_2$)	Merck KGaA, Darmstadt, Germany
Sodium azide (NaN_3)	Merck KGaA, Darmstadt, Germany
Sodium carbonate (Na_2CO_3)	Merck KGaA, Darmstadt, Germany
Sodium hydrogen carbonate ($NaHCO_3$)	Merck KGaA, Darmstadt, Germany
Sodium Pyruvate	Thermo Fisher scientific, Waltham, USA
Streptavidin-HRP	Mabtech AB, Nacka Strand, Sweden

Reagent/Chemical	Company
Sulfinipyrazone	Sigma-Aldrich Chemie GmbH, Taufkirchen, Germany
Sulfuric acid	Carl Roth GmbH + Co. KG, Karlsruhe, Germany
T4 ligase	Thermo Fisher scientific, Waltham, USA
TransIT transfection reagent	Mirus Bio LLC, Madison, USA
Triton X	Sigma-Aldrich Chemie GmbH, Taufkirchen, Germany
TRIzol reagent	Thermo Fisher scientific, Waltham, USA
Trypane blue	Sigma-Aldrich Chemie GmbH, Taufkirchen, Germany
Trypsine/EDTA	Thermo Fisher scientific, Waltham, USA
Tween 20	Sigma-Aldrich Chemie GmbH, Taufkirchen, Germany
Yeast tRNA	Thermo Fisher scientific, Waltham, USA

1.9 Kits

Table 12. Kits

Kit	Purpose	Company
AffinityScript Multiple Temperature cDNA Synthesis Kit	Reverse transcription of mRNA into cDNA	Agilent Technologies, Santa Clara, USA
Ambion™ Poly(A) Tailing Kit	Polyadenylation of in vitro transcribed RNA	Thermo Fisher scientific, Waltham, USA
BD OptEIA™ Human IL-2 ELISA Set	Cytokine measurement in cell culture supernatants	BD Biosciences, Franklin Lakes, USA
BD OptEIA™ Human IFN-γ ELISA Set	Cytokine measurement in cell culture supernatants	BD Biosciences, Franklin Lakes, USA
BD OptEIA™ TMB Substrate Reagent Set	Cytokine measurement in cell culture supernatants	BD Biosciences, Franklin Lakes, USA
DNA blood and tissue kit	gDNA isolation from tumor Mel15	QIAGEN GmbH, Hilden, Germany
Dynabeads® Untouched™ Human CD8 T Cells Kit	CD8+ T-cell isolation from PBMC	Thermo Fisher scientific, Waltham, USA
eBioscience™ Intracellular Fixation & Permeabilization Buffer Set	Intracellular cytokine staining	Thermo Fisher scientific, Waltham, USA
HotStarTaq Plus Master Mix Kit	TCR repertoire PCR	QIAGEN GmbH, Hilden, Germany
Human total RNA Master Panel II	RNA expression of TAA in healthy tissues	Clontech Laboratories, Inc., Mountain View, USA
PerfeCTa FastMix II	Real-time PCR with dual-labeled hybridization probes	QuantaBio / VWR International GmbH, Darmstadt, Germany
JETSTAR™ 2.0 Plasmid Purification Kit	Large-scale purification of DNA plasmids coding for HLA and minigene constructs; Miniprep	Genomed, Löhne, Germany
KOD Hot Start Polymerase Kit	PCR	Merck KGaA, Darmstadt, Germany
mMESSAGE mMACHINE® T7 Transcription Kit	In vitro transcription of HLA constructs	Thermo fisher scientific, Waltham, USA
NEB® 5-alpha Competent E. coli	Transformation of vector products	New England BioLabs Inc., Frankfurt am Main, Germany
NucleoBond® Xtra Maxi EF	Endotoxin-free plasmid purification of TCR constructs	MACHEREY-NAGEL GmbH & Co. KG, Düren, Germany
Nucleospin Gel and PCR Cleanup kit	Purification of DNA from Gel and PCR mixtures	MACHEREY-NAGEL GmbH & Co. KG, Düren, Germany
RNeasy Mini Kit	RNA extraction (tumor Mel15)	QIAGEN GmbH, Hilden, Germany
Venor GeM mycoplasma detection kit	Testing of cell lines for absence of mycoplasma infection	Minerva Biolabs GmbH, Berlin, Germany

1.10 Media and Buffers

Table 13. Composition of buffers and solutions

Buffer/solution	Application	Ingredients
Permeabilization buffer (1x Perm Buffer)	Intracellular cytokine staining	H2O + 10% Permeabilization Buffer (10x, contained in eBioscience™ Intracellular Fixation & Permeabilization Buffer Set)
TAE buffer (1x)	Gel electrophoresis	H2O + 10% Invitrogen TAE buffer (10x stock solution, Thermo Fisher scientific)
Acetate buffer	ELIspot	46.9 ml H2O + 4.6 ml C2H4O2 (0.2M) + 11 ml C2H3NaO2 (0.2M)
AEC buffer	ELIspot	500 µl AEC solution + 9.5 ml Acetate buffer, filtered (0.45 µm)
AEC solution	ELIspot	AEC tablet dissolved in 2.5 ml DMF
Blocking solution	ELISA	PBS + 1% (w/v) milk powder
ΔFCS	Multiple applications	FCS, inactivated for 20 min at 58°C
ΔHS	Multiple applications	HS, inactivated for 20 min at 58°C
ELISA coating buffer	ELISA	H2O + 0.1 mol/l NaHCO3, 0.03 mol/l Na2CO3, pH = 9.5
FACS buffer	Stainings for flow cytometry	PBS + 1% ΔFCS
FACS-azide buffer	Intracellular cytokine staining	PBS + 1% ΔFCS + 2 mM EDTA + 0.09% NaN3
HRP-complex solution	ELIspot	10ml PBS + 50 µl von Strp. / HRP + 50 µl ΔFCS
Isolation buffer	T-cell isolation	PBS + 2% ΔHS, 2 mM EDTA
Multimer staining buffer	Tetramer and Pentamer staining	PBS + 50% ΔFCS, 2 mM EDTA
Washing buffer	ELIspot, ELISA	PBS + 0.05% v/v Tween 20

Table 14. Composition of media

Medium	Ingredients
AIM-V	AIM-V (Thermo Fisher scientific), no supplements
cDMEM	DMEM supplemented with 10% ΔFCS, 10 mM non-essential amino acids, 1 mM sodium pyruvate, 2 mM L-Glutamine, 100 U/ml Penicillin and 100 µg/ml Streptomycin
cRPMI	RPMI supplemented with 10% ΔFCS, 10 mM non-essential amino acids, 1 mM sodium pyruvate, 2 mM L-Glutamine, 100 U/ml Penicillin and 100 µg/ml Streptomycin
cMEM	MEM supplemented with 10% ΔFCS, 10 mM non-essential amino acids, 1 mM sodium pyruvate, 2 mM L-Glutamine, 100 U/ml Penicillin and 100 µg/ml Streptomycin
Freezing medium	90% ΔFCS + 10% DMSO
LB medium	10 g Bacto-Tryptone, 5 g Bacto-Yeast extract and 10 g NaCl dissolved in 1l H2O, autoclaved after preparation
OptiMEM	OptiMEM (Thermo Fisher scientific), no supplements
T-cell medium (TCM)	RPMI 1640 supplemented with 5% ΔFCS, 5% ΔHS, 10 mM non essential amino acids, 1 mM sodium pyruvate, 2 mM L-Glutamine, 100 U/ml Penicillin, 100 µg/ml Streptomycin, 10 mM HEPES buffer and 16.6 µg/ml Gentamycin

1.11 Recombinant cytokines

Table 15. Cytokines and TLR ligands

Substance	Company
CL075	InvivoGen, San Diego, USA
OKT3	Kindly provided by Elisabeth Kremmer, Helmholtz Zentrum München
Poly-I:C	InvivoGen, San Diego, USA

Substance	Company
rh GM-CSF	PeproTech, London, UK
rh IFN-g	PeproTech, London, UK
rh IL-15	PeproTech, London, UK
rh IL-1b	PeproTech, London, UK
rh IL-21	PeproTech, London, UK
rh IL-4	PeproTech, London, UK
rh IL-7	PeproTech, London, UK
rh TNF-a	PeproTech, London, UK

1.12 Peptides

Table 16. Peptides used for immunogenicity assessment and T cell stimulation

Peptide	Sequence	Company
NCAPG2^{P333L}	KLILWRGLK	Genscript Biotech Corporation, Piscataway, USA
NCAPG2^{WT}	KPILWRGLK	Genscript Biotech Corporation, Piscataway, USA
SYTL4^{S363F}	GRIAFFLKY	Genscript Biotech Corporation, Piscataway, USA
SYTL4^{WT}	GRIAFSLKY	Genscript Biotech Corporation, Piscataway, USA
KIF2C^{P13L}	RLFLGLAIK	Genscript Biotech Corporation, Piscataway, USA
KIF2C^{WT}	RLFPGLAIK	Genscript Biotech Corporation, Piscataway, USA
seq723	KIFNFYPRK	Genscript Biotech Corporation, Piscataway, USA
seq429	KMKNFFFTK	Genscript Biotech Corporation, Piscataway, USA
seq311	RMLRRRAQK	Genscript Biotech Corporation, Piscataway, USA
seq136	TLYSPRGEK	Genscript Biotech Corporation, Piscataway, USA
seq1144	AMYQRAKLK	Genscript Biotech Corporation, Piscataway, USA
seq993	SLLTPPSTK	Genscript Biotech Corporation, Piscataway, USA
seq24	RLMFFRPIK	Genscript Biotech Corporation, Piscataway, USA
seq1127	SLYLKIHLK	Genscript Biotech Corporation, Piscataway, USA
seq1128	KIYAAGTFY	Genscript Biotech Corporation, Piscataway, USA
seq254	YLFFIQGYK	Genscript Biotech Corporation, Piscataway, USA
seq897	TTYSPIGEK	Genscript Biotech Corporation, Piscataway, USA
seq756	RLYKLILWR	Genscript Biotech Corporation, Piscataway, USA
seq37	KTYPCKIFY	Genscript Biotech Corporation, Piscataway, USA
seq163	SLQPRGSFK	Genscript Biotech Corporation, Piscataway, USA
seq933	KVINLSPFK	Genscript Biotech Corporation, Piscataway, USA
seq1075	CLFFGIPWK	Genscript Biotech Corporation, Piscataway, USA
seq711	KQFSAMALK	Genscript Biotech Corporation, Piscataway, USA
seq990	LLINRGFSK	Genscript Biotech Corporation, Piscataway, USA
seq1022	RLKCPFYGK	Genscript Biotech Corporation, Piscataway, USA
seq156	KVMTDPSRK	Genscript Biotech Corporation, Piscataway, USA
seq227	RIAGKALKK	Genscript Biotech Corporation, Piscataway, USA
seq650	KLYQCNECK	Genscript Biotech Corporation, Piscataway, USA
seq869	RRFSSLYSF	Genscript Biotech Corporation, Piscataway, USA
seq1201	RRLLILGRI	Genscript Biotech Corporation, Piscataway, USA
seq62	FRMFLTQGF	Genscript Biotech Corporation, Piscataway, USA

Peptide	Sequence	Company
seq448	ARWTAFFGV	Genscript Biotech Corporation, Piscataway, USA
seq1027	GRWALHSAF	Genscript Biotech Corporation, Piscataway, USA
seq472	KRFLHRQPL	Genscript Biotech Corporation, Piscataway, USA
seq495	ARFAVNLRL	Genscript Biotech Corporation, Piscataway, USA
seq565	WRNSFLLRY	Genscript Biotech Corporation, Piscataway, USA
seq975	YRIYDIPPK	Genscript Biotech Corporation, Piscataway, USA
seq905	ARLFLGLAI	Genscript Biotech Corporation, Piscataway, USA
seq59	YRHLFKVFR	Genscript Biotech Corporation, Piscataway, USA
seq341	FRFFTRKSL	Genscript Biotech Corporation, Piscataway, USA
seq1023	RRHCRSYNR	Genscript Biotech Corporation, Piscataway, USA
seq1201	KRRLLILGR	Genscript Biotech Corporation, Piscataway, USA
seq1127	FRQSLYLKI	Genscript Biotech Corporation, Piscataway, USA
seq382	RRTQRYFMK	Genscript Biotech Corporation, Piscataway, USA
seq750	FRICPIFVF	Genscript Biotech Corporation, Piscataway, USA
seq144	KRTNVGILK	Genscript Biotech Corporation, Piscataway, USA
seq386	LRILRIKLR	Genscript Biotech Corporation, Piscataway, USA
seq238	KRHEVPVPL	Genscript Biotech Corporation, Piscataway, USA
seq556	HRYFFFVAM	Genscript Biotech Corporation, Piscataway, USA
seq1136	FRFFATPAL	Genscript Biotech Corporation, Piscataway, USA
seq628	LRFSIIEEF	Genscript Biotech Corporation, Piscataway, USA
seq279	SRVILFSPL	Genscript Biotech Corporation, Piscataway, USA
CDH8^{S350F}	ETKKFYTLK	Dgpeptides., Ltd, Hangzhou city, China
MAP2K1^{F53L}	KRLEALLTQK	Dgpeptides., Ltd, Hangzhou city, China
CTNNA2^{P361L}	EKGDLLNIAIDK	Dgpeptides., Ltd, Hangzhou city, China
ATF4P4^{R86T}	TAFSSSVAVTDK	Dgpeptides., Ltd, Hangzhou city, China
HLA-J^{K83R}	RRKSSVTHF	Dgpeptides., Ltd, Hangzhou city, China
ITGA6^{G308A}	DAAFLSLTQR	Dgpeptides., Ltd, Hangzhou city, China
MAP2K1^{F53L}	RKRLEALLTQK	Dgpeptides., Ltd, Hangzhou city, China
OPN5^{E348K}	TVRKSSAVLK	Dgpeptides., Ltd, Hangzhou city, China
PTPN2P1^{M17V}	RIVEKELVK	Dgpeptides., Ltd, Hangzhou city, China
RPS23P2^{A26T}	KAHLGTTPK	Dgpeptides., Ltd, Hangzhou city, China
THUMPD1P1^{M103I}	KAFLKDIKK	Dgpeptides., Ltd, Hangzhou city, China
TIGD6^{T221I}	NASGIEKMR	Dgpeptides., Ltd, Hangzhou city, China
DDX21^{S517F}	FVPPTAISHF	Dgpeptides., Ltd, Hangzhou city, China
NUP153^{P706L}	ETLKPGTCVKR	Dgpeptides., Ltd, Hangzhou city, China
TP53BP2^{A494V}	SSEDILRDV	Dgpeptides., Ltd, Hangzhou city, China

Table 17. Peptides for alanine/threonine scanning

pp18_al_1	**ALFLGLAIK**	**Genscript Biotech Corporation, Piscataway, USA**
pp18_al_2	RAFLGLAIK	Genscript Biotech Corporation, Piscataway, USA
pp18_al_3	RLALGLAIK	Genscript Biotech Corporation, Piscataway, USA
pp18_al_4	RLFAGLAIK	Genscript Biotech Corporation, Piscataway, USA
pp18_al_5	RLFLALAIK	Genscript Biotech Corporation, Piscataway, USA
pp18_al_6	RLFLGAAIK	Genscript Biotech Corporation, Piscataway, USA
pp18_al_8	RLFLGLAAK	Genscript Biotech Corporation, Piscataway, USA

pp18_al_9	RLFLGLAIA	Genscript Biotech Corporation, Piscataway, USA
pp18_tr_1	TLFLGLAIK	Genscript Biotech Corporation, Piscataway, USA
pp18_tr_2	RTFLGLAIK	Genscript Biotech Corporation, Piscataway, USA
pp18_tr_3	RLTLGLAIK	Genscript Biotech Corporation, Piscataway, USA
pp18_tr_4	RLFTGLAIK	Genscript Biotech Corporation, Piscataway, USA
pp18_tr_5	RLFLTLAIK	Genscript Biotech Corporation, Piscataway, USA
pp18_tr_6	RLFLGTAIK	Genscript Biotech Corporation, Piscataway, USA
pp18_tr_7	RLFLGLTIK	Genscript Biotech Corporation, Piscataway, USA
pp18_tr_8	RLFLGLATK	Genscript Biotech Corporation, Piscataway, USA
pp18_tr_9	RLFLGLAIT	Genscript Biotech Corporation, Piscataway, USA

1.13 Antibodies

Table 18. Fluorescently labeled antibodies used for flow cytometry

Antibody	Clone	Conjugation	Company
anti-human CD3	HIT3a	APC	BD Biosciences, Franklin Lakes, USA
anti-human CD3	UCHT1	PE, AF®700	BD Biosciences, Franklin Lakes, USA
anti-human CD4	RPA-T4	PE, APC-CyTM7	BD Biosciences, Franklin Lakes, USA
anti-human CD8	RPA-T8	APC, V450, APC-CyTM7	BD Biosciences, Franklin Lakes, USA
anti-human CD8	HIT8a	FITC	BD Biosciences, Franklin Lakes, USA
anti-human CD45RA	HI100	APC	BD Biosciences, Franklin Lakes, USA
anti-human CD45RO	UCHL1	PE, AF®700	BD Biosciences, Franklin Lakes, USA
anti-human CD62L	DREG-56	PE, V450	BD Biosciences, Franklin Lakes, USA
anti-human CD137	4B4-1	APC	Miltenyi Biotec GmbH, Bergisch Gladbach, Germany
anti-murine TCR (TCRmu)	H57-597	PE	BD Biosciences, Franklin Lakes, USA
Isotypes	MOPC-21	FITC, PE, APC, AF®700, V450, APC-CyTM7	BD Biosciences, Franklin Lakes, USA
Isotype	X40	V500, BV510	BD Biosciences, Franklin Lakes, USA
anti-murine TCR (TCRmu)	H57-597	APC	BD Biosciences, Franklin Lakes, USA
anti-murine TCR (TCRmu)	H57-597	FITC	BD Biosciences, Franklin Lakes, USA
Isotype	Hα4/8	FITC	BD Biosciences, Franklin Lakes, USA

1.14 Multimers

Table 19. Multimers

pMHC-Multimer	Peptide	HLA allele	Structure	Source
SYTL4^{S363F}-pMHC	GRIAFFLKY	B27:05	Pentamer (C67S)	ProImmune Ltd., Oxford, UK
SYTL4^{WT}-pMHC	GRIAFSLKY	B27:05	Pentamer (C67S)	ProImmune Ltd., Oxford, UK
SYTL4^{S363F}-pMHC	GRIAFFLKY	B27:05	Tetramer (C67S)	AG Busch, TU München, Germany
SYTL4^{WT}-pMHC	GRIAFSLKY	B27:05	Tetramer (C67S)	AG Busch, TU München, Germany
SYTL4^{S363F}-pMHC	GRIAFFLKY	B27:05	Tetramer (WT)	AG Busch, TU München, Germany
SYTL4^{WT}-pMHC	GRIAFSLKY	B27:05	Tetramer (WT)	AG Busch, TU München, Germany
KIF2C^{P13L}-pMHC	RLFLGLAIK	A03:01	Tetramer	AG Busch, TU München, Germany

KIF2C^{WT}-pMHC	RLFPGLAIK	A03:01	Tetramer	AG Busch, TU München, Germany
NCAPG2^{P333L}-pMHC	KLILWRGLK	A03:01	Tetramer	AG Busch, TU München, Germany
NCAPG2^{WT}-pMHC	KLILWRGLK	A03:01	Tetramer	AG Busch, TU München, Germany

1.15 Primers

Table 20. Primers for sequencing

Primer	Sequence	Application
MP71 fwd	TGAAAATTAGCTCGACAAAG	Sequencing of cloned inserts in pMP71
MP71 rev	GTAAATGATTGCCCCACCA	Sequencing of cloned inserts in pMP71

Table 21. Primer for S1 downgrading

Primer	Sequence
RD114_env_fwd	AACGGGTCAGTCTTCCTCTG
RD114_env_rev	AGGTCCAGTCCCCTCCTATT

Table 22. Primers for TCR alpha and beta chain repertoire

TCRAV gene segment family-specific primers			**TCRBV gene segment family-specific primers**		
Primer	**Sequence**	**C_{WORK}**	**Primer**	**Sequence**	**C_{WORK}**
P-5'αST	CTG TGC TAG ACA TGA GGT CT	2.5 µM	**5βST**	AAG CAG AGA TCT CCC ACA C	5 µM
P-3'αST	CTT GCC TCT GCC GTG AAT GT	2.5 µM	**P-3βST**	GAG GTG AAG CCA CAG TCT G	5 µM
3'T-Cα	GGT GAA TAG GCA GAC AGA CTT GTC ACT GGA	5 µM	**P-3CβII**	GAT GGC TCA AAC ACA GCG ACC TC	5 µM
Vα1	AGA GCC CAG TCT GTG ASC CAG; S=C/G	2.5 µM	**Vβ1**	GCA CAA CAG TTC CCT GAC TTG GCA C	5 µM
Vα1.1	AGA GCC CAG TCR GTG ACC CAG; R=A/G	2.5 µM	**Vβ2**	TCA TCA ACC ATG CAA GCC TGA CCT	2.5 µM
Vα2	GTT TGG AGC CAA CRG AAG GAG	5 µM	**Vβ3**	GTC TCT AGA GAG AAG AAG GAG CGC	2.5 µM
Vα3	GGT GAA CAG TCA ACA GGG AGA	2.5 µM	**Vβ4**	ACA TAT GAG AGT GGA TTT GTC ATT	2.5 µM
Vα4	TGA TGC TAA GAC CAC MCA GC	5 µM	**Vβ5.1**	ATA CTT CAG TGA GAC ACA GAG AAA C	2.5 µM
Vα5	GGC CCT GAA CAT TCA GGA	2.5 µM	**Vβ5.2**	TTC CCT AAC TAT AGC TCT GAG CTG; Vβ5.2 + Vβ5.2T 1:1 MIX	5 µM
Vα6	GGT CAC AGC TTC ACT GTG GCT A	2.5 µM	**Vβ6.1**	GCC CAG AGT TTC TGA CTT ACT TC	2.5 µM
Vα7	ATG TTT CCA TGA AGA TGG GAG	5 µM	**Vβ6.2**	ACT CTG ASG ATC CAG CGC ACA; S=C/G	2.5 µM
Vα8	TGT GGC TGC AGG TGG ACT	5 µM	**Vββ6.3**	ACT CTG AAG ATC CAG CGC ACA	2.5 µM
Vα9	ATC TCA GTG CTT GTG ATA ATA	5 µM	**Vβ7**	CCT GAA TGC CCC AAC AGC TCT C	2.5 µM
Vα10	ACC CAG CTG CTG GAG CAG AGC CCT	5 µM	**Vβ8**	ATT TAC TTT AAC AAC AAC GTT CCG	2.5 µM
Vα11	AGA AAG CAA GGA CCA AGT GTT	2.5 µM	**Vβ8.3**	GCT TAC TTC CGC AAC CGG GCT CCT	5 µM
Vα12	CAG AAG GTA ACT CAA GCG CAG ACT	2.5 µM	**Vβ9**	CCT AAA TCT CCA GAC AAA GCT	2.5 µM

TCRAV gene segment family-specific primers			TCRBV gene segment family-specific primers		
Vα13	GAG CCA ATT CCA CGC TGC G	2.5 µM	**Vβ10**	CTC CAA AAA CTC ATC CTG TAC CTT	2.5 µM
Vα14.1	CAG TCC CAG CCA GAG ATG TC	2.5 µM	**Vβ11**	TCA ACA GTC TCC AGA ATA AGG ACG	5 µM
Vα14	CAG TCT CAA CCA GAG ATG TC	2.5 µM	**Vβ12**	AAA GGA GAA GTC TCA GAT	5 µM
Vα15	GAT GTG GAG CAG AGT CTT TTC	2.5 µM	**Vβ13.1**	CAA GGA GAA GTC CCC AAT	5 µM
Vα16	TCA GCG GAA GAT CAG GTC AAC	2.5 µM	**Vβ14**	GTC TCT CGA AAA GAG AAG AGG AAT	2.5 µM
Vα17	GCT TAT GAG AAC ACT GCG T	2.5 µM	**Vβ15**	AGT GTC TCT CGA CAG GCA CAG GCT	5 µM
Vα18	GCA GCT TCC CTT CCA GCA AT	2.5 µM	**Vβ16**	AAA GAG TCT AAA CAG GAT GAG TCC	2.5 µM
Vα19	AGA ACC TGA CTG CCC AGG AA	2.5 µM	**Vβ17**	CAG ATA GTA AAT GAC TTT CAG	2.5 µM
Vα20	CAT CTC CAT GGA CTC ATA TGA	2.5 µM	**Vβ18**	GAT GAG TCA GGA ATG CCA AAG GAA	2.5 µM
Vα21	GTG ACT ATA CTA ACA GCA TGT	5 µM	**Vβ19**	CAA TGC CCC AAG AAC GCA CCC TGC	2.5 µM
Vα22	TAC ACA GCC ACA GGA TAC CCT TCC	2.5 µM	**Vβ20**	AGC TCT GAG GTG CCC CAG AAT CTC	2.5 µM
Vα23	TGA CAC AGA TTC CTG CAG CTC	2.5 µM	**Vβ21**	AAA GGA GTA GAC TCC ACT CTC	2.5 µM
Vα24	GAA CTG CAC TCT TCA ATG C	2.5 µM	**Vβ22.1**	CAT CTC TAA TCA CTT ATA CT	5 µM
Vα25	ATC AGA GTC CTC AAT CTA TGT TTA	2.5 µM	**Vβ23**	GCA GGG TCC AGG TCA GGA CCC CCA	2.5 µM
Vα26	AGA GGG AAA GAA TCT CAC CAT AA	5 µM	**Vβ24**	ATC CAG GAG GCC GAA CAC TTC T	5 µM
Vα27	ACC CTC TGT TCC TGA GCA TG	2.5 µM			
Vα28	CAA AGC CCT CTA TCT CTG GTT	2.5 µM			
Vα29	AGG GGA AGA TGC TGT CAC CA	2.5 µM			
Vα30	GAG GGA GAG AGT AGC AGT	2.5 µM			
Vα31	TCG GAG GGA GCA TCT GTG ACT A	2.5 µM			
Vα32	CAA ATT CCT CAG TAC CAG CA	2.5 µM			

Table 23. Primers for molecular cloning

Primer	Sequence	Application
SYTL4_fwd	TAGCGGCCGCCACCATGAGTACGATCGGCAGCAT	Cloning of mutated and wt minigene
SYTL4_rev	TAGTCGACCTTGGCTTCATCAGCATAGG	Cloning of mutated and wt minigene
NCAPG2_fwd	TAGCGGCCGCCACCATGTCTCCAGTGCATTCCAA	Cloning of mutated and wt minigene
NCAPG2_rev	TAGTCGACCATGAAGGTTTGGATCC	Cloning of mutated and wt minigene
TCR KIF2C-PBC1 alpha variable chain	TAGCGGCCGCCACCATGTCACTTTCTAGCCTGCT	Cloning of native TCR chains

Primer	Sequence	Application
TCR KIF2C-PBC1 beta variable chain	TAGCGGCCGCCACCATGGGCACCAGTCTCCTATG	Cloning of native TCR chains
TCR KIF2C-PBC2 alpha variable chain	TAGCGGCCGCCACCATGAAATCCTTGAGAGTTTT	Cloning of native TCR chains
TCR KIF2C-PBC2 beta variable chain	TAGCGGCCGCCACCATGGGCACAAGGTTGTTCTT	Cloning of native TCR chains
TCR alpha constant chain	TAGTCGACGCTGGACCACAGCCGCAGCG	Cloning of native TCR chains
TCR beta constant chain	TAGTCGACGCCTCTGGAATCCTTTCTCT	Cloning of native TCR chains
KIF2C_fwd	ATGCGGCCGCCAACATGGCCA	Cloning of KIF2C minigene
KIF2C_rev	ATGTCGACTTCTGGGTTTATTGC	Cloning of KIF2C minigene
iRFP	GTAGATCATCACTCTGTCGAAG	Cloning of iRFP
NCAPG2-SYTL4-KIF2C minigene_fwd	ATGCGGCCGCCACCATGGC	Cloning of mut/wt tandem minigenes
NCAPG2-SYTL4-KIF2C minigene_rev	ATGTCGACCCTGAGGCCGGCCTC	Cloning of mut/wt tandem minigenes
GFP-Luciferase_fwd	ATGTCGACTCTCCCTTATCGTCAATCTTCT	Cloning of GFP-Luciferase
GFP-Luciferase_rev	ATGAATTCAAGGCCTTGTAAGTTGGCGA	Cloning of GFP-Luciferase

1.16 Software and web-based tools

Table 24. Software tools

Software	Application	Company
CloneManager 7, v7.03	In-silico cloning	Scientific & Educational Software, Denver, USA
SerialCloner 2.6.1		SerialBasics
EndNoteTM X7	Citation management	Thomson Reuters, New York City, USA
FlowJo v7.6.5 and 10.6.2	Flow cytometry analysis	Tree Star, Ashland, USA
Graphpad Prism v10	Data processing and analysis	GraphPad Software, Inc., La Jolla, USA
Immunospot software 5.4.0.1	ELIspot analyses	CTL-Europe, Bonn, Germany
Microsoft Office (Word, Excel, Powerpoint), 2010	Data processing and presentation	Microsoft Corporation, Redmond, USA
Sequencher v5.0	Sequence alignment	GeneCodes Corporation, Ann Arbor, USA
StepOne Software v2.3	Processing of real-time PCR data	Life Technologies Corporation, USA

Table 25. Web-based tools

Tool	Application	Homepage
CBS Prediction Servers (NetMHCpan 2.8, NetMHC 4.0 and others)	In-silico epitope prediction	http://www.cbs.dtu.dk/services/NetMHC/
EMBOSS needle	Protein sequence alignment	http://www.ebi.ac.uk/Tools/psa/emboss_needle/
Ensembl GRCh38.78	Sequence extraction from reference genome	http://www.ensembl.org/index.html
Genevestigator	Antigen expression analysis	https://genevestigator.com/
Human Protein Atlas	Protein expression analysis	http://www.proteinatlas.org/

Tool	Application	Homepage
IMGT	TCR sequence identification	http://www.imgt.org/
NCBI Basic Local Alignment Search Tool (BLAST)	TCR reconstruction; Primer blast	https://blast.ncbi.nlm.nih.gov/Blast.cgi
Oncomine	Antigen expression analyses in cancer tissues	https://www.oncomine.org/resource/login.html
Primer3	Primer and probe design	http://bioinfo.ut.ee/primer3/
SYFPEITHI	In-silico epitope prediction	http://www.syfpeithi.de/
UCSC Genome Browser Gateway (BLAT)	Antigen expression analysis	http://genome-euro.ucsc.edu
Primer3web	Design of real-time primers and probes	
OligoArchitect Online	Design of real-time primers and probes	

1.17 Mouse model

NOD.Cg-Prkdc^{scid}Il2rg^{tm1Wjl}/SzJ (NSG), The Jackson Laboratory, Bar Harbor, Maine, US.

Methods

1.18 Cell culture methods

1.18.1 Primary human material

Informed consent of all healthy donors and patients was obtained following requirements of the institutional review board (Ethics Commission, Faculty of Medicine, TU München). An overview about patient Mel15 clinical courses is given in **Figure 2**.

Patient Mel15 was diagnosed in 2008 with malignant melanoma and received surgical resection of primary tumor in the same year. Since 2013, the patient was treated at the Klinikum Rechts der Isar, TU München, when the disease had spread to the lung and intestine, and was histologically confirmed with a lung biopsy (B_{Lung}; 2013). The patient received two cycles of chemotherapy which led to shrinkage of the intestinal metastasis (M_{Int}), while the lung metastasis (M_{Lung}) kept progressing. In November of the same year patient Mel15 started treatment with four cycles of anti-CTLA-4 mAb (Ipilimumab) to which M_{Lung} initially responded whereas the intestinal metastases did not. Therefore, the patient received abdominal surgery in 2014 for removal of M_{Int} and two adjacent lymph nodes (day 96 from start of Ipilimumab), and thoracic surgery in 2016 for resection of the then again progressing M_{Lung} and one lymph node (day 796). After second surgery the patient received anti-PD-1 mAb Pembrolizumab for one year and is in complete remission since then. TILs were extracted from M_{Lung} tumor tissue (E. Bräunlein et al., 2021).

M_{Lung} fresh sample was used for isolation and expansion of TILs. Briefly, TILs were expanded by culturing minced tumor tissue in T-cell medium (TCM) supplemented with 1000 U/ml IL-2 and 30 ng/ml OKT3, in presence of γ-irradiated feeder PBMCs (30 Gy). Medium was exchanged every 2-3 days with fresh TCM supplemented with 300 U/ml IL-2. TILs were expanded for 2-3 weeks and cryopreserved until use (Bassani-Sternberg et al., 2016).

EDTA-anticoagulated whole blood was collected from patients and healthy donors by blood withdrawal or apheresis products and PBMCs were isolated by density-gradient centrifugation (Ficoll-Hypaque, Biochrom) immediately upon receipt and stored in liquid nitrogen. PBMCs and T cells were cultivated in T-cell medium, RPMI 1640 (Invitrogen, Carlsbad, CA, USA) supplemented with Penicillin/Streptomycin (Pen/Strep) (PAA, Pasching, Austria), 5% ΔFCS, 5% human serum, 10 mM Hepes (Invitrogen) and Gentamycin (Biochrom, Berlin, Germany), or serum-free AIM-V (Invitrogen) as indicated (Bassani-Sternberg 2016).

1.18.2 Cell lines

Cell lines used in this study are: T2 (ATCC), human metastatic melanoma cell line A2058 (Sigma-Aldrich), human colon carcinoma cell line MDST8 (Sigma-Aldrich) and B cell lymphoma cell line U-698-M (DSMZ) (**Table 8**). T2 cell line was retrovirally transduced with the HLA restriction elements HLA-A03:01 (T2-A3) and B27:05 (T2-B27) as previously described (Klar et al., 2014) (**Table 9**). Mel15-derived and LCL-8 B-cell lymphoblastoid line were generated in-house by immortalization with EBV supernatants, other lines were provided by Steve Marsh (**Table 10**). RD114 packaging cell line was adopted for production of retroviral vectors. Suspension target cell lines were maintained in cRPMI, while adherent cell lines were cultivated in cDMEM, except A2058 cell line which was maintained in MEM. Cell lines were split twice per week and/or according to cell density. Adherent cell lines were rinsed with PBS and detached from the flask through incubation with Trypsin/EDTA for 2-3 min at 37°C. Cell lines were routinously observed under the light microscope and culture supernatants tested for the absence of mycoplasma infection, using a mycoplasma detection kit (Venor GeM) according to the manufacturer's instructions.

1.18.3 Isolation of PBMCs from whole peripheral blood

PBMCs were obtained from whole blood or leukapheresis products using density gradient centrifugation (Ficoll). Briefly, whole blood and leukapheresis products were diluted in RPMI medium (respectively 1:1 and 5:1). Diluted solutions were gently laid on Ficoll, and centrifuged at 880 g for 25 min with light acceleration and no brakes. Afterwards leukocytes were carefully collected, pooled and washed twice with RPMI. Purified PBMCs were immediately stored in liquid nitrogen or used fresh for further experiments.

1.18.4 PBMC-derived T cell recall responses assessed with accelerated co-culture dendritic cell assay (acDC)

For stimulation and expansion of antigen specific T cells, a modified version of the previously published stimulation acDC protocol (Martinuzzi et al., 2011) was established by Dr. Bräunlein (Bassani-Sternberg et al., 2016) and adopted for all stimulations here reported. Patient-derived PBMCs (3-5×10^5/well) were cultured in AIM-V medium supplemented with 100 ng/ml IL-4 and 100 ng/ml GM-CSF in a flat-bottom 96-well plate. After 24 hours (h), a single peptide or a pool of peptides (**Table 26**) (C_{END} = 1 μM), Poly-I:C (20 μg/ml) and IL-7 (0.5 ng/ml) were added to the culture. After 24 h, cells were rinsed twice with RPMI and transferred onto a pre-coated ELIspot plate (p. 1.21.1) and cultured overnight. After incubation, cells were harvested from the ELIspot plate and transferred to a round-bottom 96-well plate for expansion in TCM supplemented with IL-7 and IL-15 (5 ng/ml each). Cytokines were freshly added every 2-3 days. The ELISpot plate was developed as explained in p. 1.21.1

("early-timepoint"). Cells were split and expanded according to cell density. Reactivity was confirmed 10-15 days later by co-culturing expanded T cells with pulsed T2 target cells (2×10^4/well; E:T=1:1) in TCM on a coated ELISpot plate (p. 1.21.1) for 72h ("late timepoint"). Expanded T cells from "early timepoint" for which reaction was confirmed, were used for single-cell cloning and isolation of TCRs (p. 1.18.5).

Table 26. Arrangement of peptide pools for immunogenicity assessment. Table adapted from (E. Bräunlein et al., 2021)

Subpool	Peptide	Variation	Predicted affinity (nM)	Pools
A1	KIFNFYPRK	L > F	6.8	Pool 1 / 6
	KMKNFFFTK	S > F	7.4	
	RMLRRRAQK	E > K	8.7	
	TLYSPRGEK	E > K	9.2	
	AMYQRAKLK	S > L	9.5	
A2	SLLTPPSTK	P > S	9.6	Pool 2 / 7
	RLMFFRPIK	S > F	9.8	
	SLYLKIHLK	L > K	11	
	KIYAAGTFY	H > Y	11.2	
	YLFFIQGYK	S > F	12.5	
A3	TTYSPIGEK	G > E	14.5	Pool 3 / 8
	RLYKLILWR	P > L	14.7	
	KTYPCKIFY	S > F	16.6	
	SLQPRGSFK	P > S	18.2	
	KVINLSPFK	E > K	18.6	
A4	CLFFGIPWK	S > I	19.2	Pool 4 / 9
	KQFSAMALK	P > S	21.4	
	RLFLGLAIK	P > L	21.6	
	KLKLPIIMK	M > I	23.3	
	LLINRGFSK	D > N	25.2	
A5	RLKCPFYGK	H > Y	26.1	Pool 5 / 10
	KVMTDPSRK	A > V	28.7	
	RIAGKALKK	P > L	31.5	
	KLYQCNECK	S > L	32.7	

Subpool	Peptide	Variation	Predicted affinity (nM)	Pools
B1	RRFSSLYSF	G > R	11.5	Pool 1 / 10
	RRLLILGRI	G > R	11.5	
	FRMFLTQGF	P > L	15	
	ARWTAFFGV	S > F	17.1	
	GRWALHSAF	S > F	17.5	
B2	KRFLHRQPL	P > L	20.2	Pool 2 / 6
	ARFAVNLRL	G > R	20.7	
	WRNSFLLRY	S > F	24	
	YRIYDIPPK	V > I	24	
B3	ARLFLGLAI	P > L	25.7	Pool 3 / 7
	YRHLFKVFR	G > R	26.6	
	FRFFTRKSL	E > K	26.9	
	RRHCRSYNR	D > N	27.6	
	KRRLLILGR	G > R	28	
B4	FRQSLYLKI	L > K	29.2	Pool 4 / 8
	RRTQRYFMK	E > K	29.3	
	FRICPIFVF	R > C	32.3	
	KRTNVGILK	E > K	33.3	
	LRILRIKLR	M > I	35.6	
B5	KRHEVPVPL	Y > H	36.8	Pool 5 / 9
	HRYFFFVAM	S > F	37.5	
	FRFFATPAL	S > F	38.3	
	LRFSIIEEF	T > I	45.9	
	SRVILFSPL	N > S	46	

Pool 11 = Pool 1 + SYTL4^{S363F}

1.18.5 Cloning of neoantigen-reactive T cell lines

For isolation of peptide-specific TCRs, an aliquot (ca. $1x10^5$ cells) of expanded reactive T-cell lines was stored in Trizol; the rest was cultured for 24 h with irradiated (100 Gy) T2 cells pulsed with peptide of interest (E:T = 3:1) in presence of IL-7. As negative control 1/10 of available T cells were cocultured with T2 cells pulsed with an irrelevant peptide. Activated cells were enriched for $CD137^+$ activation marker expression (p. 1.21.4) and cloned by limiting dilutions at a concentration of 0.5, 1 and 10 cells per well on γ-irradiated feeder PBMCs ($5×10^4$/well; 30 Gy), 50 U/ml IL-2 (Peprotech) and 30 ng/mL OKT-3 (provided by Elisabeth Kremmer). IL-2 was added twice a week to a final concentration of 50 ng/ml. Proliferating T-cell clones were screened for reactivity to the specific peptide in a time span between 2 and 3 weeks. Half of each clone was used for co-culture with peptide-pulsed T2 cells and detection of IFN-γ secretion with ELISA assay. After proof or reactivity an aliquot of cells was stored in TRIzol reagent for RNA extraction (one-fourth of T cells) and repertoire PCR (**Table 22**). Remaining cells were further expanded by adding different γ-radiated PBMC-feeder pools to the culture every two weeks.

1.18.6 Magnetic separation of $CD8^+$ T cell sub-population

$CD8^+$ T cells were isolated from fresh or freshly thawed PBMCs using the kit "Dynabeads® Untouched™ Human CD8 T Cells" following the manufacturer's instructions. Briefly, cells were thawed, counted and resuspended in isolation buffer. Reagent volumes are scaled according to cell numbers as indicated in the datasheet. Non-specific sites on cell surface are blocked with ΔFCS before the labelling with an antibody mix provided in the kit. After incubation and washes, beads are added. The tube is then placed in a magnet and all cells labeled with antibody mix and magnetic beads are retained, while $CD8^+$ cells remained in the unlabeled fraction and can be collected. The kit allows the depletion of all cells positive for the following antigens: CD4, CD14, CD16, CD19, CD36, CD56, CDw123 and CD235a. Aliquots of PBMCs and isolated CD8 was saved for quality control of performed isolation through flow cytometry (1.23.1). Isolated $CD8^+$ T cells were activated in culture (1.18.7).

1.18.7 In vitro activation of isolated $CD8^+$ T cells

$CD8^+$ T cells were activated in culture immediately after isolation (1.18.6). For activation T cells were resuspended in TCM at a density of $1×10^6$/ml with 30/ml IL-2 and 50µl/ml of pre-washed Human T-Activator CD3/CD28 Dynabeads™. Before use beads were vortexed, pipetted into a tube with the same amount of isolation buffer and placed in a magnet for 2 min. Supernatant was removed and beads resuspended in TCM. T cells were activated for 2 or 3 days at 37°C.

After incubation T cells were collected, spun down and resuspended in 6-8 ml RPMI. Cell suspension was placed in a magnet for 2 min to remove activation beads. Activated $CD8^+$ T cells were the used for retroviral transduction (1.22.2).

1.18.8 TCR in vitro functional characterization

1.18.8.1 Assessment of TCR specificity for the epitope

TCR-transduced T cells were incubated with target cells (LCL-1) transduced with different minigene constructs or pulsed with relative peptides (1 μM). Mutated neoantigens, wt counterparts and/or irrelevant antigens were taken as controls for TCR specificity. Assays for detection of cytokine secretion were performed in triplicates (E:T = 1:1; 10,000 target and effector cells per well).

1.18.8.2 TCR functional avidity assessment

Functional avidity was assessed by incubating transgenic T cells with T2 target cells (ATCC® CRL-1992™) pulsed with graded amounts of peptide (E:T = 1:1; 10,000 cells/well). IFN-γ secretion was quantified by ELISA and values obtained were fitted into a nonlinear variable-slope regression curve on GraphPad Prism 7. The peptide concentration required to reach half-maximal IFN-γ secretion (EC_{50}) was calculated through the formula:

$$Y = Bottom + \frac{(Top - Bottom)}{1 + 10^{(Log(EC_{50} - x) \cdot Hillslope)}}$$

Functional avidity assay was performed at least three times for at least two different transductions and donors showing comparable results (E. Bräunlein et al., 2021).

1.18.8.3 TCR-T cell co-culture at different effector to target ratios

For co-culture of T cells with target cells in different ratios, LCL-1 target cells endogenously expressing mut and wt antigens, were rinsed and resuspended in appropriate volume of TCM. T cells transduced with TCRs were harvested for culture, washed and different dilutions prepared. Number of target cells was kept constant (5,000/well), while T cells were seeded in different ratios (10:1, 2:1, 0.4:1 etc.). After 20 h incubation IFN-γ secretion was quantified with ELISA.

1.18.8.4 Alanine-Threonine scanning

Target T2 cells were pulsed for 2h at 37°C with peptide antigens of interest carrying a single amino acid substitution in each position. This assay was performed with both alanine and threonine-single substitutions in direct comparison to the original mutated identified neoantigens. TCR-transgenic T cells were cocultured with peptide-pulsed target cells in a E:T=1:1 (10,000:10,000). After 20 h incubation

IFN-γ secretion was quantified with ELISA. IFN-γ values from every condition were calculated as a percentage on the positive control (neoantigen).

1.18.8.5 TCR cross-reactivity testing

For alloreactivity evaluation, TCR-transduced T cells were stimulated with respective to neoantigens presented in the context of different HLA class I alleles. To this end, effector cells were cultured with LCL cell lines (**Table 10**) with a broad variety of HLA alleles, pulsed with mutated peptides (E:T = 1:1; 10,000 cells/well). To exclude the recognition of the allogenic HLA complexes presenting other endogenously presented peptides, non-pulsed LCLs were also included in the analysis. As readout, IFN-γ production was quantified by ELISA.

1.18.8.6 Real-time in vitro monitoring of TCR-mediated cytotoxicity with the "xCELLigence system"

For real-time monitoring of T-cell mediated cytolitic activity on target cells, two different adherent cell lines were adopted, according to the naturally expressed HLA-allotypes. MDST8 cell line (HLA-B27:05^{+}) was selected for the testing of SYTL4^{S363F}-specific TCRs; A2058 (HLA-A03:01) for KIF2C^{P13L} and NCAPG2^{P333L}-specific TCRs. Both cell lines were engineered to express mutant and wt tandem minigenes coding for all three identified neoantigens, and cloned (p. 1.18.5). Cytotoxicity assays were performed with impedance-based xCELLigence assays (ACEA BioSciences). First, culture media was added to 96 well E-Plates (ACEA Biosciences) for background impedance measurement (Hamidi, Lilja, & Ivaska, 2017). Target cells were seeded on the plate at different densities, according tothe cell line (A2058$^{MUT/WT}$ – 50,000/well; MDST8$^{MUT/WT}$ – 20,000/well). The E-plate was then transferred to the RTCA MP instrument, inside a cell culture incubator for 24h, during which impedence was measured every 30 min. The measurement was paused for addition of T cells, after which impedence was measured every 15 minuts for the first 8 h and every 30 for the following 16 h. . Target cells only, target cells and non-transduced T cells served as controls. In order to allow direct comparison of TCRs targeting different cell lines, cytolysis was calculated by normalizing Cell Index (CI) values from each measurement on CI from coculture of target cells and non-transduced T cells with the following formula:

$$TCR\ specific\ cytolysis = 100 - \left(\frac{CIx}{CInontransd} \times 100\right)$$

1.18.8.7 In vitro detection of TCR mediated cytotoxicity with "europium release assay"

This assay was performed with LCL-1/HOM2 as target cell line transduced with single minigenes coding for three neoantigens and their wt counterparts. For loading of the cell lines, 10,000 cells per condition were calculated. Numbers were rounded up to 0,5 or 1 x 10^6 cells in 0.5 or 1mL culture medium, to be pulsed with 2.5 or 5 µL bis(acetoxymethyl) 2,2':6',2''-terpyridine-6,6''-dicarboxylate

(BATDA) and incubated for 30 minutes at +37°C. 3. After loading cells were spun down and resuspended in PBS. Washing step in PBS was repeated 3 times. The pellet was resuspended in RPMI and cell number adjusted to about 1 x 10^5 cells/ml. 100 µl target cells were seeded in a round bottom 96-well plate. Wells for detection of background, spontaneous release and maximum release were set. The background is measured on wells containing just medium used for cell resuspension. Spontaneous release is from target cells only and maximum release is from target cells lysed with Triton X 1%.

Effector cells were added of varying cell concentrations in order to have different effector to target ratios (1:1, 0.3:1, 0.1:1). The coculture was incubated for 4 h in a humidified 5 % CO_2 atmosphere at 37°C. After 4 h, 20 µl of the supernatant were transferred to a 96 well flat-bottom ELISA plate and 180 µL of Europium Solution were added on top. The plate was incubated on a shaker for 15 minutes and fluorescence was measured with a time-resolved fluorometer. Specific release was calculated by applying the following formula:

$$\%\ Specific\ release = \frac{Experimental\ release\ (counts) - Spontaneous\ release\ (counts)}{Maximum\ release\ (counts) - Spontaneous\ release\ (counts)}\ x\ 100$$

1.18.9 Detection of TIL recall responses and expansion of neoantigen-specific T cells

To test immunogenicity of peptides identified with immunopeptidomic 2018 pipeline, TILs were mixed with autologous irradiated Mel15 PBMCs (ratio 1:1) and acDC protocol was carried out (p. 1.18.4). TILs were stimulated with peptides illustrated in **Table 27**.

Table 27. Tested peptides identified with immunopeptidomic 2018 pipeline

Gene	Sequence	a.a. Alt	HLA restriction; affinity (nM); % rank; binding level	MaxQuant database	Biotype Ensembl	Reads exome M_{Int} Ref:Alt	Reads exome M_{Lung} Ref:Alt	Reads RNA M_{Int} Ref:Alt	Reads RNA M_{Lung} Ref:Alt
CDH8	ETKKFYTLK	S350F	A*68:01; 10.3; 0.100; SB	M_{Int} exome	Nonsense mediated decay	76:6	98:8	0:0	NA
MAP2K1	KRLEALLTQK	F53L	A*03:01; 181.7; 0.700; WB	M_{Int} RNA, M_{Lung} exome	Protein coding	66:1	109:10	73:36	47:25
CTNNA2	EKGDLLNIAIDK	P361L	A*03:01; 543.4; 1400; WB	M_{Int} exome	Protein coding	36:7	9:0	NA	2:0
HLA-J	RRKSSVTHF	K83R	B*27:05; 48.2; 0.200; SB	M_{Int} RNA	Processed transcript	97:0	160:1	8:6	3:0
ITGA6	DAAFLSLTQR	G>A	A*68:01; 16.9; 0.250; SB	M_{Int} RNA	Protein coding	78:0	117:1	6:4	8:3
MAP2K1	RKRLEALLTQK	F53L	B*27:05; 701.7; 1700; WB	M_{Int} RNA	Protein coding	66:1	109:10	73:36	47:25
OPN5	TVRKSSAVLK	E348K	A*03:01; 53.4; 0.250; SB	M_{Int} exome	Protein coding	165:14	74:4	0:0	NA

Gene	Sequence	a.a. Alt	HLA restriction; affinity (nM); % rank; binding level	MaxQuant database	Biotype Ensembl	Reads exome M_{Int} Ref:Alt	Reads exome M_{Lung} Ref:Alt	Reads RNA M_{Int} Ref:Alt	Reads RNA M_{Lung} Ref:Alt
PTPN2P1	RIVEKELVK	M17V	A*03:01; 363.0; 1100; WB	M_{Int} RNA	Processed pseudogene	3:0	4:0	2:5	1:2
RPS23P2	KAHLGTTPK	A26T	A*03:01; 194.9; 0.700; WB	M_{Int} exome	Processed pseudogene	14:4	22:5	NA	NA
THUMPD1P1	KAFLKDIKK	M103I	A*03:01; 384.1; 1100; WB	M_{Int} exome	Processed pseudogene	5:3	1:0	0:0	0:0
TIGD6	NASGIEKMR	T221I	A*68:01; 17.5; 0.250; SB	M_{Int} RNA	Protein coding	58:0	91:0	6:3	3:0
DDX21	FVPPTAISHF	S517F	B*35:03; 27320,9; 3,000; --	M_{Int} exome/RNA	Protein coding	92:20	93:10	8:16	12:18
NUP153	ETLKPGTCVKR	P706L	A*68:01; 730.0; 3.000; --	M_{Int} exome/RNA	Protein coding	214:40	154:10	57:37	42:8
TP53BP2	SSEDILRDV	A494V	B*27:05; 29929,1; 39,000; --	M_{Int} exome/RNA	Protein coding	94:7	79:4	24:10	44:5

ELISpot plates were developed as explained in p. 1.21.1T cells were expanded for ca. 2 weeks and frozen. Isolation of activated T cells was carried out as explained in p. 1.21.4.

1.19 In silico methods

1.19.1 In silico prediction of mutated peptide antigens and HLA binding affinity

Putative mutated peptides were predicted by translating exome sequences bearing a SNV to 23-residue-long amino acid strings (mutated amino acid in 12th position) (Thomas Engleitner from Prof. Dr. Rad's group). SNVs were identified through a stringent variant calling on Mel15-M_{Int} exome (Bassani-Sternberg et al., 2016). Protein transcripts were downloaded from Human Ensembl GRCh38, release 86. In cases where the mutation was located closer to the 3' or 5' terminus of the gene, the string was shorter and the mutation not centrally situated. Epitopes of length ranging between 8 and 13 amino acids, and their binding affinities to patient specific HLA class I allotypes (HLA-A03:01, A68:01, B27:05 and B35:03), were predicted with NetMHC 4.0 algorithm. The database containing translated mutated peptide sequences was generated by Thomas Engleitner (Prof. Dr. Rad), while the database containing 8-13 amino acid long predicted peptides and their binding affinities was produced by Dr. Audehm and Dr. Klar.

1.19.1.1 Selection of predicted peptides for in vitro recall response assays

Selection of predicted peptides was based on size, binding affinity and HLA restriction. The list of peptides for immunogenicity assessment included nine-amino-acid-long candidates ranked by predicted affinity and binding to HLA-A03:01 and B27:05. The first 25 predicted binders for each HLA were

custom synthetized (Genscript) and used for T-cell recall reactivity assays. Neoantigens previously identified with MS (NCAPG2^{P333L}, ranked 24th and SYTL4^{S363F} ranked 6th) were excluded from this list shortening the number of candidates to be tested to 48 in total.

1.19.2 Immunopeptidomic 2018: mutation calling in non-coding regions of tumor genomes

The research group of Prof. Rad (TU-München) and Prof. Mann (Max Planck Institute) worked together for the improvement of previous immunopeptidomic pipeline published in 2016 (Bassani-Sternberg et al., 2016). Aim of this work was to develop a bioinformatic script for the identification of mutations in non-coding areas of the genome and to identify resulting peptides with MS which is not focus of this thesis.

Mutation calling and generation of the mutation database containing Mel15 M_{Int} and M_{Lung} sequence data from WES (1.20.4) and RNA-seq (1.20.5), was performed by the group of Prof. Dr. Rad (Dr. Sebastian Lange and Niklas de Andrade-Krätzig). Genes included in the analysis were: pseudogenes, processed pseudogenes/transcripts, immunoglobulin and T-cell receptor (TR/IG) genes, sense/antisense intronic processed transcripts, long interspersed non-coding RNA (lincRNA), small nucleolar RNA (snoRNA), small nuclear RNA (snRNA), ribosomal RNA (rRNA), micro RNA (miRNA). Transcript sequences were downloaded from Ensembl (release 92) (Kersey et al. 2017) and the identified mutations were artificially introduced into the DNA sequences. Mutations resulting in amino acid changes or causing a frame-shift were further considered. Sequences enclosing the mutation site were translated into the corresponding mutated peptide strings and used as input for MaxQuant (Tyanova, Temu, & Cox, 2016). Mutation calling was performed at false discovery rate (FDR) of 5% with variant caller Mutect2 for exome (Cibulskis et al., 2013), and Strelka2 for RNA (Kim et al., 2018). The exome PBMC data was used as control for mutation calling on RNA.

MS spectra were processed using the MaxQuant computational proteomics platform (version 1.5.9.1) by Dr. Matteo Pecoraro (Prof. Dr. Mann group, Max Planck Institute). A FDR of 0.01 was required at the peptide spectrum match level.

1.19.2.1 Mutated HLA peptides analysis and candidate selection

The output was further filtered to exclude peptides not containing mutations among peptides eliciting from non-coding regions, not annotated in the Ensembl database, and peptides deriving from RNA sequences containing SNPs. As last filtration step, HLA binding affinity for all peptide ligands identified with mass spectrometry was predicted with NetMHC 4.0 (http://www.cbs.dtu.dk/services/NetMHC/). Peptides with high binding affinity (< 500 nM) and peptides deriving from mutations detected on both RNA and exome level were tested for immunogenicity (**Table 27**). Additionally, HLA-binding affinity of MS-identified peptides was predicted with MHCflurry 1.2.3.

1.20 Molecular biology methods

1.20.1 Nucleic acid extraction from PBMCs and histology slides

For TCR-β and WES, gDNA was extracted from 2 µm formalin fixed paraffin embedded (FFPE) tissue slides (tumors, lymph node PBMC and M_{Lung}-derived TIL samples). The extraction was performed using Maxwell® RSC Blood DNA Kit (Promega), following the manufacturer's recommendations.

For RNA-Seq, extraction was performed on 2 µm FFPE tissue slides (tumor and lymph node samples) using Maxwell® RSC RNA FFPE Kit (Promega), following the manufacturer's recommendations.

For reverse transcription PCR and TCR repertoire PCR, RNA was extracted from PBMCs and T cell clones using TRIzol reagent. Amounts of reagents used varied according to cell numbers ($0.2\text{-}2\times10^5$ for T-cell clones and lines; $0.5\text{-}1\times10^6$ for PBMCs and cell lines) as indicated in **Table 28**. Cell pellets were resuspended in TRIzol and added with yeast t-RNA in case cell number was below 2×10^5. Bromo-3-choloro-propan was added and the mix vortexed and incubated for 10 min at RT. Samples were spun down for 15 min at 12000 rpm and the clear layer containing RNA was pipetted into a new tube containing isopropanol. The mixture was incubated over night at -20°C and then centrifuged for 20 min at 12000 rpm, 4°C. Supernatants were discarded and pellets washed with 75% v/v Ethanol. Pellets were air-dried and dissolved in DEPC-H_2O.

Obtained nucleic acid yields were measured with *NanoDrop ND-1000*.

Table 28. Reagent amounts for RNA extraction

Reagent	$0.2\text{-}2\times10^5$ cells	$0.5\text{-}1\times10^6$ cells
TRIzol	200 µl	1000 µl
Yeast t-RNA (< 2×10^5 cells)	10 µl	
Bromo-3-choloro-propan	40 µl	100 µl
Isopropanol	100 µl	500 µl
75% Ethanol	500 µl	1000 µl
DEPC-H2O	15 µl	50 µl

1.20.2 Reverse transcription PCR

Isolated RNA was reverse transcribed into complementary DNA (cDNA) for real-time PCR and TCR repertoire PCR applications. For this purpose, *AffinityScript Multiple Temperature cDNA Synthesis Kit* (Agilent Technologies) was used. The annealing step was performed by diluting 500 -1000 ng RNA in DEPC-H_2O to a total volume of 13.5 µl, with the addition of 1µl of oligo(dT) (C_{STOCK} = 500 µg/ml). The mix was heated to 65°C for 5 min and cooled down at RT for 10 min. For reverse transcription step, 2 µl of Affinity Script Buffer, 2 µl dNTP (C_{STOCK} = 10 mM each) and 1 µl Affinity Script Reverse Transcriptase were added to the mix and incubated for 1 h at 47.5°C followed by 15 min at 70°C for heat-inactivation of the enzyme.

1.20.3 TCR-β sequencing

Extracted gDNA (p. 1.20.1) was sent to Adaptive Biotechnologies which performed TCR-β sequencing with ImmunoSEQ™ platform at the deep level (exception made for B_{Lung} gDNA which underwent TCR-β sequencing survey level only due to limited material). Results were analyzed with the ImmunoSEQ analysis software provided by Adaptive Biotechnologies.

1.20.4 Whole exome sequencing (WES)

M_{Int}, M_{Lung} and PBMC genomic gDNA (p. 1.20.1) was used for library preparation and sequencing as previously described (Bassani-Sternberg et al., 2016) in cooperation with the group of Prof. Rad.

1.20.5 RNA sequencing (RNA-seq)

RNA-Seq was performed on Illumina HiSeq4000 (Helmholtz-Zentrum Munich) on RNA extracted from the two metastases (p. 1.20.1).

1.20.6 Identification of TCR alpha and beta chains with repertoire PCR

TCR repertoire PCR was performed to determine variable alpha and beta chain usage with degenerate primers (**Table 22**) using mix indicated in **Table 29** and settings in **Table 30**.

Table 29. Reaction mix for TCR alpha and beta repertoire

Reagent	Description	Volume
HotStar MasterMix		12.5 µl
P-5' aST / P-5' bST	Primer fwd constant region	1.5 µl
P-3'aST / P-3'bST	Primer rev constant region	1.5 µl
3'-a const / CbII	Primer rev variable fragment	2 µl
Va/b x	Primer fwd variable fragment	3 µl
cDNA		0.55 µl
Coral load		2.5 µl
DEPC H_2O		1.45 µl
V_{END}		25 µl

Table 30. Thermal profile of TCR repertoire PCR

Temperature	Time	Cycles
95°C	15 min	
94°C	1 min	
54°C	1 min	× 35
72°C	1 min	
72°C	10 min	

PCR products were run on agarose gel (1%); amplified bands from variable chains were excised and sent for sequencing with variable fragment primer used in the PCR mix. Obtained CDR3 nucleotide sequences were investigated using IMGT/V-Quest (http://www.imgt.org/IMGT_vquest/vquest) and the

complete sequences were in silico reconstructed by aligning the CDR3 region to the complete corresponding variable alpha chain and constant chains on Sequencher software. Variable and constant chains were downloaded from Ensembl database and aligned to corresponding variable chains.

1.20.7 Cloning of identified native TCR chains

Primers were designed (**Table 23**) to amplify the full length TCR loci and insert Not I and Sal I restriction sites at 5´ and 3´ respectively. TCR sequences were amplified (1.20.7) from cDNA obtained from T cell clones (1.20.1; 1.20.2), digested and cloned into pMP71 vector upstream reporter genes, respectively eGFP for beta and iRFP for alpha chain (vectors available in the lab). Digestion of vector and PCR product was performed as reported in p. 1.20.8.

1.20.8 Optimization of TCR sequences

TCR sequences were modified in silico by substitution of the constant chains with murine ones, insertion of an additional cysteine for the creation of a disulphide bridge and codon optimization (Kuball et al., 2007; Scholten et al., 2006) (BioCat). Beta and alpha chains separated by a self-cleaving P2A element were cloned into pMP71 backbone.

1.20.9 Cloning of minigenes and tandem minigenes

SYTL4 and NCAPG2 mutated and wt minigenes were cloned as previously described (Bassani-Sternberg et al., 2016). KIF2C minigenes, comprising 100 bp up- and downstream of mutation position, were in silico designed, synthetized (Genscript) and cloned into pMP71 backbone. Following primer sequences used for the cloning of KIF2C minigenes: KIF2C_fwd 5'-ATGCGGCCGCCAACATGGCCA-3´; KIF2C_rev 5'-ATGTCGACTTCTGGGTTTAT TGC-3'. Additionally, constructs containing mutant and wt sequences of minigenes coding for $KIF2C^{P13L}$/$KIF2C^{WT}$, $SYTL4^{S363F}$/$SYTL4^{WT}$ and $NCAPG2^{P333L}$/$NCAPG2^{WT}$ in tandem separated by P2A elements and flanked by NotI and SalI restriction enzymes, were in silico designed, synthetized (Genscript) and cloned into pMP71 backbone. A reporter gene dsRed ExpressII, was cloned downstream the minigene sequences to allow sorting of transgenic cells. All vectors were amplified using NEB® 5-alpha Competent E. coli (New England BioLabs) and purified with NucleoBond® Xtra Midi/Maxi (Macherey-Nagel).

1.20.10 Digestion with restriction enzymes and ligation of PCR products

Table 31. Digestion mix

Reagent	C_{STOCK}	Vector	Insert
Vector DNA/PCR product	1 µg/µl / variable	15 µl	20 µl
Buffer O	10 X	10 µl	10 µl

Restriction Enzyme 1	10 U/µl	2 µl	2 µl
Restriction Enzyme 2	10 U/µl	2 µl	2 µl
DEPC-H_2O		71 µl	66 µl
V_{END}		100 µl	100 µl

Ligation was calculated according to the formula:

$$V(insert) = n \times y\ (vector) \times \frac{vector\ (C)}{insert\ (C)} \times \frac{insert\ (bp)}{vector\ (bp)}$$

Where "n" represents the chosen molecular ratio (3:1 or 10:1) and "y" the µl of vector corresponding to 100 ng of DNA (in optimal cases 1µl). Ligation was performed at RT for 1h or 16°C for 16 h.

Table 32. Ligation mix

Reagent	Volume
Vector	variable
Insert	variable
T4 Buffer 10 X	1 µl
T4 Ligase	1 µl
DEPC-H_2O	variable
V_{END}	10 µl

Ligated vector constructs were amplified by transforming NEB5-alpha competent E. coli cells with ligation product. Transformation and plating on LB-agar plates supplemented with Ampicillin (100 µg/ml) was performed as indicated by the manufacturer. Grown colonies were picked and expanded in 3 ml LB medium (supplemented with 100 µg/ml ampicillin), for subsequent DNA vector purification.

1.20.11 PCR for amplification and cloning of constructs of interest

cDNA retrotranscribed from RNA extracted from cell lines or primary human cells was adopted as template for the amplification of specific minigenes. KOD Hot Start DNA Polymerase Kit was used for PCR experiments. Reaction mix was prepared as reported in **Table 33** and thermocycler was programmed as shown in **Table 34**.

Table 33. Reaction mix for standard PCR using KOD polymerase

Reagent	C_{STOCK}	C_{END}	Volume
10X KOD Buffer	10X	1	10 µl
$MgSO_4$	25 mM	1.5 mM	6 µl
dNTPs	2 mM	0.2 mM	10 µl
5' fwd Primer	10 µM	300 pM	3 µl
3' rev Primer	10 µM	300 pM	3 µl
cDNA			2 µl
KOD Polymerase	103 U/ml	2 U/100 µl	2 µl
H_2O			64 µl
V_{END}			100 µl

Table 34. Thermal profile PCR with KOD polymerase

Temperature	Time	Cycles
94 °C	**2 min**	
97 °C	**30 sec**	
57 °C	**30 sec**	**×35**
72 °C	**1 min**	
72 °C	**10 min**	
4° C	**pause**	

1.20.12 Purification of DNA plasmids

Amplified DNA vectors were purified from 2 ml bacterial culture using *NucleoSpin plasmid - plasmid Miniprep kit*, according to the manufacturer's instructions. Digestion of 1µg of purified vector with enzymes of choice was performed as described in p. 1.20.8 and analyzed by gel electrophoresis, as control of the molecular cloning. Vector constructs showing expected fragment lengths, were sent for Sanger sequencing to MWG Eurofins. Successfully cloned vectors were used for re-transformation of E. coli (100 ng) and plating on LB-agar plates added with ampicillin. Two to three bacterial colonies were picked and expanded in 3 ml LB medium (supplemented with 100 µg/ml Ampicillin) for 6-8 h at 37°C. The pre-growth was inoculated in 300 ml LB medium and incubated over night at 37°C.. Vectors were purified from 300 ml bacterial cultures using *NucleoBond® Xtra Maxi EF* according to the manufacturer's instructions. Extracted plasmid DNAyield was analyzed using *NanoDrop-1000* and stored at -20°C.

1.21 Immunological assays and sorting

1.21.1 IFN-γ ELISpot assay

ELISpot plates MAHAS4510 were coated with IFN-γ capture antibody 1-D1K (C_{END}=10µg/ml in PBS) and incubated over night at 4°C. The next day, coated plates were rinsed four times with PBS by incubating for 10 min at RT. A blocking step with TCM followed for 45 min at 37°C. Patient-derived PBMCs, were transferred on blocked ELISpot plates and incubated over night at 37°C. Before development of the ELISpot plate, cells were removed and expanded in culture as explained in p. 1.18.4, to be tested at a later time point.

For reactivity confirmation of expanded T-cell lines or assessment of TILs (p.1.18.4 and 1.18.9), 2×10^4 effector T cells were incubated with peptide-pulsed PBMCs or LCLs (E:T=1:1) on the blocked ELISpot plate and incubated for 72 h at 37°C. As positive control PMA (C_{END} = 1 µg/ml) and Ionomycin (2 µg/ml) were used and as negative DMSO (1 µl) or TCM. After incubation, 150 µl of supernatant was removed and stored at -20°C for further analyses. Cells were then discarded and ELIspot plates were washed six times with washing buffer. Secondary anti-IFN-γ antibody 7-B6-1-Biotin was added to each well (C_{END} 2 µg/ml in PBS + 0.5% BSA) and incubated for two h at RT. Plates were washed again (six

times) before incubation with HRP-complex solution for 90 min in the dark. For development, AEC substrate was pipetted immediately after two washes with washing buffer and two with PBS. The reaction was incubated in the dark for ca. 10-15 min, when the positive control was visible. The reaction was stopped with running tap water and plates were air-dried overnight protected from the light until analysis. Read-out was performed on an ImmunoSpot S6 Ultra-V Analyzer using Immunospot software 5.4.0.1.

1.21.2 IFN-γ ELISA assay

ELISA assay was performed on supernatants of effector/target cell cocultures with *BD OptEIA™ Human IFN-γ* or *IL-2 ELISA Set* following manufacturer's recommendations with slight modifications. ELISA plates were coated with IFN-*γ* capture antibody diluted in coating buffer (1:250) and incubated over night at 4°C or 1h at 37°C. Plates were washed three times with washing buffer and incubated 1h with blocking solution at room temperature. IFN-*γ* standard curve was prepared by reconstituting lyophilized standard from the kit in TCM to a concentration of 1000 pg/ml and by performing six serial 1:2 dilutions and one blank (TCM only). Plates were washed three times before application of supernatants and standard curve, followed by 1h incubation at RT. Plates were washed five times and incubated for 1h in the dark with detection antibody (1:250) and enzyme conjugate (1:250) dissolved in blocking solution. For substrate reaction, solution A and B from *BD OptEIA™ TMB Substrate Reagent Set* (BD Biosciences) were mixed in a ratio of 1:1 and pipetted after washing the plates for seven times with washing solution. Plates were incubated at RT in the dark for 10-20 min, until the standard curve was well visible. The reaction was stopped by adding sulfuric acid on top of the substrate. The readout was given by absorbance at 450 nm and a reference of 570 nm with *Sunrise™ absorbance reader* (Tecan).

1.21.3 Preparation of peptide pools for acDC assay

In case the number of peptides to screen was above 10-12, generation of pools was necessary, due to limited samples from patients. After prioritization of peptides, pools of 10 peptides were designed to contain five HLA-A predicted binders (sub-pool A) and five HLA-B predicted binders (sub-pool B), arranged as depicted in (**Table 35**). Peptides belonging to the same sub-pool (binders of the same HLA-allotype) have similar predicted HLA binding affinity, so that binding competition between peptides was minimized. Sub-pools A and B were combined differently in order to quickly narrow down reactivity to a group of five peptides and test each sub-pool twice (**Table 36**). Each peptide was dissolved in DMSO to a concentration of 2 mM and combined with the other eight or nine so that the final concentration of each peptide added to the culture would be 1 µM.

314 Table 35. Composition of sub-pools for HLA-A03:01 and B27:05 predicted ligands

HLA-A03:01			
Sub-pool	**Peptide sequence (aa)**	**Mutation (aa)**	**Predicted affinity (nM)**
A1	KIFNFYPRK	L > F	6.8
	KMKNFFFTK	S > F	7.4
	RMLRRRAQK	E > K	8.7
	TLYSPRGEK	E > K	9.2
	AMYQRAKLK	S > L	9.5
A2	SLLTPPSTK	P > S	9.6
	RLMFFRPIK	S > F	9.8
	SLYLKIHLK	L > K	11
	KIYAAGTFY	H > Y	11.2
	YLFFIQGYK	S > F	12.5
A3	TTYSPIGEK	G > E	14.5
	RLYKLILWR	P > L	14.7
	KTYPCKIFY	S > F	16.6
	SLQPRGSFK	P > S	18.2
	KVINLSPFK	E > K	18.6
A4	CLFFGIPWK	S > I	19.2
	KQFSAMALK	P > S	21.4
	RLFLGLAIK[a]	P > L	21.6
	KLKLPIIMK	M > I	23.3
	LLINRGFSK	D > N	25.2
A5	RLKCPFYGK	H > Y	26.1
	KVMTDPSRK	A > V	28.7
	RIAGKALKK	P > L	31.5
	KLYQCNECK	S > L	32.7

HLA-B27:05			
Sub-pool	**Peptide sequence (aa)**	**Mutation (aa)**	**Predicted affinity (nM)**
B1	RRFSSLYSF	G > R	11.5
	RRLLILGRI	G > R	11.5
	FRMFLTQGF	P > L	15
	ARWTAFFGV	S > F	17.1
	GRWALHSAF	S > F	17.5
B2	KRFLHRQPL	P > L	20.2
	ARFAVNLRL	G > R	20.7
	WRNSFLLRY	S > F	24
	YRIYDIPPK	V > I	24
B3	ARLFLGLAI	P > L	25.7
	YRHLFKVFR	G > R	26.6
	FRFFTRKSL	E > K	26.9
	RRHCRSYNR	D > N	27.6
	KRRLLILGR	G > R	28
B4	FRQSLYLKI	L > K	29.2
	RRTQRYFMK	E > K	29.3
	FRICPIFVF	R > C	32.3
	KRTNVGILK	E > K	33.3
	LRILRIKLR	M > I	35.6
B5	KRHEVPVPL	Y > H	36.8
	HRYFFFVAM	S > F	37.5
	FRFFATPAL	S > F	38.3
	LRFSIIEEF	T > I	45.9
	SRVILFSPL	N > S	46

315 Table 36. Combination of sub-pools within peptide pools

Pool	Sub-pool
Pool 1	A1+B1
Pool 2	A2+B2
Pool 3	A3+B3
Pool 4	A4+B4
Pool 5	A5+B5
Pool 6	A1+B2
Pool 7	A2+B3
Pool 8	A3+B4
Pool 9	A4+B5
Pool 10	A5+B1
Pool 11	A1+B1+SYTL4^{S363F}

1.21.4 Sorting of CD137$^+$ activated T cells

Stimulated T cells (p. 1.18.5) were resuspended in isolation buffer and labelled with anti-CD137-APC antibody for 10 min at 4°C. After rinsing and resuspension in isolation buffer, anti-APC-microbeads were added and the cells were incubated for 15 min at 4°C. Labeled cells were washed once and then run through a LS column, which was washed twiced. The flow through, consisting of unlabeled cells, was collected.. Labeled CD137$^+$ cells were eluted, spun down, resuspended in TCM and expanded as lines or clones (p. 1.18.5). CD137 expression levels of T cells stimulated with antigen of interest (before labeling with beads) were compared to the negative control and unlabeled fraction, with flow cytometry.

1.22 Retroviral gene transfer for T cell engineering and generation of target cells

1.22.1 Production of retroviral vectors

For production of viral vectors, RD114 cells were seeded 3-4 days before first transduction in a tissue culture treated plate in cDMEM (3-4.5×10^5/well). Transfection of packaging cells was performed when they were well attached and reached a confluency of 60-70%. The transfection solution for each construct was prepared by adding 3 µl TransIT to 200 µl DMEM, vortexing and incubating 20 min at RT. Retroviral vector, containing the transgene of interest was added to the mixture (1 µg), gently mixed and incubated for 30 min at RT. The mix was added drop by drop on the packaging cell line and incubated for 48-72 h at 37°C.

1.22.2 Generation of effector and target cells

Non-tissue treated plates were coated with RetroNectin (RN) diluted in PBS to a final concentration of 12.5 µg/ml at 4°C overnight. Plates were then blocked with PBS + 2% BSA for 30 min at 37°C, washed twice with PBS + 2.5 % v/v HEPES and stored at 4°C until use.

Activated CD8$^+$ T cells were harvested (p. 1.18.7) and resuspended in TCM to a density of ca. 1×10^6 cells/ml. Suspension cell lines (**Table 8** and **Table 10**) were harvested from culture, washed and resuspended to a density of 3-5×10^5 cells/ml in cRPMI.

T cells and suspension cell lines were seeded on blocked-RN-coated plates, while in the case of adherent cell lines, they were seeded the day before transduction on tissue-culture treated plates at a density of 1-3×10^5 cells/well.

All media containing cells on the day of transduction were supplemented with 10 mM HEPES (C_{END} = 5 mM) and 8 µg/ml Protamine sulfate (C_{END} = 4 µg/ml). For T cells 200 U/ml IL-2 (C_{END} =100 U/ml) were also added. Final concentrations refer to a V_{END} = 2 ml/well, given by 1 ml cell suspension plus 1 ml retroviral supernatant for each well.

Supernatants containing viral vectors were harvested from RD114 culture (p. 1.22.1), filtered with a 0.45 µm filter and added to each well containing the cells to be transduced.

Plates were centrifuged at 820 g for 90 min at 32°C without brakes followed by 24 h incubation at 37°C. For the second round of transduction, suspension cell lines were harvested, washed and seeded in a new RN-coated and blocked plate. Each condition was split in two. T cells were collected, washed and resuspended in TCMum supplemented with IL-2, Protaminsulfate and HEPES. Adherent cells were kept in the same culture plate for second transduction. The rest of RD114 viral supernatants was harvested and filtered and transduction was performed as described above. After 24 h, cells were washed and resuspended in appropriate culture media. T cells were expanded in TCM supplemented with 5 ng/ml IL-7 and 5 ng/ml IL-15.

Neoantigen-coding and wt counterpart minigenes were transduced in LCL-1, U-698-M, A2058 and MDST8 cell lines. LCL-1 cell line was transduced with single minigenes, while other cell lines with tandem constructs (**Table 7**). TCR single native chains and optimized constructs were transduced in $CD8^+$ healthy donor derived T cells and expanded for 7 to 10 days with IL-7 and IL-15 (5ng/mL; Peprotech) before functional characterization.

Transduced cell lines were cloned by limiting dilutions and grown for about 2-3 weeks, after which expression and clonality of the population was verified with flow cytometry thanks to a reporter gene expression (dsRed).

Expression and co-expression of single native TCR chains was also assessed through detection of reporter genes (TCR-β GFP; TCR-α iRFP).

1.23 Flow cytometry methods

For staining of surface markers cells were washed with FACS buffer and blocked with 100% ΔHS for 10 min at 4°C. After washing and resuspension of the cells in 50µl FACS buffer, 1.5 µl of each surface marker antibody and 1 µl 7-AAD (cEND = 0.5 mg/ml) for dead cells discrimination were added. The staining was incubated for 20-30 min on ice in the dark. Cells were washed with 1 ml FACS buffer, fixed with 1% PFA and stored at 4°C in the dark until measurement.

All flow cytometry measurements were performed with LSRII flow cytometer (BD Biosciences) and analyzed with FlowJo Software (version 7.6.5 and 10.6.2).

1.23.1 Assessment of $CD8^+$ T cell subset isolation

To prove the efficacy of $CD8^+$ T cell isolation, thawed or fresh healthy-donor derived PBMCs were counted and a small aliquot of cells was stored on ice before negative selection. $CD8^+$ T cells negatively selected fraction was also counted and activated in culture (p. 1.18.7) and an aliquot saved for flow cytometry. PBMCs and $CD8^+$ T cells were stained in parallel with antibody mixes shown in **Table 37** containing markers for CD4 and CD8 lineages and for main T-cell subcompartments.

Table 37. Antibody mixes for CD8+ T cell isolation assessment

Mix	Antibodies
1	anti-CD8-FITC, -CD62L-V450, -CD3-AF700, -CCR7-PE, -CD4-APC, 7AAD
2	Anti-CD8-FITC, -CD45RA-APC, -CD45RO-PE

1.23.2 Assessment of reporter gene expression

For reporter gene expression assessment in T cells and target cell lines, cells were collected from culture, washed in PBS, stained with 7-AAD and resuspended in PFA 1%. Cells were directly measured at the flow cytometer.

1.23.3 Staining of transduced TCRs on T cells

Transduction efficiency was determined by staining of TCR surface expression with an antibody specific to murine constant beta chain (TCRmu-FITC Hamster anti-mouse TCRβ, BD Biosciences) and CD8 surface marker. Gates for TCR positivity were set on 7-AAD negative, CD8 positive T cells, according to isotype control (FITC Hamster IgG2, λ1 isotype control).

1.23.4 Multimer staining of transduced TCRs on T cells

For multimer staining Strep-tagged mutated and wild-type peptide-MHC complexes (mut pMHC; wt pMHC) (e.g. $KIF2C^{P13L}$ and $KIF2C^{WT}$), kindly customized and provided by Prof. Busch, were multimerized on a fluorophore labeled Strep-Tactin backbone (Strep-Tactin APC; Iba GmbH) for 30 min on ice in the dark in a 1 µg : 1 µl ratio in FACS Buffer. After multimerization, 0.5×10^6 T cells were resuspended in 25µl of multimer and incubated for 45 min on ice in the dark. After 25 min additional surface staining antibodies were added to the cells.

In the case of HLA-B27 multimers, two different tetramers were available, one bearing mutation C56S and one wt, besides commercially available pentamers purchased from ProImmune (mutation C67S). Staining with pentamers was performed with following current recommendations and protocols from CIMT Immunoguiding Program (http://www.cimt.eu/workgroups/cip).

Transduced T cells were stained with tetramers, anti-CD8 (BD Biosciences) and 7-AAD (Sigma-Aldrich) and fixed in PFA 1%.

1.23.5 Intracellular TCR staining

Intracellular staining was used to characterize the expression quality of different TCR. Therefore, the T cells were blocked with human serum added with ethidium monoazide bromide (EMA) at a final concentration of 1:500 for 10 min on ice in the dark. Following this, the samples were exposed to light, on ice for additional 10’ min to bind the EMA dye. After EMA-staining, the cells were washed in FACS-

buffer followed by surface antibody staining for markers CD3, CD8 and TCRmu with saturating concentrations of the antibodies (double volume as standard staining).

Cells were washed again and then fixed with IC fixation buffer (eBioscience) for 20’ min on ice in the dark. Following fixation, the cells were washed twice with 1x permeabilization (eBioscience) buffer. Subsequently, the cells were stained for intracellular TCRmu according to the manufacturer’s recommendations for 20’ min on ice protected from light. Finally, the cells were washed with 1x permeabilization buffer and once more with FACS-buffer containing 0.1% sodium azide before the cells were suspended in the same buffer for analysis at the flow cytometer.

Surface TCR was marked with FITC, while intracellular TCR with APC fluorophore.

1.23.6 Quantification of TCR mediated multi-cytokine secretion

Supernatants of T cell and minigene transduced target clone co-cultures were additionally used for assessment of a diverse cytokine panel with MACSPlex 12 Cytokines Kit (Miltenyi Biotech). Cytokines present in the culture were stained with the beads and antibodies provided in the kit following the manufacturer's recommendations. The standard curve was generated by preparing six dilutions of the standards in the kit in TCM allowing quantification of single cytokines in the supernatant samples. For plot and gate setting, Setup Beads provided with the kit were run, plots and gates were created as indicated in the user manual for acquisition. For standard curve and samples, the mean fluorescence intensity (MFI) in APC channel was calculated as geometric mean in FlowJo software. Cytokine concentration was inferred from the standard curve.

MACSPlex Cytokine Capture Beads are added to unknown samples and to serial dilutions of the MACSPlex Cytokine Standard. During a 2 h incubation period, the cytokines are captured by the MACSPlex Capture Beads. Subsequently, MACSPlex Cytokine Detection Reagent containing a mixture of APC-conjugated anti-cytokine antibodies, is added in order to form sandwich complexes during a 1-h incubation period. Standard curves for each of the cytokines are generated. The median of the APC fluorescence of each capture bead population gives the concentration of each cytokine in the unknown samples.

1.23.7 Flow cytometry of mouse organs and tumors to assess TCR-T biodistribution

Cells isolated from tumors, bone marrow, spleen and blood were stained for surface markers with a mix containing anti-TCRmu-FITC, anti-CD8-APC and 7-AAD and fixed with PFA 1%.

1.24 Synthetic peptides

Synthetic peptides for mutated HLA peptides spectra validation were ordered from Genscript and DGpeptidesCo., Ltd.

1.25 In vivo study

All experimental procedures using animals were carried out in accordance with local guidelines and regulations. NOD.Cg-Prkdc^{scid} Il2rg^{tm1Wjl}/SzJ (NSG) mice were subcutaneously injected with U-698-M cell clones (10x10^6 cells/flank) transduced with tandem minigenes coding for neoantigens (pMP71 #316) and wt counterpart (pMP71 #317). In each mouse mut-mg transduced cells were injected in the right flank, while wt-mg transduced cells in the left flank. Procedure for transduction of human CD8$^+$ T cells was started one day prior tumor injection as explained in p. 1.22.2.

Starting from nine days after tumor implantation, tumor volumes were measured in vivo by external digital caliper (marca). The volume size was determined by measuring the greatest longitudinal diameter (length) and the greatest transverse diameter (width) and multiplying to obtain the tumor surface in mm^2.

At day 11 post tumor cell injection, TCR-transduced T cells were injected intravenously. Transduced T cells were diluted with non-transduced T cells in order to obtain a homogeneous number of effector cells (ca. 10% of all T cells) for the different TCRs. Ca. 2x10^6 effector cells on a total of 20x10^6 T cells were injected, exception made for those TCRs where transduction rates were lower as 10% (KIF2C-PBC1, NCAPG2-PBC1 and SYTL4-TIL2). Number of mice injected for each TCR are indicated in **Table 38**.

Table 38. Experiment set-up to assess in vivo anti-tumor potential of TCRs

TCRs	Number mice	Number of cells (x10^6)
KIF2C-PBC1	5	20
KIF2C-PBC2	5	20
NCAPG2-PBC1	4	16.9
SYTL4-TIL1	5	20
SYTL4-TIL2	3	20
SYTL4-PBC1	5	20
SYTL4-PBC2	4	17.3
Non-transduced	5	20

Tumor growth and/or shrinkage was monitored for 10 days with digital caliper. On day 11 tumors (when present), spleen, blood (from the heart) and bone marrow were excised. Organs and femur bones were kept in dPBS buffer on ice. Blood was added with EDTA (20 µl). Single-cell suspensions from tumors and spleens were prepared by passing cells through 70 µm cell strainers. Femurs or tibias were excised, and one end of the bones was open and bone marrow was centrifuged out (10,000 rpm, 30 seconds, 4°C). Erythrocyte lysis was performed by applying 500 µl Ammonium-Chloride-Potassium (ACK) lysing buffer to each cell pellet and incubating at room temperature for 1 minute. Around 10 ml cold PBS/ΔFCS was then added to terminate the reaction. Cells were spun down and re-suspended in PBS/ΔFCS.

1.26 Statistics

Significance of differences within TCR EC_{50} values were investigated by Pearson correlation calculated with one-way ANOVA for multiple comparisons (Tukey's test). With regard to in-vivo rejection potential of the TCRs, differences in tumor growth were calculated with two-way ANOVA test (time; treatment) and Dunnett's test for multiple comparisons. Flow cytometry results from in-vivo experiment were evaluated with Kruskal-Wallis test and uncorrected Dunn's test for multiple comparisons. To calculate the statistical significance of the increase in SASA, a standard independent two-sample t-test was used. Statistical analyses were performed with GraphPad Prism 7.04 software.

Results

1.27 Clinical course of Mel15

Clinical course of melanoma patient Mel15 is explained in the Methods (p. 1.18.1) and illustrated in **Figure 2**.

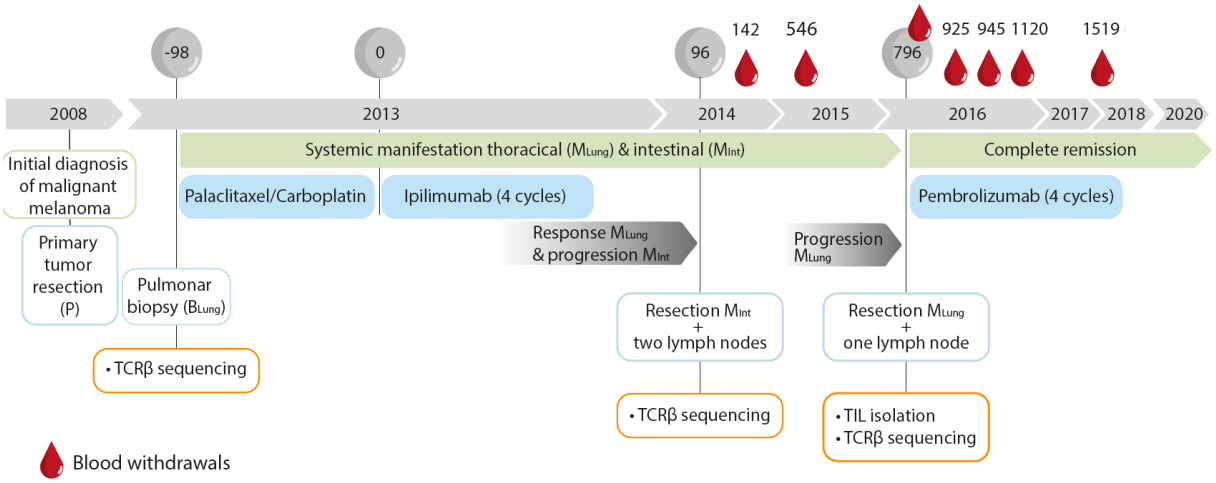

Figure 2. Clinical course of disease of patient Mel15. Patient Mel15 was diagnosed with malignant melanoma in 2008 and underwent surgery for resection of the primary tumor in the same year. In 2013, metastases were detected, respectively in the lung and in the intestine. A lung biopsy (BLung) was performed for histological analysis. The patient was treated with carboplatin and paclitaxel, that mediated a mixed response of the metastatic disease. The patient was subsequently treated with the anti-CTLA-4-antibody Ipilimumab. After the treatment, the intestinal metastasis (MInt) progressed, which was eventually removed in 2014 together with two non-malignant lymph nodes (LNs). In 2016, the lung metastasis (MLung) progressed and was removed in conjunction with one adjacent non-malignant LN. After surgery Pembrolizumab was administered to the patient for 18 months. Mel15 is currently in complete remission without any anticancer treatment. Analyses performed on tissue samples and time points of blood withdrawals are depicted. Figure adapted from Bräunlein et al., 2021.

1.28 In-silico predictions complement MS-based neoantigen identification

In order to investigate if critical neoantigens may have been missed by MS, a sequence-based prediction approach was applied. Putative mutated peptide ligands and their HLA binding affinity were analyzed using NetMHC 4.0 (Andreatta & Nielsen, 2016) on the previously generated mutation calling dataset (Bassani-Sternberg et al., 2016). 1,196 missense mutations were called from M_{Int}-tumor tissue, leading to prediction of ~4670 peptides (8-12 amino acid long) with binding affinity < 500nM. By sorting nine-amino-acid-long putative peptides according to HLA-binding affinity predicted by NetMHC 4.0, previously identified neoantigens $SYTL4^{S363F}$ and $NCAPG2^{P333L}$ ranked 6^{th} and 24^{th} in the HLA-B27:05 and HLA-A03:01 lists respectively (Appendix 1.42).

Immunogenicity of selected nonamers binding to HLA-A03:01 and B27:05 allotypes was investigated by detecting recall autologous T-cell responses of patient Mel15. PBMCs from time points 925 and 945 (**Figure 2**) were stimulated with peptide pools arranged as shown in **Table 26**.

Reactivity against pool 4 and pool 9 was observed for both time points (only 925 is shown; **Figure 3A**) and narrowed down to one single antigen by repeating the stimulation according to the protocol for recall responses (p. 1.18.4). T cells reactive to pool 4 and 9 were expanded for 2 weeks and challenged with the peptides shared by the two pools (subpool A4; **Table 26**). Autologous T cells showed reactivity against peptide RLFLGLAIK (KIF2C^{P13L}; **Figure 3B**), ranking in position 18th of nonamer HLA-A03:01 binding peptides according to NetMHC 4.0 (Appendix 1.42). Previously MS-identified peptide SYTL4^{S363F} was included in pool 11 as internal positive control, however did not elicit any reactivity in these experiments (Pool 11).

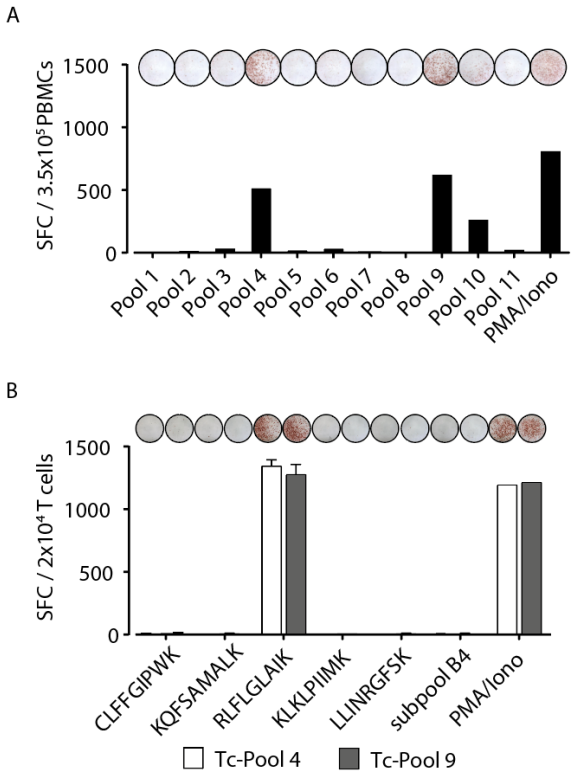

Figure 3. IFN-γELISpot for immunogenicity assessment of in-silico predicted peptides. A) recall responses detected from PBMCs derived from Mel15 blood withdrawal 925, two days after in-vitro stimulation with peptide pools. B) Response of expanded T cells to co-culture T2 cells pulsed with single peptides shared by Pool4 and 9 (A).

Stimulations of PBMCs with single peptides SYTL4^{S363F}, KIF2C^{P13L} and NCAPG2^{P333L} allowed detection of reactivities throughout disease course, indicating a variable detectability of neoantigen-specific functional T-cell responses (**Figure 4**).

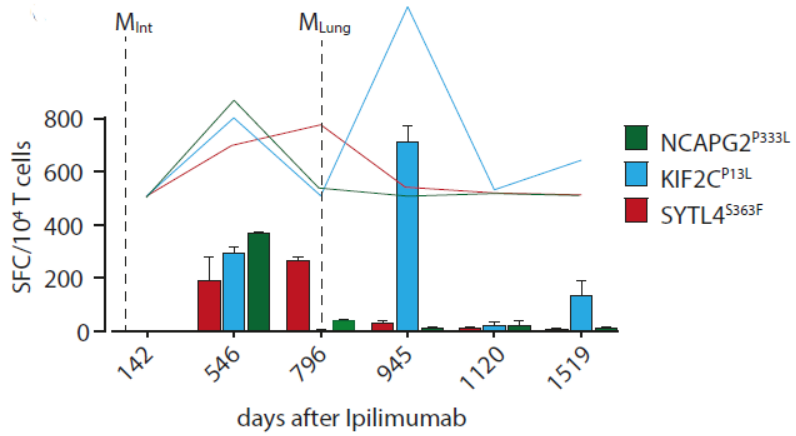

Figure 4. PBMC-derived neoantigen reactivity over time. IFN-γ ELIspot spot counts resulting from late stimulation of PBMC-expanded T cells through co-culture with peptide-pulsed target cells (E:T=1:1; peptide conc. 1µM).

1.29 KIF2C^{P13L} stimulated T cells show an activation phenotype

T-cell lines reactive to peptide Pool 4 and Pool 9 from time points 925 and 945 showed a high percentage of CD137^{+} cells after overnight stimulation with neoantigen KIF2C^{P13L}, while no positive population is detected in case of stimulation with an irrelevant peptide. These results confirm that 50-70% of expanded CD8^{+} T cells are specific to peptide KIF2C^{P13L} and show an activated phenotype (**Figure 5**).

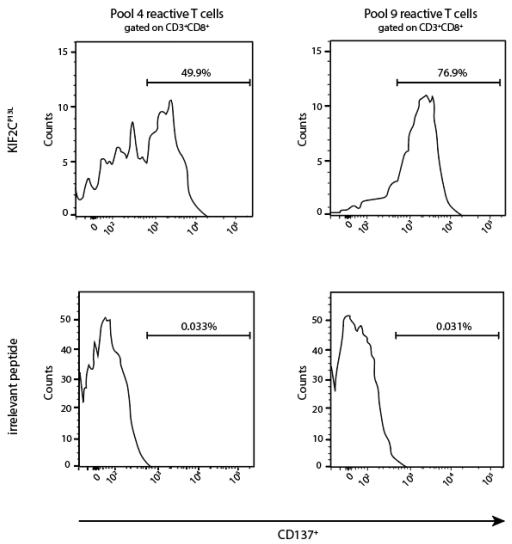

Figure 5. Enrichment of KIF2C reactive T cells. Flow cytometry plot of pool reactive expanded T cells re-stimulated over night with KIF2C^{P13L} pulsed target cells and stained with anti-CD137 antibody. As negative control T cells were stimulated with an irrelevant peptide.

1.30 Screening of T-cell clones for reactivity to KIF2C^{P13L} neoantigen

Proliferating T-cell clones resulting from limiting dilutions of activated T cells, maintained responsiveness to neoantigen KIF2C^{P13L} between week 2 and 3 after start of specific stimulation (**Figure 6**).

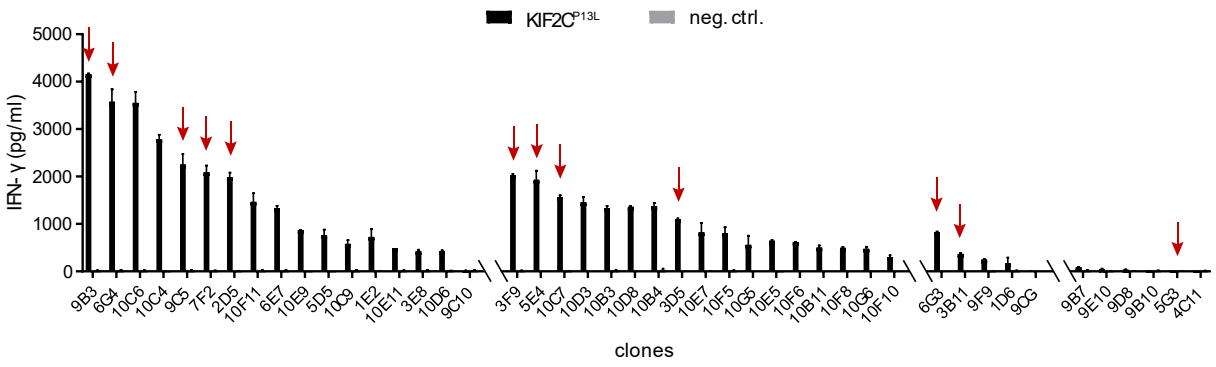

Figure 6. T-cell clone reactivity against KIF2C^{P13L}. T-cell clones were co-cultured in duplicate with peptide-pulsed T2 target cells. Pro well 1/4 of the T-cell pellet and 10^4 pulsed target cells were seeded. As negative control peptides NACPG2^{WT} or KIF2C^{WT} were used. Separate IFN-γ ELISA assays are represented by gaps in the x-axis.

After detection of specific reactivity of expanded T-cell clones, variable regions of TCR alpha and beta chains were identified using a TCR repertoire-specific PCR (**Table 22**) followed by agarose gel electrophoresis. Out of 20 investigated T-cell clones, 15 clones revealed bands Vα2 and Vβ12 (**Figure 7**) and 5 clone bands Vα6 Vβ6.1, 6.2 and 6.3. variable chain (not shown).

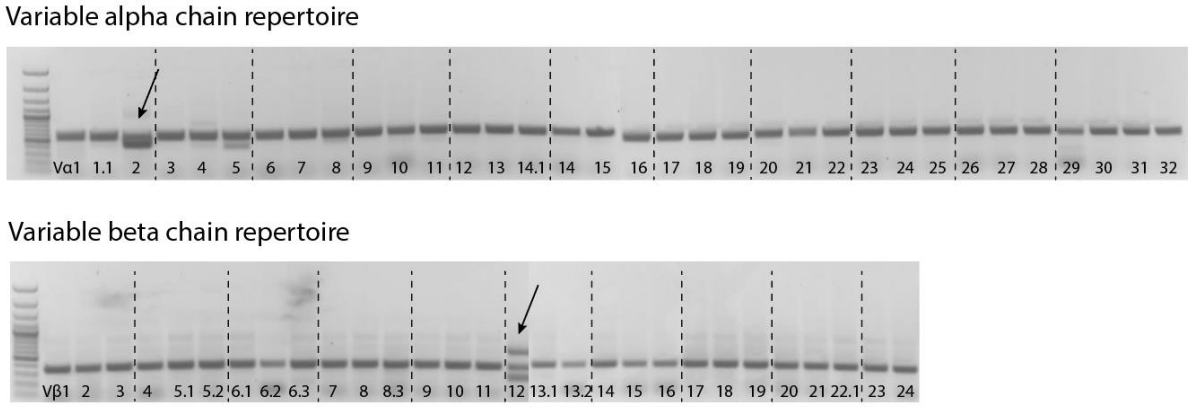

Figure 7. TCR variable chain repertoire PCR on cDNA from T cell clone 3D5. Agarose gel 1%, Marker 1kb Peqlab.

Bands were excised and sent for sequencing, subsequently complete sequence of the TCR was in silico reconstructed on Ensembl database to allow design of primers and expansion of the full TCR sequence from cDNA obtained from clone RNA. Alpha and beta chain sequences were retrieved for 12 clones (**Table 39**).

An overview of analyzed clones and detailed information about TCR CDR3 regions is provided in **Table 39**.

Table 39. Sequence details of alpha and beta chains isolated from KIF2C^{P13L} reactive T-cell clones.

Clone	CDR alpha	CDR beta	Identified variable chains	Constant beta chain	Stimulus	Time point	TCR name
5E4	CAMREQNNNARLMF	CASSLTRMGDRGEFF	TRAV14/DV4, TRBV7-6	TRBC2	Pool 4	945	KIF2C-PBC1
10C7	CAMREQNNNARLMF	CASSLTRMGDRGEFF	TRAV14/DV4, TRBV7-6	TRBC2	Pool 4	945	KIF2C-PBC1
2D5	CAVKERASGGSYIPTF	CAISDTSGGLWTDTQYF	TRAV12-2, TRBV10-3	TRBC2	Pool 9	925	KIF2C-PBC2
3D5	CAVKERASGGSYIPTF	CAISDTSGGLWTDTQYF	TRAV12-2, TRBV10-3	TRBC2	Pool 9	925	KIF2C-PBC2
3F9	CAMREQNNNARLMF	CASSLTRMGDRGEFF	TRAV14/DV4, TRBV7-6	TRBC2	Pool 9	925	KIF2C-PBC1
3B11	CAMREQNNNARLMF	CASSLTRMGDRGEFF	TRAV14/DV4, TRBV7-6	TRBC2	Pool 9	925	KIF2C-PBC1
5G3	CAMREQNNNARLMF	CASSLTRMGDRGEFF	TRAV14/DV4, TRBV7-6	TRBC2	Pool 9	925	KIF2C-PBC1
6G3	CAVKERASGGSYIPTF	CAISDTSGGLWTDTQYF	TRAV12-2, TRBV10-3	TRBC2	Pool 9	925	KIF2C-PBC2
6G4	CAVKERASGGSYIPTF	CAISDTSGGLWTDTQYF	TRAV12-2, TRBV10-3	TRBC2	Pool 9	925	KIF2C-PBC2
7F2	CAVKERASGGSYIPTF	CAISDTSGGLWTDTQYF	TRAV12-2, TRBV10-3	TRBC2	Pool 9	925	KIF2C-PBC2
9C5	CAVKERASGGSYIPTF	CAISDTSGGLWTDTQYF	TRAV12-2, TRBV10-3	TRBC2	Pool 9	925	KIF2C-PBC2
9B3	CAVKERASGGSYIPTF	CAISDTSGGLWTDTQYF	TRAV12-2, TRBV10-3	TRBC2	Pool 9	925	KIF2C-PBC2

1.31 TCR-β repertoire analyses in tumor samples and peripheral blood

To investigate spatial and temporal distribution of tumor antigen-specific TCRs, TCR-β sequencing was performed on genomic DNA extracted from primary biopsy tissue (B_{Lung}), tumor metastases (M_{Int} and M_{Lung}), lymph nodes (M_{Int}-LN1, -LN2 and M_{Lung}-LN) and PBMCs from different time points by Adaptive Biotechnologies company (**Figure 2**). From the sequencing data, it was possible to infer the frequency of the neoantigen specific TCRs in the different samples. KIF2C-TCRs expanded in M_{Lung} compared to M_{Int}, whereas SYTL4-TCRs shrank or remained unchanged (**Figure 8A**; **Table 40**).

In peripheral blood, all specific TCRs could be detected in at least four out of the six sequenced samples (**Figure 8B**). Productive frequencies of SYTL4-TCRs ranged between 0.0008% to maximal 0.013%, whereas KIF2C-PBC1, KIF2C-PBC2 and NCAPG2-PBC1 showed higher frequencies between 0.013% and 0.54% in analyzed blood samples (**Table 40**). TCR KIF2C-PBC1 showed high frequencies over time and was the 4th most abundant TCR from the whole repertoire at time point 945. Frequency of KIF2C-PBC2 increased up to the time point of lung metastasis resection and decreased afterwards. NCAPG2-PBC1 was present in the bloodstream, however it could not be detected either in M_{Lung} nor in expanded TILs derived from the same tissue (**Figure 8C**).

The relative frequency of the beta chains, attributable to the seven known neoantigen-specific TCRs, out of all identified CDR3 sequences, ranged from 0.11% to 1.53% in tumors and associated non-malignant lymph nodes (**Figure 8C**). Thereby, KIF2C-TCRs were the most abundant amongst known neoantigen specific TCRs, in the metastases and in the lymph nodes.

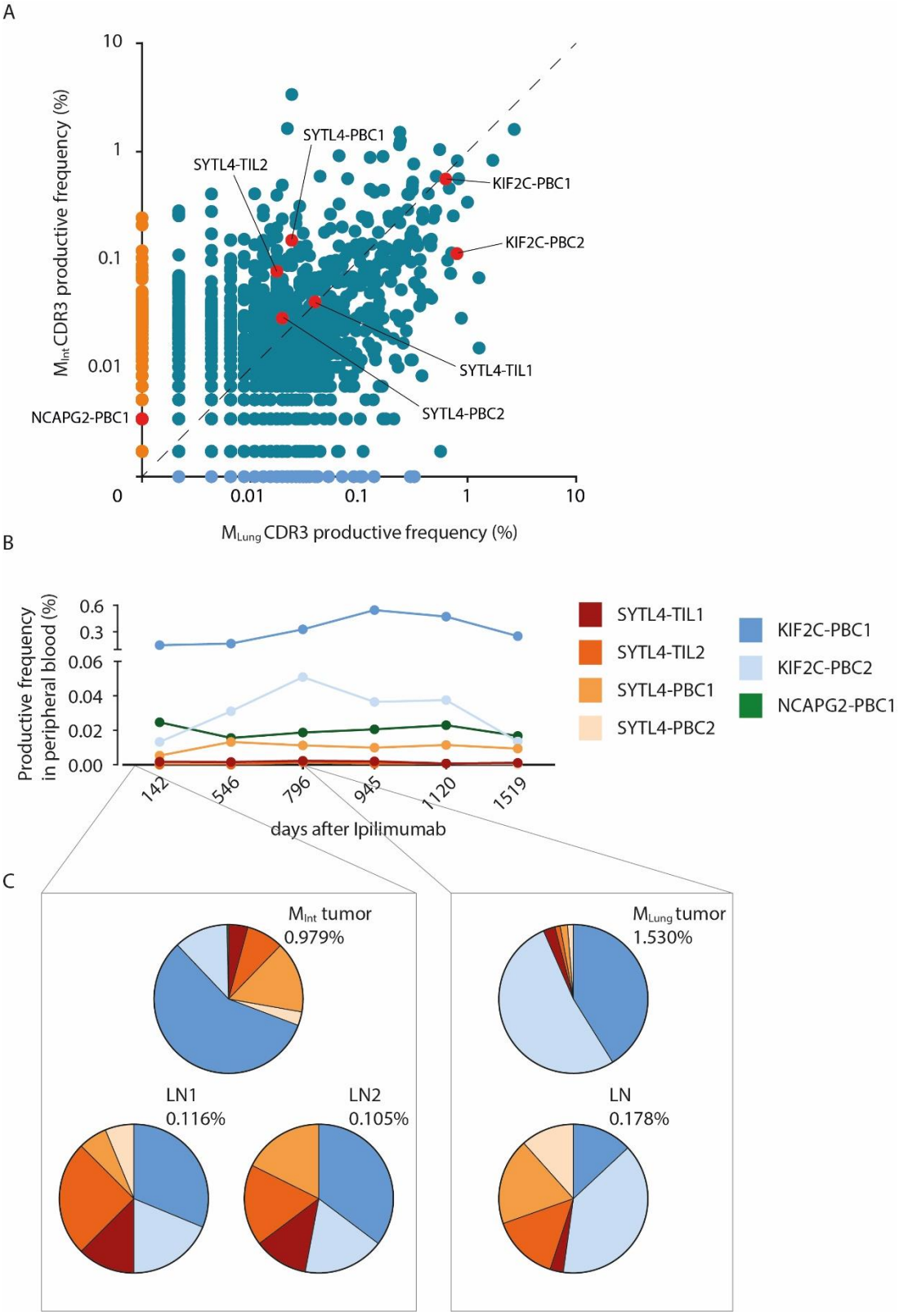

572

573 Figure 8. Temporal-spatial monitoring of neoantigen-specific TCR β-chain frequencies using deep sequencing of
574 TCRb chains. A) Productive frequency of TCR clonotypes (CDR3 amino acid rearrangements) in M_{Int} and M_{Lung}.
575 Scatter plot dataset was generated with Adaptive Biotechnologies ImmunoSEQ analysis software. B) Productive
576 frequency expressed as percentage of neoantigen-specific clonotypes in the peripheral blood at different time
577 points after start of treatment with Ipilimumab. C) Distribution of neoantigen-specific TCRs in resected tumor and

adjacent lymph node tissues. Figure adapted from Bräunlein et al., 2021.

Table 40. Productive frequencies (%) of neoantigen-specific TCR β-chains in tumor and blood samples.

%	M_{Int}			M_{Lung}			Blood samples					
TCRs	**Tumor**	**LN1**	**LN2**	**Tumor**	**LN**	**TILs**	142	546	796	945	1120	1519
SYTL4-TIL1	0.041	0.036	0.012	0.039	0.005	0.126	0.0018	0.0016	0.0022	0.0020	0.0008	0.0010
SYTL4-TIL2	0.079	0.022	0.019	0.017	0.026	0.040	-	-	0.0015	0.0007	0.0008	0.0010
SYTL4-PBC1	0.152	-	0.019	0.024	0.034	0.030	0.0053	0.0132	0.0112	0.0099	0.0115	0.0094
SYTL4-PBC2	0.029	0.014	-	0.020	0.021	0.126	-	0.0008	0.0015	0.0007	0.0008	-
KIF2C-PBC1	0.560	0.029	0.037	0.629	0.023	1.756	0.1489	0.1672	0.3273	0.5449	0.4715	0.2505
KIF2C-PBC2	0.115	0.007	0.019	0.800	0.070	7.890	0.0132	0.0311	0.0509	0.0365	0.0376	0.0136
NCAPG2-PBC1	0.003	0.007	-	-	-	-	0.0247	0.0156	0.0187	0.0205	0.0230	0.0167

Overlap of TCR-β clonotypes was investigated in all three metastatic tissues, the lung biopsy (B_{Lung}, day 96), intestinal metastasis (day 98) lung metastasis (day 796) and primary tumor (P) (**Figure 9**). The two metastases share 3,072 sequences with the same TCR-derived complementarity-determining regions (CDR3) (14.76%). Despite the very few rearrangements sequenced from B_{Lung} prior to immune checkpoint modulation, KIF2C-PBC1 could be detected within this tissue. Moreover, B_{Lung} shares 33 and 30 of 48 identified CDR3 clonotypes with M_{Int} and M_{Lung} respectively. In the primary tumor (P) from 2004, 29 clonotypes were sequenced, however none of the β-chains from known neoantigen-specific TCRs were detected (**Figure 9**). Of note, only scarce material was available from the biopsy and primary tumor samples.

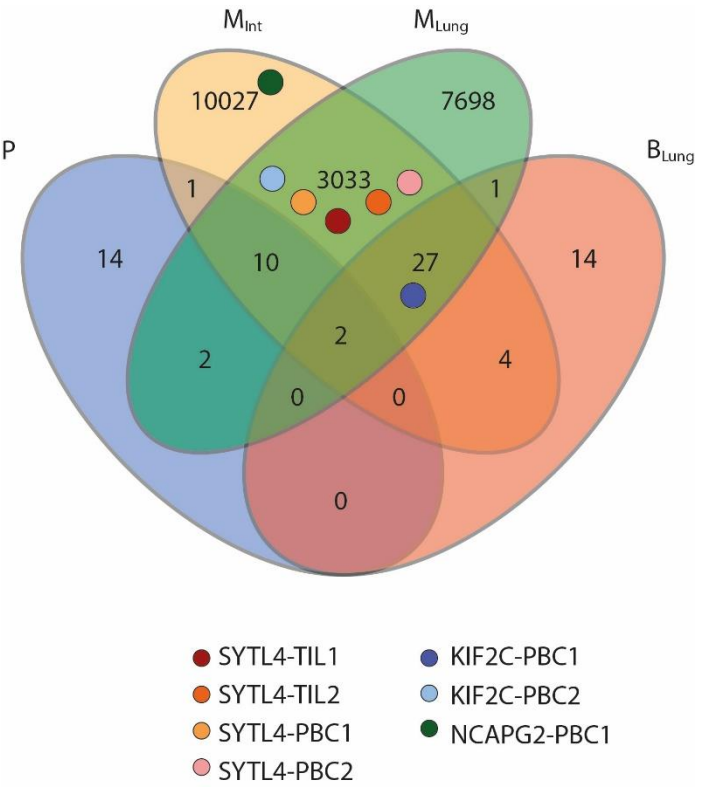

Figure 9. Venn diagram from variable TCR-β chain overlap in metastases, biopsy and primary tumor. Patient samples and number of β-chain clonotypes sequenced in each sample are depicted. Overlaps within samples are represented by intersection of the ovals. Clonotypes from identified neoantigen-specific TCRs are indicated as

small circles inside the ovals.

1.32 Transduction and functionality assessment of native-chain transduced CD8$^+$ T cells

Vectors containing TCR single alpha and beta native chain genes were co-transduced in primary isolated CD8$^+$ T cells to observe co-expression levels. CD8$^+$ T cells were isolated from healthy donors' derived PBMC and analyzed by flow cytometry for the expression of main lineage markers.

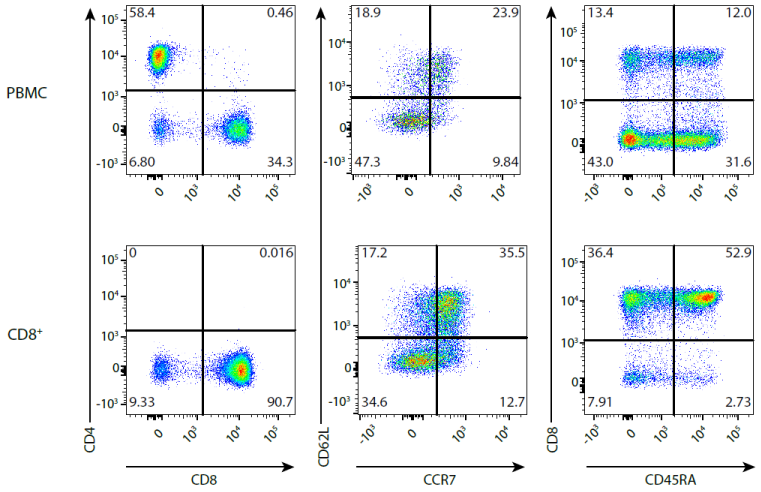

Figure 10. Isolation of CD8$^+$ T cells from healthy-donors' derived PBMC. Flow cytometry staining of PBMC and isolated CD8$^+$ showing main T-cell lineage markers: CD62L$^+$/CCR7$^+$ naïve; CD62L$^-$/CCR7$^-$ effector; CD45RA$^+$ effector/naïve; CD45RA$^-$ memory.

Isolated CD8-T cells were co-transduced with two vectors for the expression of native alpha and beta TCR chains (native chains; nc) respectively. 30-40% of T cells displayed expression of the beta chain only, however in ca. 10% of the cells both alpha and beta chains were expressed for both TCRs KIF2C-PBC1nc and KIF2C-PBC2nc.

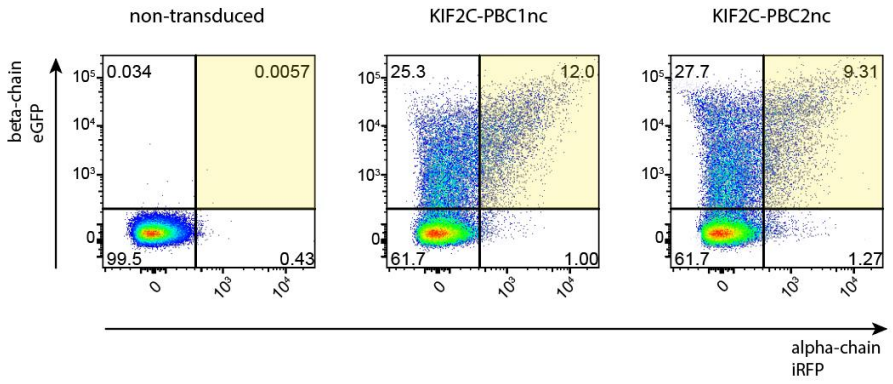

Figure 11. Expression of TCR alpha and beta native chains in CD8$^+$ T cells. The expression of single native TCR chains is directly detected through the expression of reporter genes coding for fluorophores eGFP and iRFP. T cells transgenic for both chains are in the yellow gate. The suffix "nc" next to the TCR name is to indicate the

transduction with native chains.

Co-culture of transgenic $CD8^+$ T cells with peptide-pulsed T2 target cells (**Figure 12A**) and LCL-1 minigene-transduced target cells (**Figure 12B**) provided proof of TCR functionality and defined neoantigen specificity as well as proper neoantigen processing and presentation by target cells.

A peptide titration experiment showed similar dose-response curves for ncKIF2C-TCRs to $KIF2C^{P13L}$ neoantigen and no reactivity to wt cognate antigen or to the irrelevant antigen at high doses (**Figure 13C-D**). From this experiment MHC/TCR complex avidity was estimated (EC_{50}) and resulted to be in the nanomolar range and very similar for both ncTCRs (**Figure 13E**).

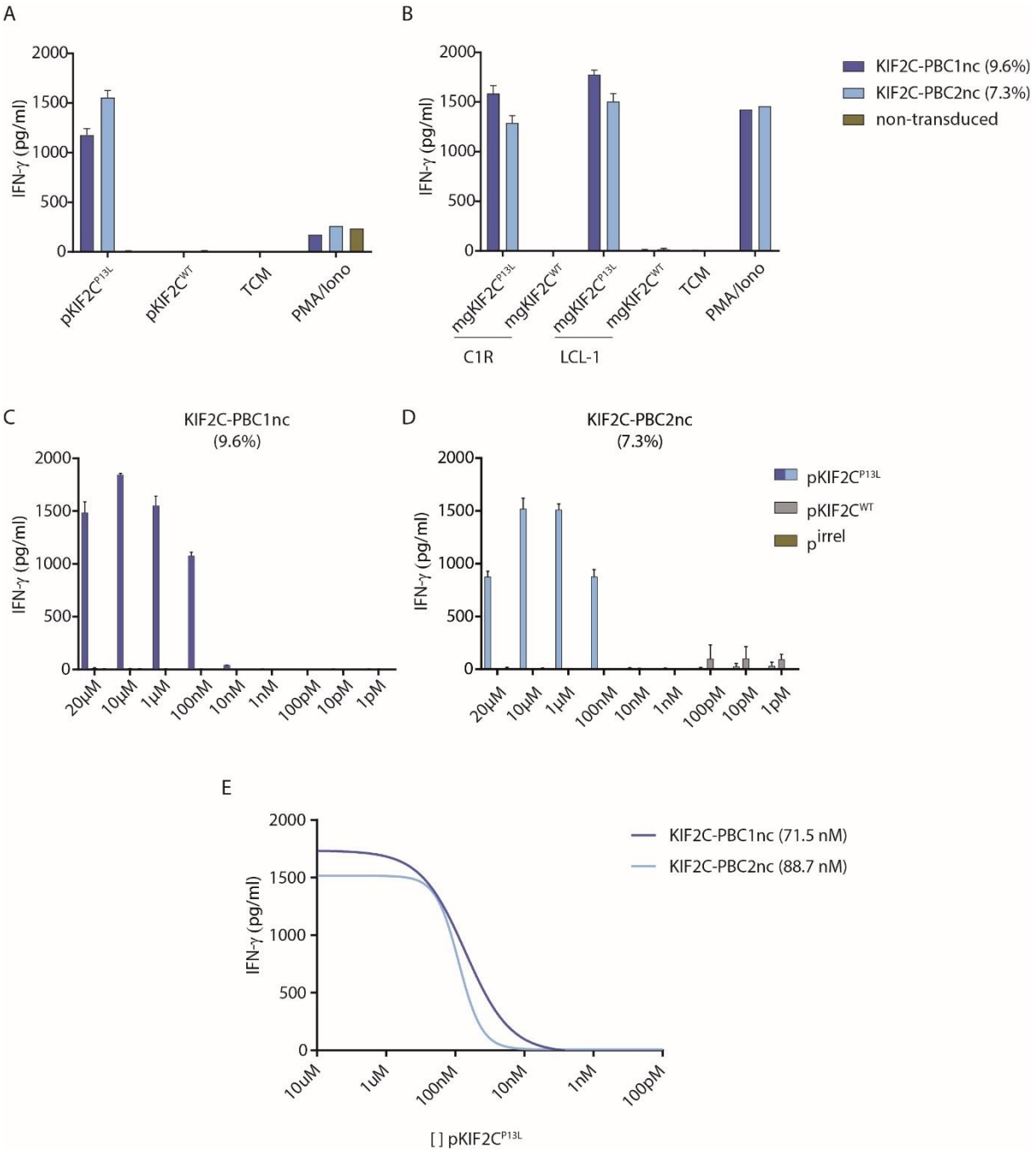

Figure 12. Functional analysis of CD8$^+$ T cells transduced with native TCR chains. KIF2C-PBC1 and -PBC2 TCR alpha and beta native chains mediate IFN-γ secretion upon co-colture with (A) peptide pulsed T2 cells, (B) minigene-transduced LCL-1 and C1R cells. C and D) Transduced T cells were co-cultured with T2 pulsed with graded amounts of mutated, wt and irrelevant peptides. E) Fitting of non-linear regression curve in GraphPad Prism 7 through data points of C and D for calculation of the slope, representing functional avidity of the ncTCRs for KIF2C^{P13L}.

1.33 Expression of optimized TCR constructs

1.33.1 Detection of transgenic codon optimized TCRs through murine constant chain

Expression of codon optimized TCRs on primary CD8$^+$ T cells was assessed by staining the alpha murine constant chain (**Figure 13**).

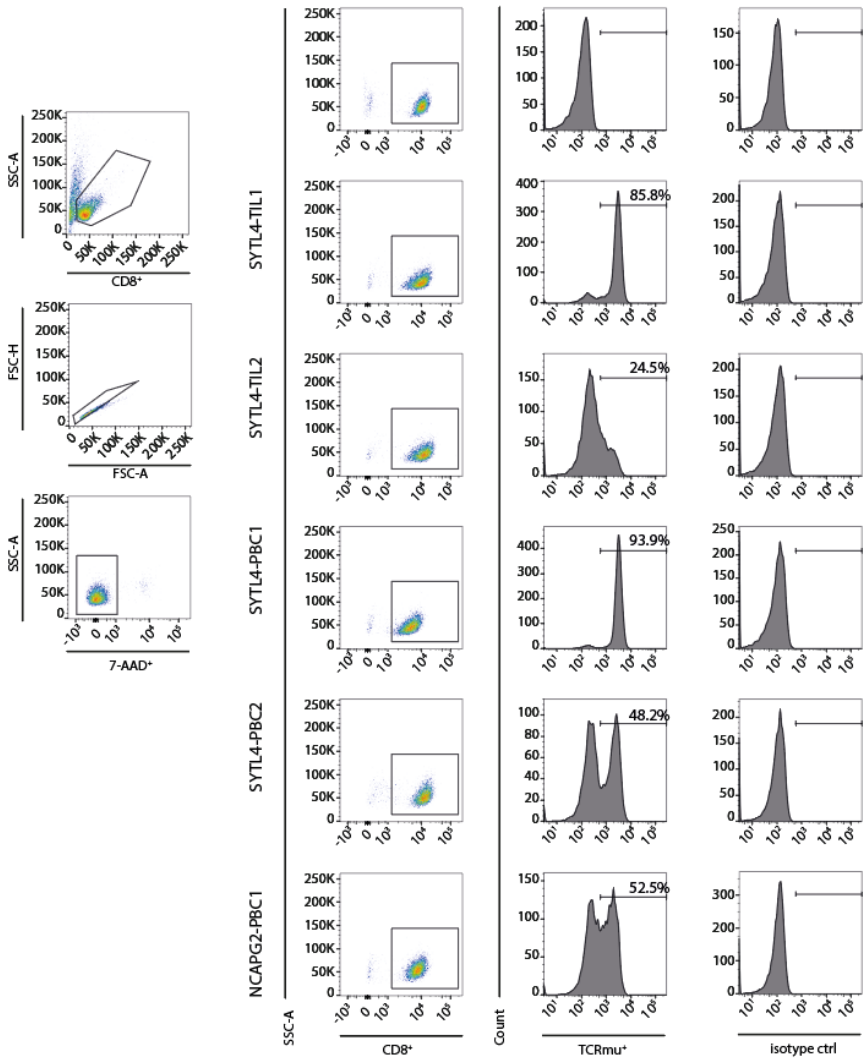

Figure 13. Surface expression of transduced neoantigen-specific TCRs on human CD8$^+$ T cells. Flow cytometry plots of TCR-transduced-CD8$^+$ T cells stained for CD8, and transgenic TCRs (TCRmu$^+$); the dot plots were gated

on singlets, living cells (7-AAD$^-$) and CD8$^+$ T cells. The bar plots represent the percentage of CD8$^+$-T cells expressing the murinized TCRs in direct comparison to the isotype staining. Transduction efficiency was assessed for all transductions showing consistent results for the different TCRs. The figure is representative of more than three staining experiments.

1.33.2 Detection of transgenic codon optimized TCRs through multimer staining

HLA class I multimer staining was performed for all TCRs using neoantigen- as well as wt-peptide multimers. Staining of SYTL4-TCRs was performed with three different kinds of multimers. Staining of these four TCRs with tetramerized HLA-B27 bearing mutation C56S failed to detect a positive population for SYTL4-TIL2 and -PBC2 (**Figure 14A**). Staining performed with tetramerized HLA-B27 wt led to the same result with a less efficient staining of reactive T cell population (**Figure 14B**). In addition, staining with commercial pentamers bearing mutation C67S reflected the same results, but in addition displayed a population of T cells binding the wt peptide (wt p), which is opposite to all functional results (**Figure 14C**). All other multimers containing SYTL4^{WT} did not bind to transgenic TCRs (**Figure 14A-B**).

Detection of KIF2C- and NCAPG2-TCRs with HLA-A03 tetramers completely matched functional data showing T cells reacting to the mutated peptides, but not to the wt (**Figure 15A-B**).

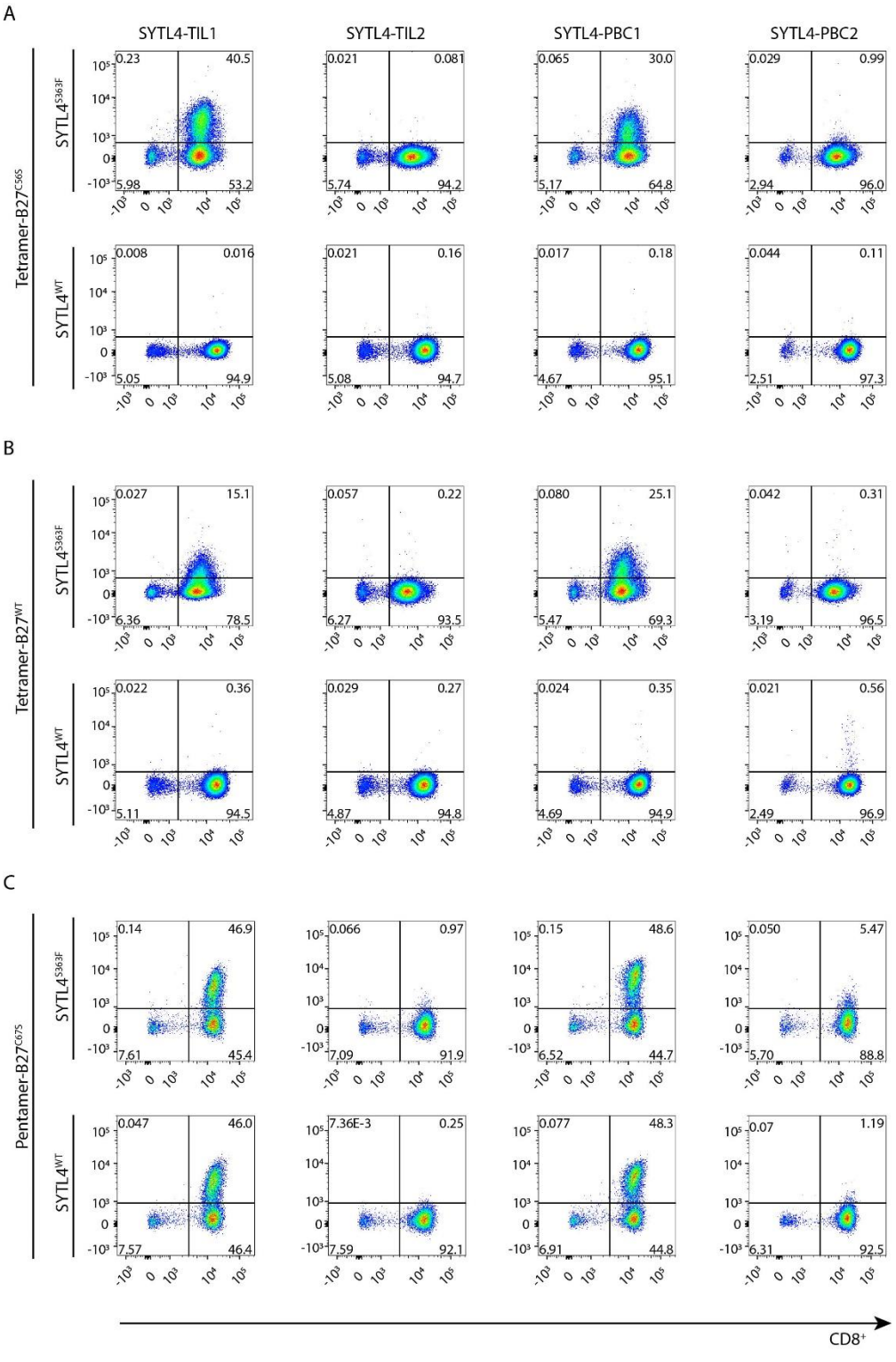

Figure 14. Expression of transduced SYTL4^{S363F}-specific TCRs on the surface of CD8$^+$ T cells assessed by multimer staining. Flow cytometry plots show staining with tetramers HLA-B27:05^{C56S}-SYTL4$^{S363F/WT}$ (A), HLA-B27:05^{WT}-SYTL4 $^{S363F/WT}$ (B) and pentamers HLA-B27:05^{C67S}-SYTL4 $^{S363F/WT}$ (C). TCR-transgenic-CD8$^+$ T cells were stained for CD8 expression. The dot plots were gated on singlets and living cells (7-AAD$^-$) (not shown). The values in upper right quadrant represent the percentage of multimer-positive CD8$^+$-T cells. The gates were set by comparison to non-transduced T cells and isotype control. Depicted staining is representative of three experiments

with T cells from two different healthy donors.

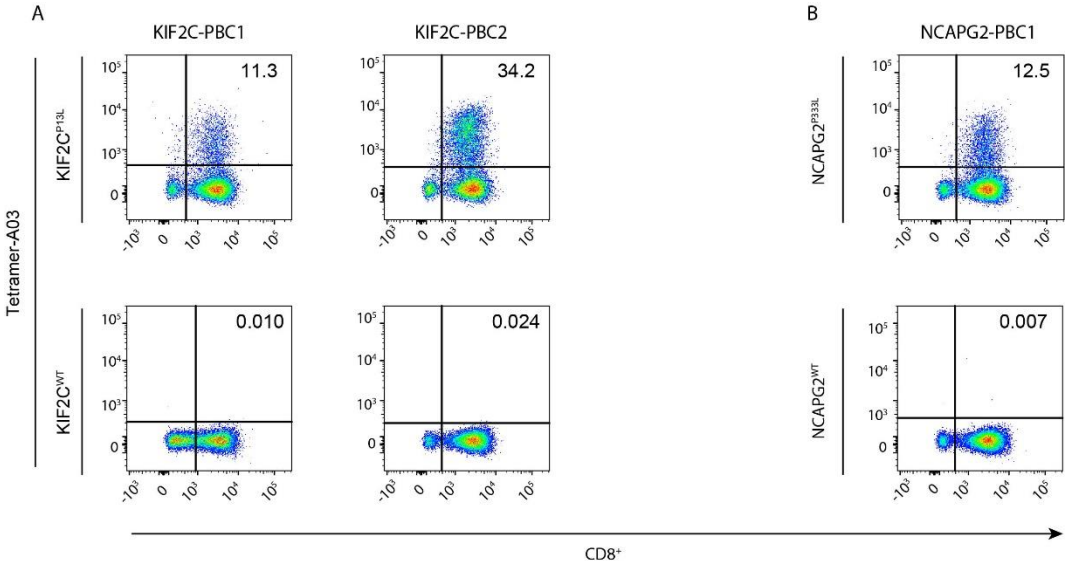

Figure 15. Expression of transduced KIF2C^{P13L} and NCAPG2^{P333L}-specific TCRs on the surface of CD8$^+$ T cells assessed by multimer staining. Flow cytometry plots show a staining with indicated multimers: HLA-A03:01-KIF2C$^{P13L/WT}$ (A) and HLA-A03:01-NCAPG2$^{P333L/WT}$ (B). TCR-transduced-CD8$^+$ T cells were stained for CD8 expression. The dot plots were gated on singlets and living cells (7-AAD$^-$) (not shown). The values in the upper right quadrant represent the percentage of multimer-positive CD8$^+$-T cells. The quadrants were set by comparison to non-transduced T cells and isotype control. Depicted staining is representative of three experiments with T cells from two different healthy donors.

1.33.3 Flow cytometry intracellular staining of transgenic TCRs

In the attempt to understand the reasons behind low expression of some TCRs despite optimization, an intracellular staining of the transgenic TCRs was performed, saturating first all TCR molecules on the surface and performing a second staining after fixation and permeabilization. Intracellular staining did not show a higher frequency of cells with intracellular expression of TCR. Double-positive events (4%) for KIF2C-PBC2 can be represented by surface receptors which were not completely saturated from the first surface staining and therefore might have been stained again during performance of the intracellular staining (**Figure 16**).

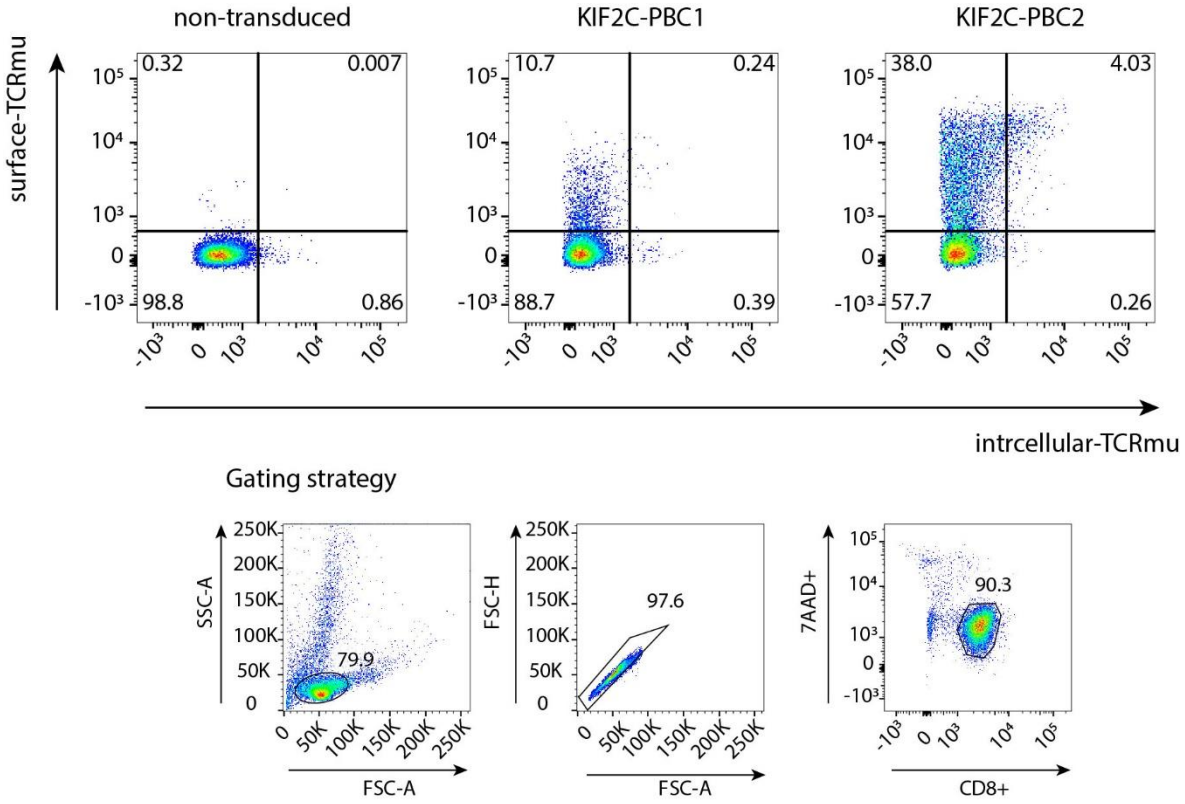

Figure 16. Surface and intracellular staining of TCRs KIF2C-PBC1 and KIF2C-PBC2. TCR-transduced $CD8^+$ T cells were stained with saturating amounts of antibody for CD8 and transgenic TCR surface marker. After permeabilization T cells were stained for transgenic TCR. The dot plots were gated on singlets and living cells (7-AAD^-). The values in the upper and lower right quadrants represent the percentage of surface TCR and retained TCR.

1.34 In-depth characterization of immune responses against three neoantigens

KIF2C-TCRs were murinized, codon-optimized, complemented with an additional cysteine (om.c) and transduced in primary $CD8^+$ T cells (**Figure 10**). Optimization of the sequence allowed a better expression and pairing of the TCR chains on the surface of transduced cells (**Figure 17**). KIF2C-PBC1 consistently showed a lower transduction rate and a lower density on the surface compared to KIF2C-PBC2.

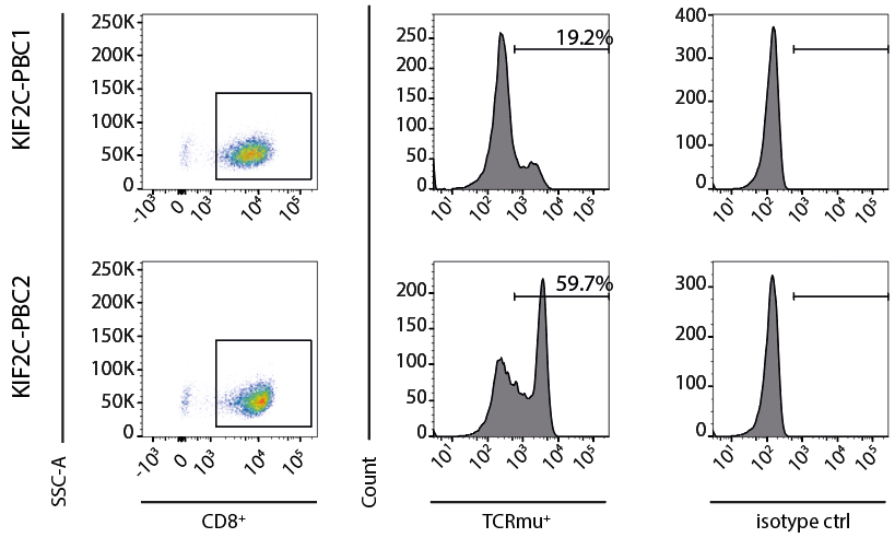

Figure 17. Surface expression of codon-optimized KIF2C-TCRs. Flow cytometry panels showing expression of optimized KIF2C-PBC1 and -PBC2 detected by anti-murine constant TCR chain monoclonal antibody (TCRmu). Gates for TCR-transduced T cells were set accordingly to an isotype control.

Despite differences in expression, no significant difference is observed by quantifying IFN-γ cytokine secretion mediated by the TCRs upon stimulation with pulsed- or minigene transduced-target cells. Both TCRs showed high specificity for the neoantigen and no reactivity towards the wt cognate or irrelevant peptide (**Figure 18A**). This specificity is retained also in case the TCRs are challenged with high concentration of peptides (**Figure 18**, **B** and **C**). Furthermore, the two TCRs show similar functional avidities (average of all experiments: KIF2C-PBC1 – 510nM; KIF2C-PBC2 – 561nM) (**Figure 18D**). By comparing optimized TCRs to ncTCRs, an increase in surface expression and IFN-γ levels was observed whereas functional avidity of optimized TCRs seems to be decreased. However, analysis of functional avidity with native chain TCRs was performed once and would need to be confirmed, while experiments with optimized chains were coducted at least three times and by different operators.

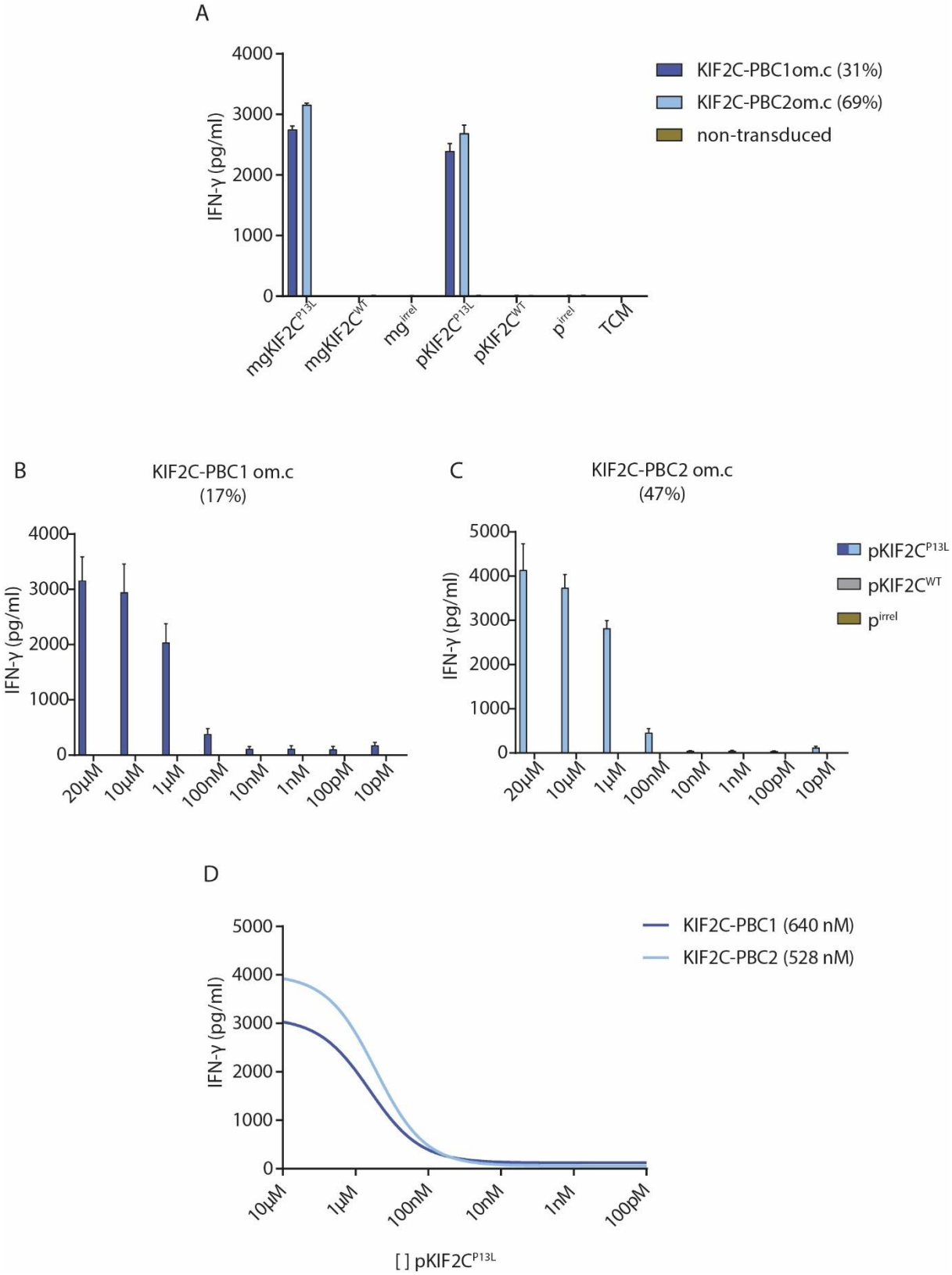

Figure 18. Functionality of CD8$^+$ T cells transduced with optimized TCRs. A) KIF2C-PBC1 and -PBC2om.c mediate IFN-γ secretion upon co-colture with peptide pulsed T2 cell. B and C) Transduced T cells were co-cultured with T2 pulsed with graded amounts of mutated, wt and irrelevant peptides. D) Fitting of a non-linear regression curve in GraphPad Prism 7 through data points of B and C for calculation of the slope, representing functional avidity of the TCRs om.c for KIF2C^{P13L}. Experiments performed with Dr. Bräunlein. In total, seven autologous

TCRs were identified from Mel15 patient. Five of them were previously isolated by Dr. Bräunlein after validation of two MS-detected neoantigens (Bassani-Sternberg et al., 2016) and functionally characterized in close cooperation. All seven TCRs were murinized, added with a disulfide cysteine bridge and codon optimized. TCR-transgenic $CD8^+$ T cells displayed IFN-γ secretion upon recognition of target cells pulsed with mutant peptide or transduced with minigenes coding for mutated peptides (Figure 19, A-C). No reactivity was observed against wt cognate or irrelevant peptides as well as against the corresponding control minigenes. TCR/MHC complex avidity experiments showed half-maximum IFN-γ release (EC_{50}) values in the range 100nM–10nM for SYTL4-TIL1, -TIL1, PBC1 and NCAPG2-PBC1 TCRs, while for SYTL4-PBC2 functional avidity is higher than 100nM and for KIF2C-TCRs is closer to 1µM. SYTL4- and NCAPG2-TCRs are showed an avidity significantly higher than KIF2C-TCRs ($p\text{-value} < 0.05$) (Figure 19D).

To further assess the cytokine footprint of all seven TCRs, defined cytokines as GM-CSF, IL-2, IL-12 and TNF-α, were analyzed by multiplex analysis using supernatants of TCR-transgenic $CD8^+$ T cells stimulated with mutated or wt minigene-transduced LCL-1 target cells (**Figure 19E**). All TCR-transduced T cells showed secretion of IFN-γ and GM-CSF only upon stimulation with cells transduced with respective mutated minigene. Highest concentrations of these cytokines were observed for stimulated TCRs SYTL4-TIL1 and SYTL4-PBC1.

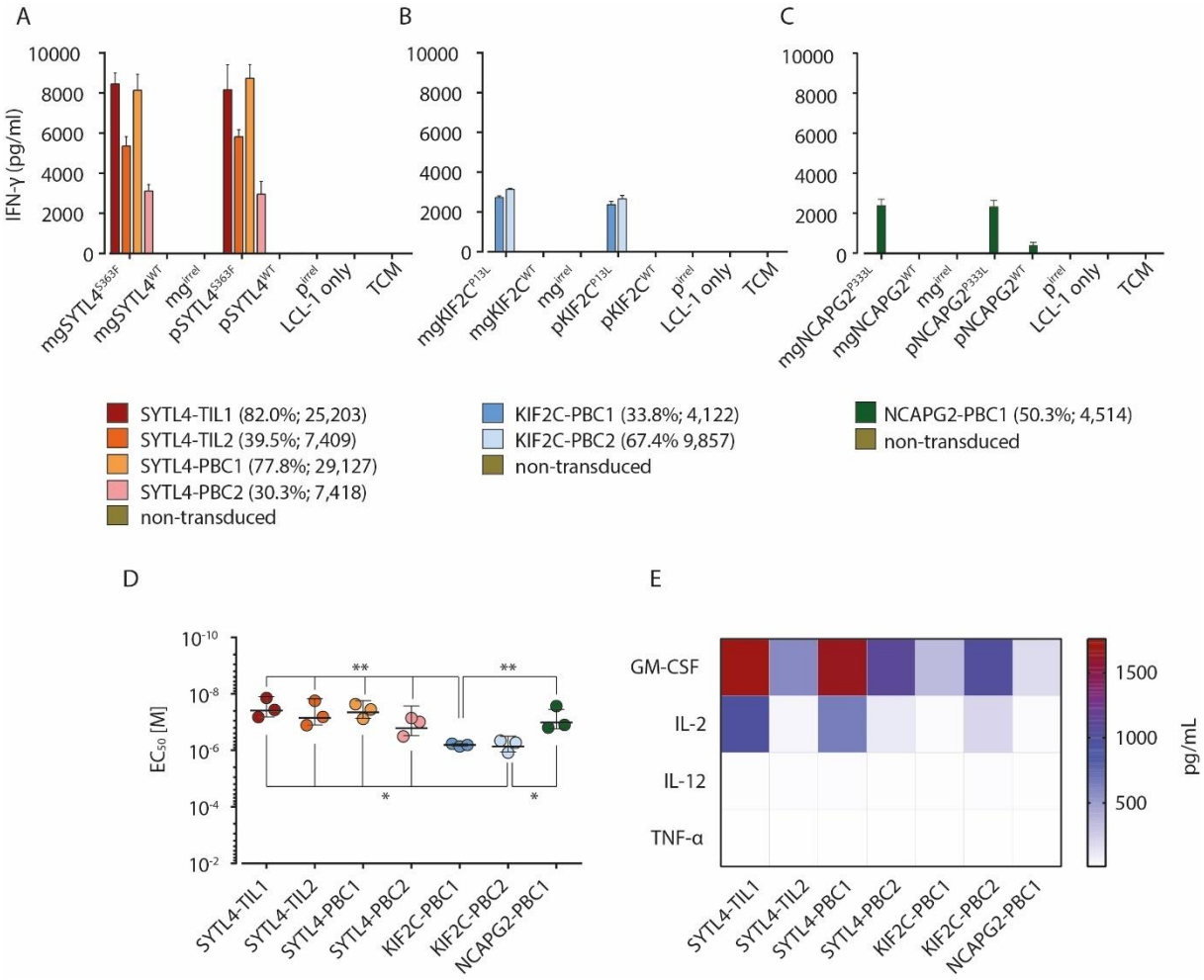

Figure 19. Functional characterization of neoantigen-specific TCR. IFN-γ ELISA assay performed on supernatants of CD8$^+$ T cells transduced with TCRs specific for SYTL4^{S363F} (A), KIF2C^{P13L} (B) and NCAPG2^{P333L} (C) after coculture with LCL-1 presenting neoantigens and respective wt counterparts (E:T = 1:1). IFN-γ secretion in response to LCL-1 transduced with minigenes (mg) encoding for mutant (mut mg), wt (wt mg) or irrelevant peptides (irrel mg) was compared to stimulation with peptide pulsed LCLs (mut p, wt p, irrel p; 1 µM peptide). Transduction efficiencies and MFI values are indicated in the legends. D) Functional avidities of neoantigen-specific TCR, calculated as EC_{50} of the corresponding mutated peptides. TCR-transgenic T cells were co-cultured with T2 target cells pulsed with different concentrations of the corresponding peptides. IFN-γ secretion was assessed on supernatants and data points were fit in a non-linear regression curve to determine the EC_{50}. The error bars in the graph represent SD from the mean value of triplicates. Significance was calculated with one-way ANOVA and Tukey multiple comparison test (* $p \leq 0.05$, ** $p \leq 0.01$). E) Multi-cytokine secretion of TCR-transduced T cells upon coculture with mutated-peptide-pulsed LCL-1 cells. All experiments were performed with three different sets of transduced T cells obtained from two different healthy donors, experiments were performed together with Dr. Bräunlein. Figure from Bräunlein et al., 2021.

1.35 Neoantigen-specific TCR show antigen-dependent binding and cross reactivity patterns

For cross-reactivity testing of identified TCRs, a set of altered peptide ligands, containing individual alanine or threonine substitutes (ala/thr scan) at every single position of the neoantigen, were used for stimulation of TCR-transgenic T cells. Highly similar binding motifs of all four SYTL4-TCRs either for alanine or for threonine substitutions were observed (**Figure 20A**; **Table 41**).

Replacement of Gly in position 1, Lys in position 7 and Tyr in position 8, enhanced recognition of the peptide by SYTL4-TIL2 and SYTL4-PBC2. KIF2C-TCRs exhibited the same pattern in the case of alanine substitutions and very different ones both inter- and intra-TCR when threonine was replaced. Replacement of Leu in position 2 with Thr exacerbated reactivity of KIF2C-PBC1 (**Figure 20B**). NCAPG2-PBC1 showed completely different pattern for the two amino acid substitutions. In particular, replacement of Leu in position 2 (unique to the neoantigen) and Leu in position 7 with Ala increased immunogenicity of the peptide compared to the original neoantigen (**Figure 20C**). This was reflected in a higher potential for cross reactivity against naturally occurring peptides within the human proteome, as indicated in silico by the ScanProsite tool (https://prosite.expasy.org/scanprosite) (De Castro et al., 2006). However this could not be experimentally confirmed with a selection of ScanProsite peptides (E. Bräunlein et al., 2021).

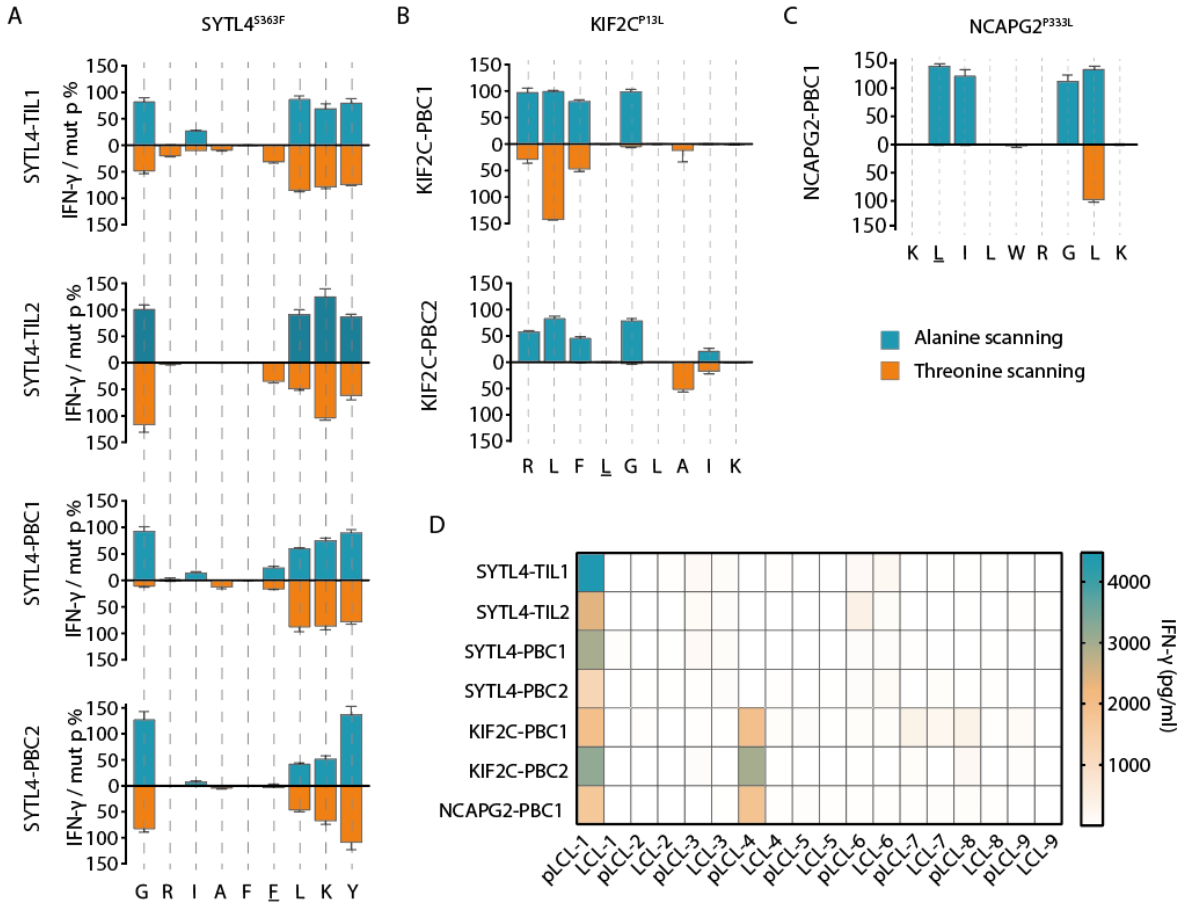

Figure 20. Cross-reactivity assessment of neoantigen-specific transgenic TCRs. TCR cross-reactivity was tested by quantification of secreted IFN-γ upon coculturing TCR-transgenic T cells with T2 target cells pulsed with ala/thr scanned peptide cognates (1 µM peptide) of ligands SYTL4^{S363F} (A), KIF2C^{P13L} (B) and NCAPG2^{P333L} (C). IFN-γ secretion values from single conditions were normalized against cytokine level in response to the defined neoantigen. D) Investigation of TCR peptide-dependent and – independent HLA alloreactivity. Reactivity of seven neoantigen-specific TCRs was tested by coculture with different LCLs expressing common HLA allotypes. LCLs were pulsed with mutated peptides of interest (pLCL; 1 µM) before coculture with TCR-transgenic T cells. As control, non-pulsed LCL target cells were adopted. All experiments were performed three times with TCR transgenic T-cells derived from two different healthy donors. Experiments performed together with Dr. Bräunlein. Figure from Bräunlein et al., 2021.

Table 41. Number of human proteins potentially targeted transgenic TCRs according to recognition motif (E. Bräunlein et al., 2021).

TCRs	Recognition motif[1]	Number of antigens[2,3]
SYTL4-PBC1	X-R-I-A-F-F-X-X-X	6
SYTL4-PBC2	X-R-I-A-F-F-X-X-X	6
SYTL4-TIL1	X-R-I-A-F-F-X-X-X	6
SYTL4-TIL2	X-R-I-A-F-F-X-X-X	6

KIF2C-PBC1	X-X-X-L-X-L-A-I-K	60
KIF2C-PBC2	X-X-X-L-X-L-X-I-K	> 400
NCAPG2-PBC1	K-X-X-L-W-R-X-X-K	4

[1]Recognition motifs are defined through T cell IFNγ production in response to alanine/threonine scanned cognate epitopes

[2]Number of human proteins containing matching recognition motif according to ScanProSite (http://prosite.expasy.org/scanprosite/)

[3]Results derived from protein sequence database UniprotKB, Swiss-Prot (splice variants included)

SYTL4- and NCAPG2-specific TCRs exhibited potential cross reactivity with four to six antigens only, while KIF2C-TCRs might recognize > 400 targets (

Table 41). To investigate the general alloreactive potential of selected TCRs, TCR-transduced T cells were co-incubated with a panel of LCLs expressing the most frequent HLA allotypes (**Table 42**) with or without previous peptide pulsing. All TCRs showed clear recognition of mutated peptide only in the context of the expected restriction elements (respectively HLA-B27:05 and HLA-A03:01) (**Figure 20D**). Overall, these results confirm low alloreactive potential for all neoantigen-specific TCRs.

Table 42. HLA alleles expressed by LCL cell lines (E. Bräunlein et al., 2021).

Alias	Cell line	HLA-A*	HLA-B*	HLA-C*
LCL-1	HOM2[1]	03:01	27:05	01:02
LCL-2	SWEIG007[1]	29:02	40:02	02:02
LCL-3	AMALA[1]	02:17	15:01	03:03
LCL-4	OZB[1]	02:09/03:01	35:01/38:01	04:01/12:03
LCL-5	RSH[1]	68:02/30:01	42:01	17:01
LCL-6	KLO[1]	02:08/01:01	50:01/08:01	07:01/06:02
LCL-7	LWAGS[1]	33:01	14:02	08:02
LCL-8		02:01	07:02/15:01	30:4/12:03
LCL-9	BM21[1]	01:01	41:01	17:01

[1]Cell lines kindly provided by Steven Marsh

1.36 Assessing target cell cytolysis potential of TCR-transgenic T cells

1.36.1 Europium-release assay

Killing potential mediated by TCRs was assessed in 4h europium release assay and showed a ratio-dependent specific cytolysis of cell line expressing neoantigens, while no lysis of cell line expressing wt antigens was detected. All TCRs showed lysis specificity and different efficacies within 4h incubation. SYTL4-TIL1, -TIL2 and NCAPG2-PBC1 reached in this specific experiment ~100% cytolysis at a 9:1 effector to target ratio, while other TCRs were not as fast. At the standard ratio of 1:1 all TCRs appear to perform poorly after 4h except NCAPG2-PBC1 which showed a killing of around 50%. Non-transduced T cells served as negative control and did not mediate any lysis of the target cell line.

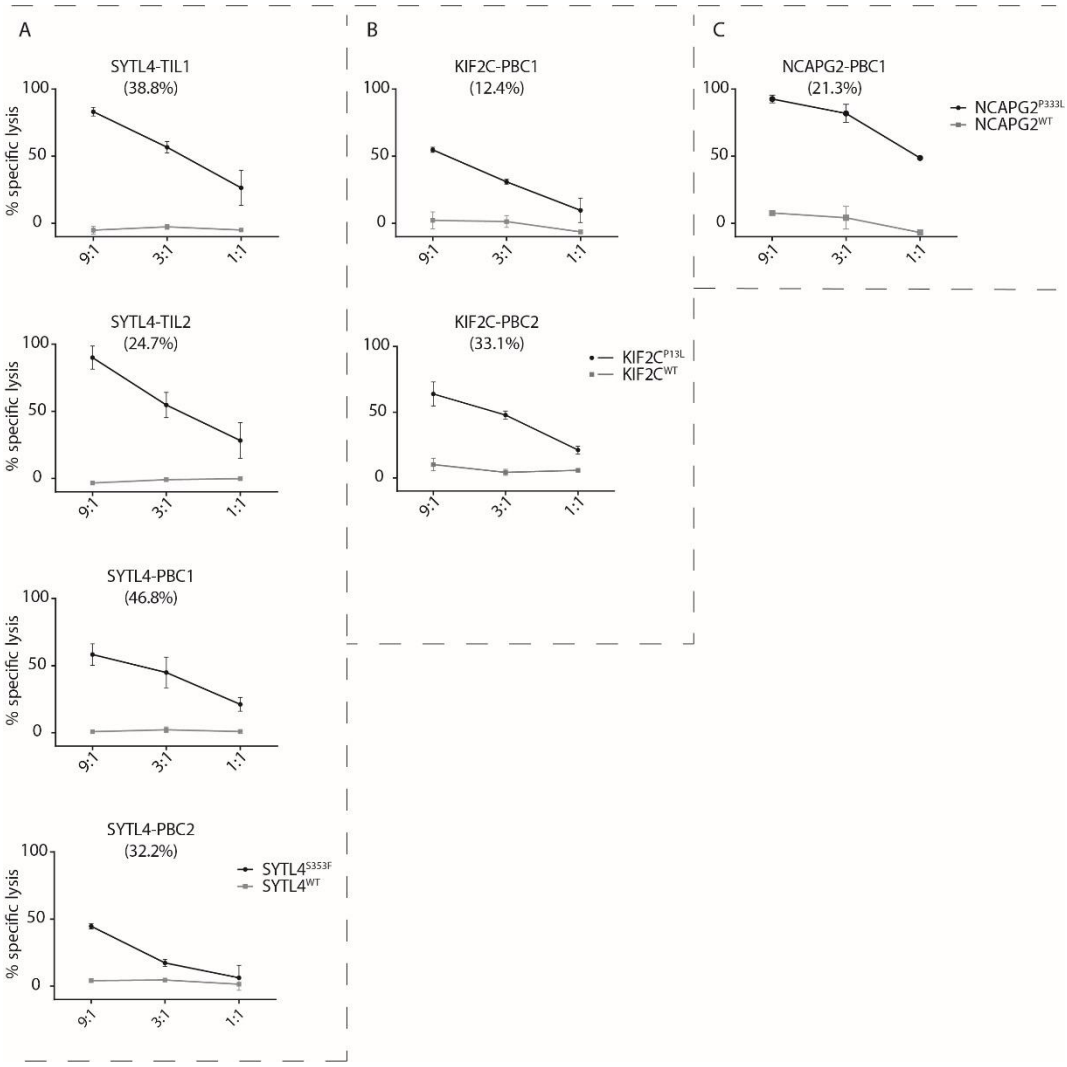

Figure 21. Standard Europium release assay for the assessment of TCR mediated cytolysis. TCR-transgenic T cells were co-incubated with LCL-1 target cells expressing neoantigens and wt counterparts at different E:T ratios (depicted on x-axis). Target cells were loaded with a dye previous co-culture (Methods p.1.18.8.7). Dye release and fluorescence resulting from Europium solution addition are proportional to specific lysis mediated by TCR-transgenic T cells after 4 h incubation. Error bars for the lysis experiments represent standard deviation of three replicates. One representative experiment of three is shown.

1.36.2 Real-Time Quantitative Cell Analysis (xCELLigence)

TCR-mediated cytotoxic activity was dynamically monitored with xCELLigence assay.

A2058 or MDST8 target cell clones (transduced with mut and wt minigenes) were seeded and proliferated for ca. 20-24h, after which TCR-transgenic T cells were added to the culture. After a lag-phase, cytotoxic effects mediated by the TCR-transgenic T cells could be observed on the target cells transduced with mutated minigenes. Target cells transduced with wt minigenes were not affected by the presence of neoantigen specific TCR-T cells. T cells transduced with three of four SYTL4-TCRs achieved 100% lysis of target cells within 8 and 12h after coculture, with SYTL4-TIL1 appearing to be

the fastest. SYTL4-PBC2 showed quick cytolysis of 25-30% of the target cells within 4h from coincubation. After 4h the target cells started proliferating again (increase in cell index), however between 8 and 23h of coculture, TCR-T cells lysed the majority of mutated minigene cells. For this TCR cytolysis never reached 100% in the example shown (**Figure 22A**), but complete lysis was observed in an independent experiment within 16-20h.

T cells transduced with KIF2C-TCRs showed very similar rejection dynamics characterized by cytolytic activity up to 75-80% within the first 4h, a plateau phase of additional 4h and a recover of the killing which reached 100% around 12h post-coculture (**Figure 22B**).

NCAPG2-PBC1 showed a killing dynamic comparable to KIF2C-TCR, however complete lysis was reached around 16h post T-cell addition (**Figure 22C**).

Addition of non-transduced T cell did not trigger any target cell detachment or lysis (**Figure 22A-B**).

Comparison of all TCR cytotoxicity dynamics is shown in **Figure 22D**.

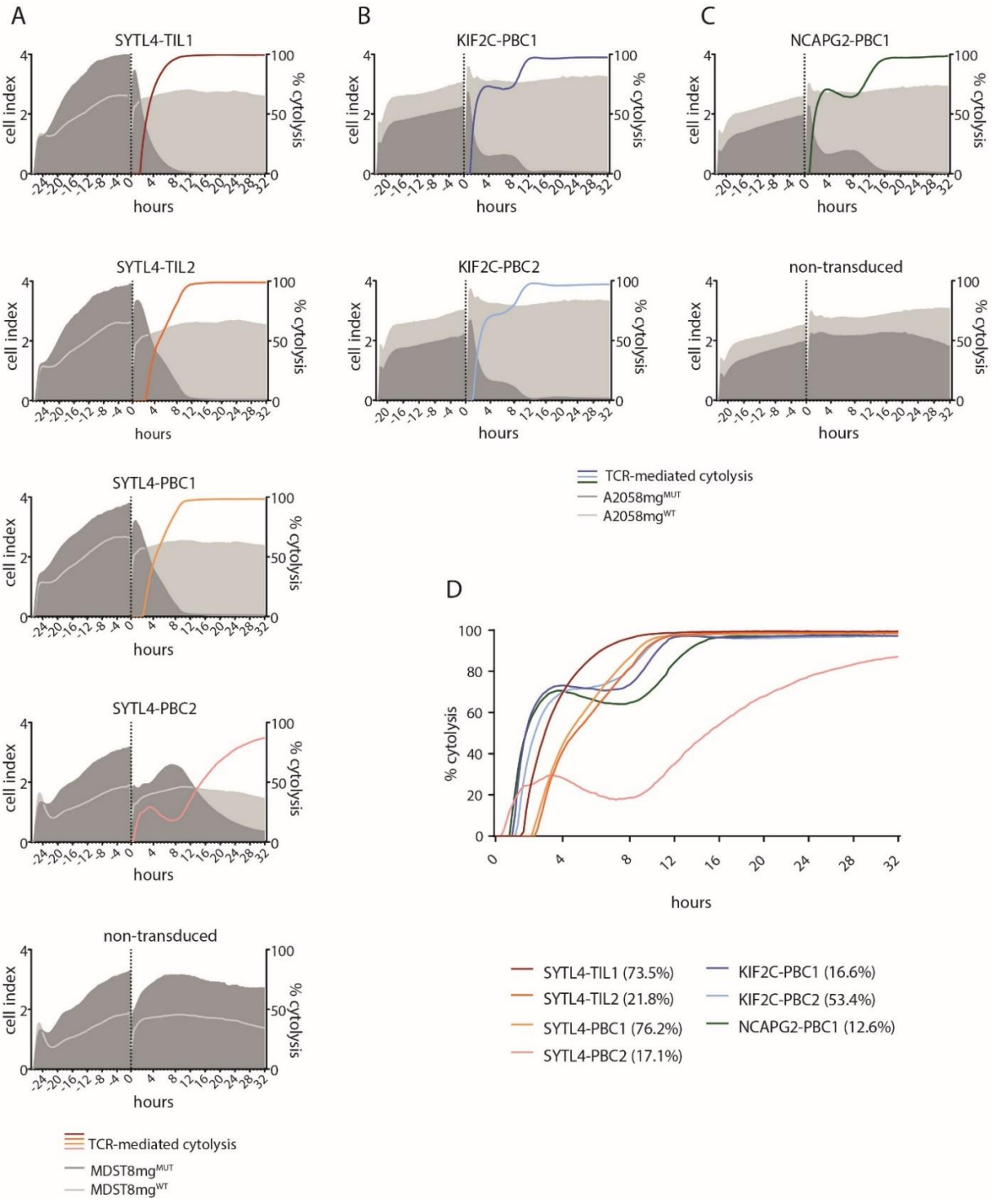

Figure 22. TCR-transgenic $CD8^+$ T cells mediate killing and detaching of target cells expressing tumor neoantigens. A-C) Proliferation of mut/wt minigene target cells is monitored for ca. 24h (measurement interval 15 min), after which TCR-T cells are added to the culture (time 0). Cytolysis of target cells is monitored for additional 30h. At time -24h $MDST8^{MUT/WT}$ (A) and $A2058^{MUT/WT}$ (B-C) cells were seeded at density of respectively 2×10^4 and 5×10^4 cells/well T cells were added at time 0 at a E:T=2:1 in respect to the initial number of target cells (4×10^4 and 1×10^5 cells/well). Cell index values of target cell lines are depicted on left y axis. Percentage of target cell lysis, calculated on non-transduced T cell, is depicted on right y axis and indicated by the colored line. D) Comparison of cytolysis mediated by all TCRs. TCR transduction efficiency is indicated in the figure legend.

Figure from Bräunlein et al., 2021.

1.37 Assessing TCR-mediated tumor rejection in an in-vivo immunocompromised xenogenic mouse model

The in-vivo rejection potential of neoantigen-specific TCRs was investigated in tumor mouse models. U698M tumor cell clones transduced with mut/wt minigene tandem vector constructs coding for all three characterized antigens, was subcutaneously injected in both flanks of each mouse (right flank: mut; left flank: wt). Growth of tumors was visually monitored three times a week after injection and subsequently measured with a digital caliper every day, as tumor lumps became palpable. When tumors reached ~25mm^2 size, transgenic T cells were injected. Staining of the transgenic TCR was conducted one day prior injection (**Figure 23A**) and again after dilution of T cells, right before injection, to reach comparable transduction rates for the seven TCRs (**Figure 23B**).

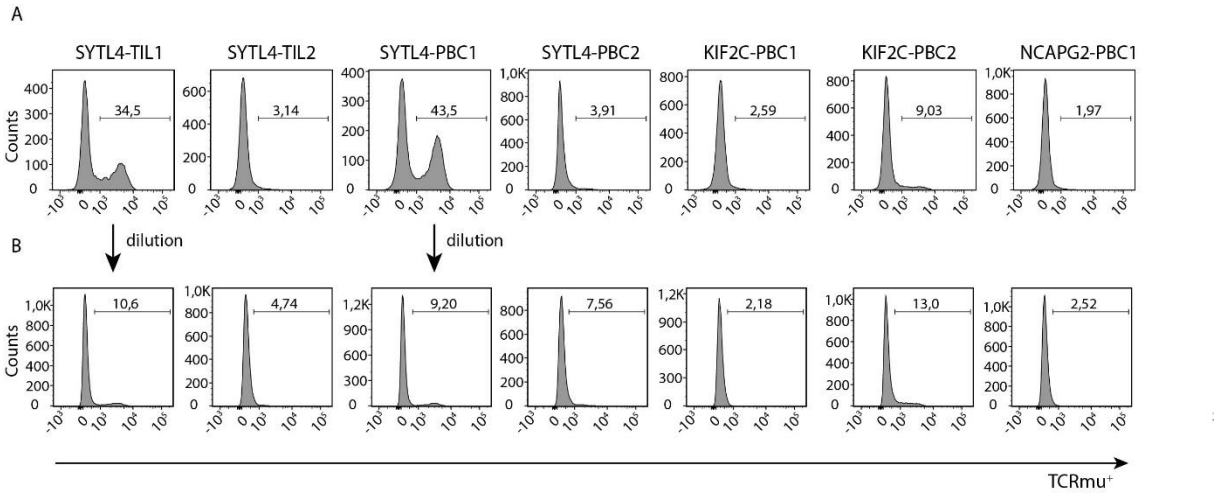

Figure 23. Assessment of TCR transduction rates for standardization of effector T cell injection. A) Flow cytometry plots of TCR-transgenic-CD8$^+$ T cells stained for CD8, and TCRmu expression. B) Flow cytometry plots of the same TCR-transduced-CD8$^+$ T cells in A, after dilution with non-transduced T cells. Plots were gated on singlets, living cells (7-AAD$^-$) (not shown) and CD8-TCRmu$^+$ T cells. The bar plots represent the percentage of CD8$^+$-T cells expressing the transgenic TCRs. Gates were set by comparison to the isotype control for each single TCR.

IFN-γ production of transgenic T cells was assessed in vitro to determine functional activity of T cells injected in vivo (**Figure 24**). Number of injected transgenic T cells in indicated in (**Table 43**).

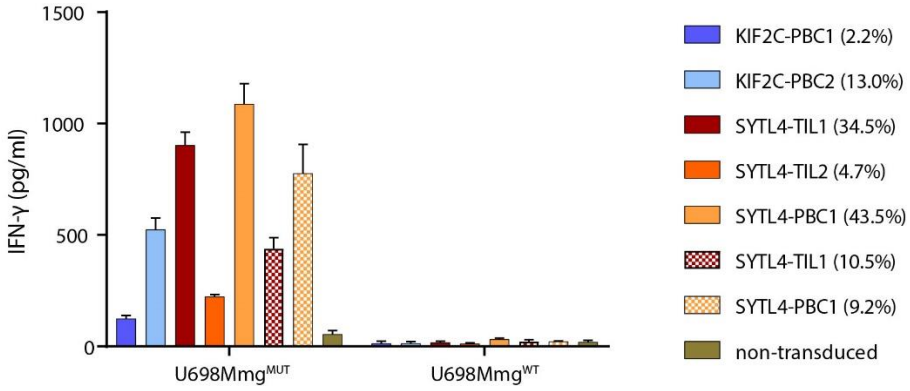

Figure 24. In vitro functional assessment of injected TCR-transgenic T cells. 10,000/well TCR-transduced T cells were co-cultured with 10,000/well mut and wt minigene U698M target cells, to assess level of IFN-γ secretion. TCR-transgenic T cells were diluted to reach transduction efficiency of ca. 10% and compared to original fraction. Bars represent average reads from three duplicates, error bars represent SD. Transduction efficiencies are indicated within the legend.

Table 43. Number of TCR-T cells injected per mouse based on transduction efficiency and mice per group.

	Transduction efficiency (%)	TCR-T cells out of 20×10^6	Nr. injected mice
SYTL4-TIL1	10,5	2.100.000	5
SYTL4-TIL2	4,7	940.000	3
SYTL4-PBC1	9,2	1.840.000	5
SYTL4-PBC2	7,6	1.520.000	4
KIF2C-PBC1	2,2	440.000	5
KIF2C-PBC2	13	2.600.000	5
NCAPG2-PBC1	2,5	500.000	4

Up to day 5 or 7 post T-cell injection, no differences could be observed within TCRs and between transgenic T cells and non-transduced T cells. After day 7, tumors of mice that received non-transduced T cells kept constantly growing, while tumors from mice injected with transgenic T cells remained significantly smaller and started to be progressively rejected to different extent depending on the TCR. T cells transgenic for all TCRs, except SYTL4-TIL2 mediated a significant inhibition of tumor growth ($p < 0.001$). No significant differences were observed within TCRs (**Figure 25**, **A-C**).

Flow cytometry data showed infiltration of all TCRmu$^+$ CD8$^+$ T cells, except SYTL4-TIL2, significantly higher than non-transduced T cells (**Figure 25D**). T cell infiltration in wt tumor was not detected (**Figure 25E**). TCRmu$^+$ CD8$^+$ T cells were also detected in peripheral blood at significant levels for SYTL4-TIL1 and KIF2C-PBC2 (**Figure 25F**) and in the spleen for SYTL4-PBC1 and KIF2C-PBC2. In the bone marrow, no transgenic T cells were observed (**Figure 25H**). Significance was calculated with Kruskal-Wallis test and uncorrected Dunn's test for multiple comparisons.

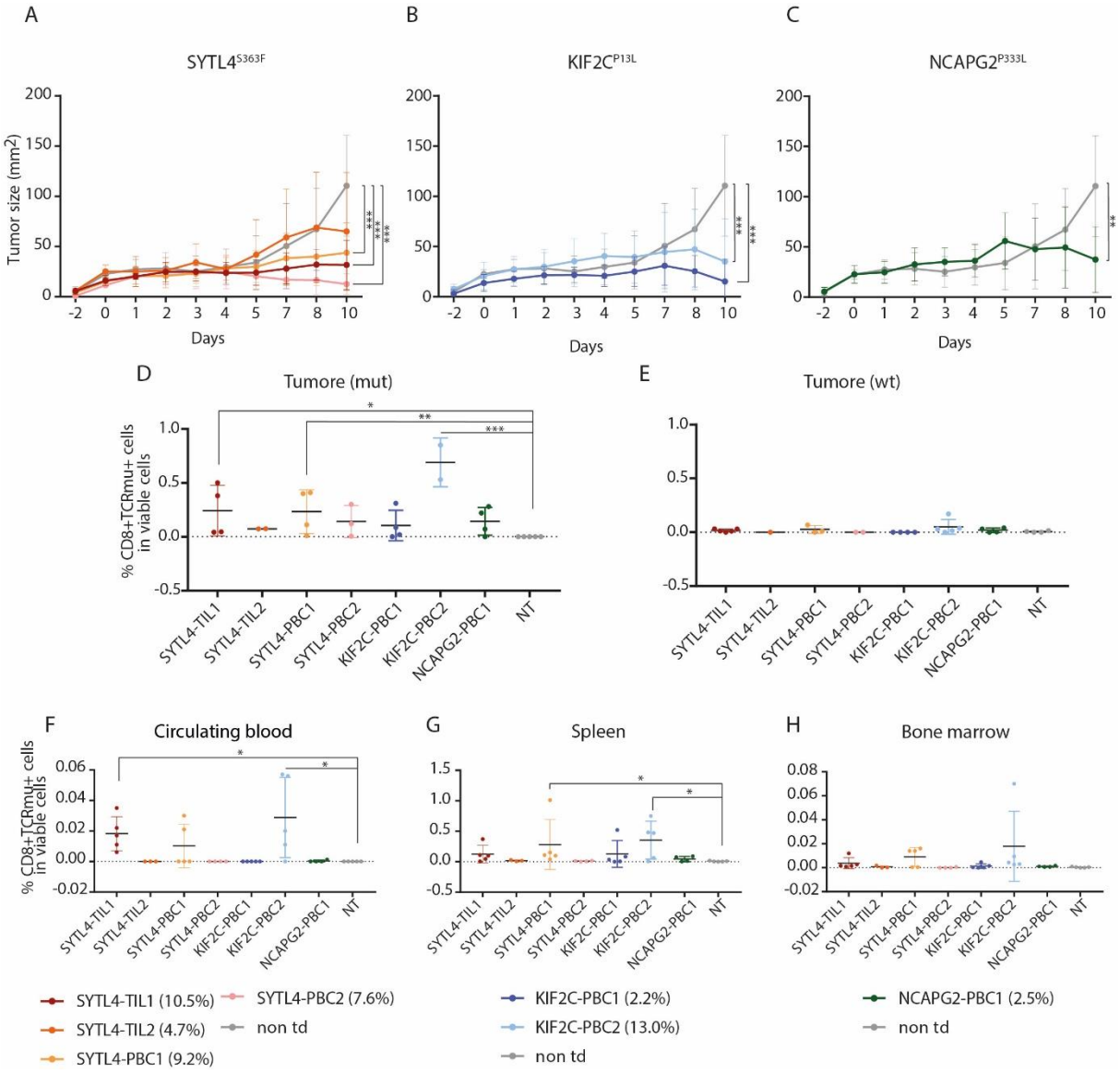

Figure 25. In vivo performance of T cells transgenic for neoantigen-specific TCRs. A) growth kinetics of U-698-M tumors mean values and SD are depicted for each group of mice bearing tumors. Animals were i.v injected with 2×10^7 T cells on day 0. Significance is calculated with two-way ANOVA (time; treatment) and multiple comparison Dunnett's test. The percentage of $CD8^+$ $TCRmu^+$ T cells calculated on total alive cells, detected in the tumor (B), and spleen (C) is depicted. Significance is calculated with Kruskal-Wallis test. TCR transduction efficiencies are indicated below the graphs. * $p < 0.033$; ** $p < 0.02$; *** $p < 0.001$. Experiment conducted together with Dario Gosmann.

By taking a closer look at each single mouse and the growth of mut and wt tumors on the flanks (**Figure 26A**), it is possible to appreciate how differently the tumors developed over time. There is a variability between each group (TCR), however there is also a variability between mut and wt tumor cell clones and an intra-individual variability between mice of each group. The majority of wt tumor masses did not engraft properly with exception of four mice (groups: SYTL4-TIL1, -PBC1 and -PBC2) which developed large wt tumors (**Figure 26B**) and mice of the group KIF2C-PBC2 (**Figure 26C**) on which

wt tumors remained of modest dimensions (KIF2C-PBC1) or comparable to the mut tumors (KIF2C-PBC2). All other mice developed rather small or undetectable wt tumors (**Figure 26**, **B-E**).

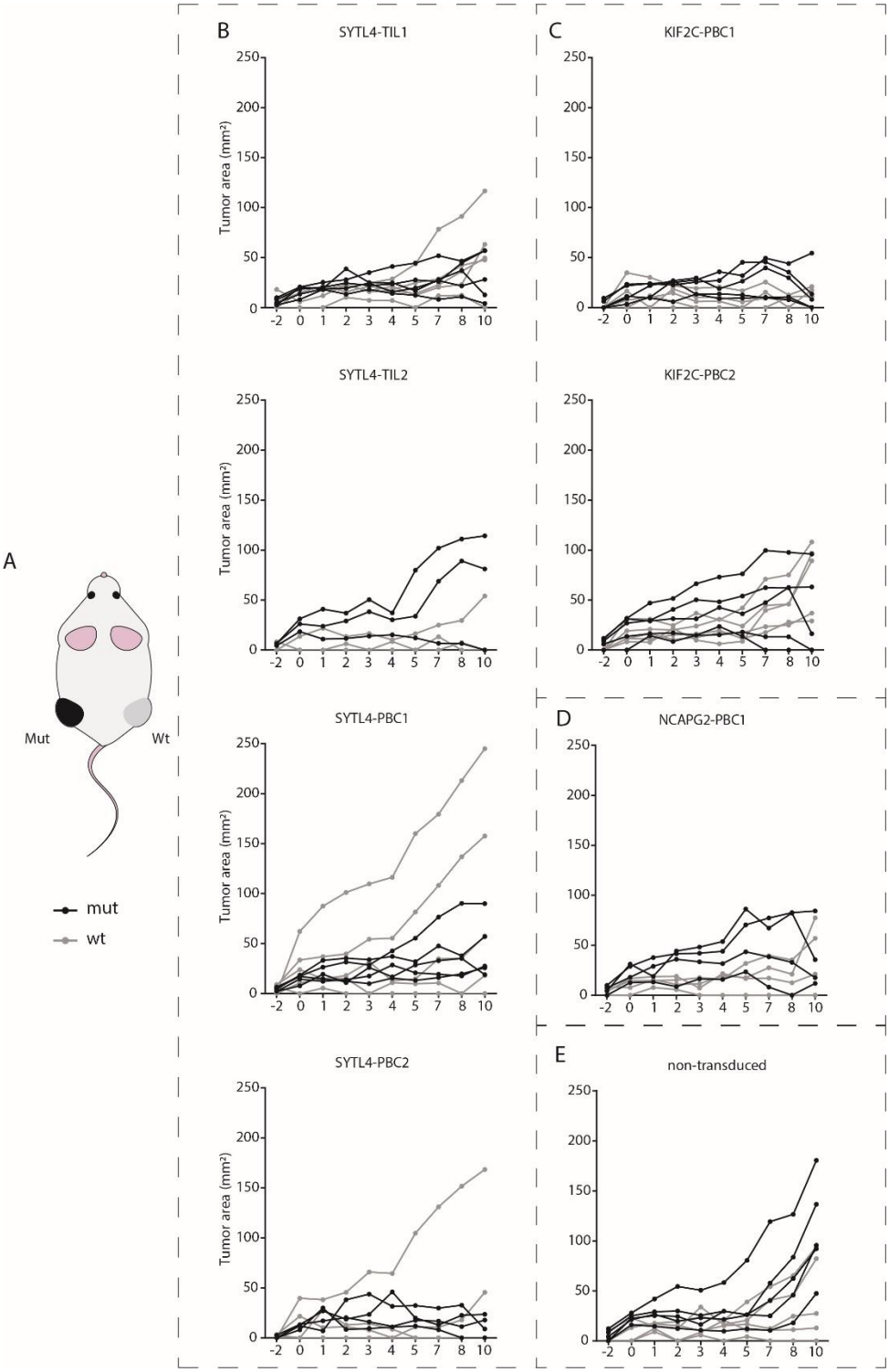

Figure 26. Growth kinetics of tumor xenografts for single mice. A) Visual representation of the xenograft mouse model bearing mut minigene U-698-M tumor on the left flank and wt on the right flank. Influence of TCR-transgenic T cell injection on tumor growth dynamics for SYTL4-TCRs (B), KIF2-TCRs (C), NCAPG2-PBC1

(D) and non-transduced T cells (E). Experiment conducted together with Dario Gosmann.

1.38 Immunogenicity assessment of mutated peptide ligands from Immunopeptidomics 2018 pipeline

TILs expanded from M_{Lung} were adopted to test immunogenicity of mutated peptides identified with Immunopeptidomic 2018 (p. 1.19.2). Fourteen new peptides were selected based on selection criteria, such as HLA binding prediction, as well as identification from both WES and RNA-Seq datasets or detection in both metastases (**Table 27**). In the Appendix 1.43 (**Table 44**) all peptides resulting from the pipeline and post MaxQuant filtering (p. 1.19.2.1) are annotated.

TILs were stimulated following the protocol for recall responses (p. 1.18.9) and showed early reactivity to novel peptides CTNNA2^{P361L}, HLA-J^{K83R} and NUP153^{P706L}, as well as reactivity to well charachterized neoantigens such as SYTL4^{S363F} and KIF2C^{P13L} (**Figure 27**). This experiment was performed once due to scarce TIL material.

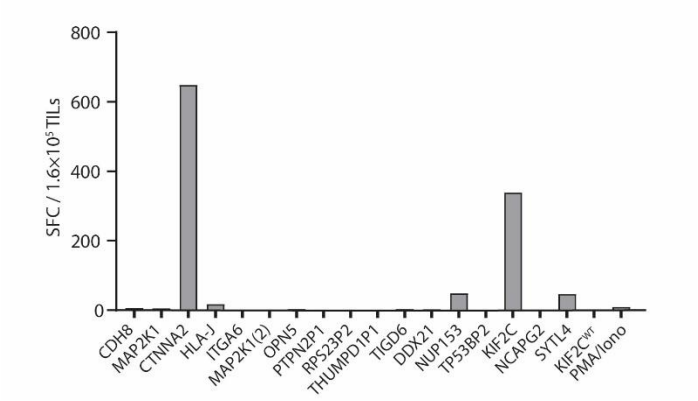

Figure 27. TIL stimulation with mutated peptides identified through Immunopeptidomics 2018. IFN-γ secretion of Mel15 TILs cultured with autologous γ-irradiated peptide pulsed PBMCs according to acDC protocol. Experiment was performed once.

After stimulation, T cells were expanded for two weeks and activated with γ-irradiated autologous LCLs of patient Mel15 pulsed with defined peptides and sorted for activation marker CD137 expression. As visible from **Figure 28** no activated CD137^{+} TILs could be isolated.

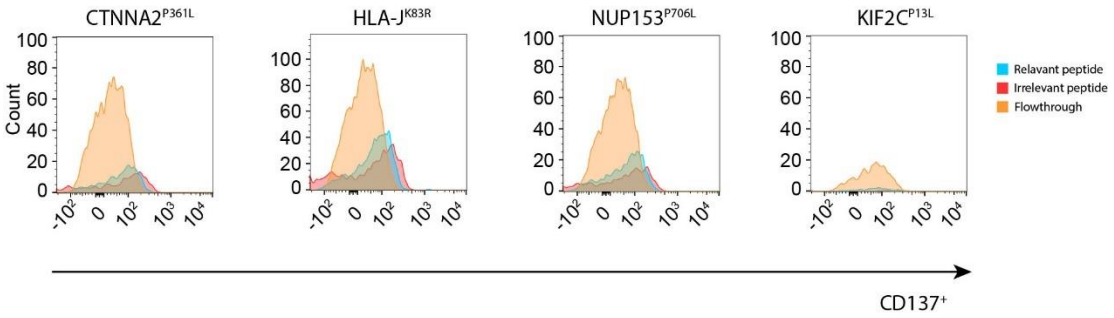

Figure 28. CD137 expression on TILs after stimulation with mutated pepitdes identified through Immunopeptidomics 2018. TILs reacting to mutated peptides were expanded and sorted according to expression of activation marker CD137 upon re-stimulation with peptide-pulsed target cells. As negative control, expanded TILs were stimulated with an irrelevant peptide. Flow-through consists of cells that were not retained by the magnetic column.

Discussion

The present dissertation evolved from a previously published research successfully identifying cancer neoantigens from metastatic melanoma patient Mel15. In this study Bassani-Sternberg et al. performed MS analysis, coupled with whole exome sequencing, on native resected tumor material. This led to the identification of eight mutated peptides from Mel15 intestinal metastasis, two of which (SYTL4^{S363F} and NCAPG2^{P333L}) were specifically recognized by autologous T-cell clones (Bassani-Sternberg et al., 2016).

The publication of this seminal piece of research prompted the question regarding the possibility to identify neoantigens potentially missed by MS, benefitting from previously acquired mutated exome sequences and bioinformatic analysis predicting HLA-peptide binding.

During the elaboration of the present dissertation the new neoantigen KIF2C^{P13L} was discovered based solely on in silico prediction analysis and could not be retrospectively identified within MS spectra from 2016 publication. This confirmed our initial hypothesis that MS analysis is still affected by technical limitations.

Moreover, two KIF2C^{P13L} reactive T-cell clones were isolated from Mel15 autologous repertoire and the TCR sequences were obtained. These receptors were in-depth characterized concurrently with four SYTL4^{S363F}- and one NCAPG2^{P333L}-specific TCRs, discovered by Dr. Bräunlein.

The characterization and comparison of in vitro and in vivo performances of seven neoantigen-specific TCRs, together with deep-sequencing data, allowed us to uncover interesting aspects and formulate hypotheses about their functionality in the patient. Particularly crucial were the results obtained from the TCR testing in the mouse model, that overthrew our initial assumptions deriving from in vitro data. In fact, cell culture experiments consistently showed a superiority of SYTL4^{S363F}-specific TCRs in terms of secreted cytokine levels, functional avidity and cytotoxicity potential.

However, in vivo experiments pointed out how other aspects might come into play and balance out for apparently less performant TCRs. Different activation profiles of the TCRs and reponse to sustained stimulation were highlighted by repeated in vitro stimulations and showed the tendency of higher avidity TCR to acquire a dysfunctional state.

These results were published on the prestigious *Journal for Immunotherapy of Cancer* (E. Bräunlein et al., 2021).

Hereafter, different considerations on neoantigen identification and TCR characterization.

1.39 Neoantigens

1.39.1 Neoantigen candidate selection and quality assessment

Currently there are three main approaches for the identification of neoantigens from tumor specimens: (1) *in silico* peptide prediction and prioritization, (2) LC-MS/MS based immunopeptidomics and (3)

unbiased immunogenicity screening of all somatic mutations from WES data (Garcia-Garijo et al., 2019).

Each one of these strategies presents advantages and drawbacks: in silico prediction relies on accuracy of algorithms, which are not equally trained for all existing HLA alleles; LC-MS/MS immunopeptidomics is limited by sensitivity of MS; immunogenicity testing of all mutations does not lead to a defined epitope and is not always feasible in presence of tumors with high mutation burden (Garcia-Garijo et al., 2019).

One of the aims of this work was to identify neoantigens in the form of defined epitopes in a patient affected by highly mutated melanoma and to investigate whether a different selection method, than MS applied to WES data, could confirm previously identified neoantigens and uncover more (Bassani-Sternberg et al., 2016). For this reason, the strategy of in silico peptide-HLA binding affinity prediction was pursued, followed by filtering and prioritization of candidate ligands according to different aspects.

To circumvent one of the limitations of prediction algorithms, the focus was kept on patient allotypes HLA-A03:01 and B27:05, rather than A68:01 and HLA-B35:03, as they are more frequent in the general population (http://www.allelefrequencies.net/); as a consequence, algorithms predicting binding affinity of ligands presented by these allotypes could be trained with more experimental data and are more reliable. Furthermore, only 9-mers were predicted and tested in this dissertation, as it was observed to be the most recurrent length for MHC class I ligands in general as well as in patient Mel15 eluted peptidome (Bassani-Sternberg et al., 2016; Trolle et al., 2016).

Predicting neoantigens from sequencing data or screening methods represents a major challenge. Particularly arduous is the prioritization of the peptides to validate, as it is becoming clear that binding affinity, and even more so predicted binding affinity, are alone not enough to predict peptide immunogenicity (Wells et al., 2020). However, with our prioritization method we were able to retrieve two neoantigens previously found with immunopeptidomics (Bassani-Sternberg et al., 2016) and we discovered a new one (E. Bräunlein et al., 2021). By testing only fifty peptides we would have therefore found three neoantigens, with the sole use of in silico affinity predictions. The fraction of "hits" on tested peptides was particularly favorable in this work. In many studies in fact, hundreds of peptides or mutations are tested for immunogenicity, with very few hits (Gros et al., 2016b; Linnemann et al., 2015; Eric Tran et al., 2015).

In the attempt to understand whether binding affinity could play a role in the immunogenicity of discovered neoantigens, affinity to the HLA allotypes was experimentally measured in the laboratory of Prof. Freund. The three tested neoantigens have similar affinities, while the corresponding wt peptides showed a wider range of affinities, which in two cases out of three was even higher than the related neoantigens (E. Bräunlein et al., 2021). For this reason, prioritization of mutated peptides with a higher affinity than the wt cognate peptides adopted by some groups (Duan et al., 2014; Ghorani et al., 2018;

Zhang et al., 2019) and advocated by the Tumor Neoantigen Selection Alliance (TESLA) (Wells et al., 2020) might miss valid candidates.

Another feature uniting all immunogenic peptides, according to TESLA, is the position of the mutation, which is never on the second amino acid (Wells et al., 2020). In our case, peptide NCAPG2^{P333L} presents the mutation in second position and was well recognized by the immune system of the patient.

Furthermore, no final neoantigen quality assessment could be made based on features such clonality or similarity to self (Nicholas McGranahan & Swanton, 2019). A quantification of neoantigen abundance or clonality might have helped in understanding whether there was a major player within identified neoantigens that mediated tumor remission in the studied patient. This analysis is not trivial when dealing with heterogenic solid tumor masses and can be pursued with multiregional sampling or targeted sequencing (Linette et al., 2019; N. McGranahan et al., 2016b). Clonality can also be estimated on bulk whole exome sequencing data, however it requires an intense bioinformatic work for normalization of factors such as sequencing depth and quality, tumor cellularity and mutation copy number (Cmero et al., 2020). These aspects were not considered, as the sequencing pipeline and the sampling strategy for this project were developed.

1.39.2 Immunoediting

The importance of identified neoantigens is proven by the evidence of immunoediting. As a matter of fact, the immunogenic neoantigen NCAPG2^{P333L} found in the first metastasis of the patient, was not detected in the second metastasis, supporting the elimination of the specific clones by T cells and outgrowth of other malignant clones. This has already been observed by other research groups in different metastatic cancers (Anagnostou et al., 2017; Matsushita et al., 2012; Rosenthal et al., 2019; Verdegaal et al., 2016).

Unfortunately it was not possible to trace identified neoantigens back to the tumor onset, as shown in patients affected by pancreatic ductal adenocarcinoma (Balachandran et al., 2017), due to scarce material from the primary tumor. This would have helped gain more insights on the development of the cancer and clonality of the mutations.

1.39.3 KIF2C^{P13L} eluded MS-guided peptide screening

Neoantigens SYTL4^{S363F} and NCAPG2^{P333L} had been identified from tumor specimens with the immunopeptidomic pipeline and their immunogenicity had been proven in the form of peptide as well as minigenes (Bassani-Sternberg et al., 2016).

As KIF2C^{P13L} neoantigen was identified from in silico predictions through immunogeniticy screening with synthetized peptides, it was necessary to prove its processing and presentation in antigen presenting cells carrying the HLA-allotypes of interest. Nevertheless, processing and presentation of a minigene alone can certainly not prove the presence of a neoantigen on the tumor surface.

To that end, the database containing peptides eluted from Mel15 cancer specimens and measured with MS was retrospectively interrogated by Dr. Pecoraro (AG Mann). Despite the favorable chemical properties of peptide KIF2C^{P13L} and the identification of the wt counterpart, the neoepitope could never be identified with certainty in this dataset.

Subsequently to the conclusion of this project, neoepitope KIF2C^{P13L} was identified from the tumor of the same patient by the group of Prof. Kuster after application of a new bioinformatic pipeline (Prosit) applied on the same MS spectra (Wilhelm et al., 2021).

1.39.4 Optimized immunopeptidomic pipeline 2018

In the attempt to identify more neoantigens coming from different sources, the group of Prof. Rad developed a new bioinformatic pipeline for mutation identification from WES and RNA-seq data. First aim of this new pipeline was to identify mutations in non-coding DNA sequences and therefore the inclusion of RNA-seq data, that covers transcribed portions of the genome, which do not belong to the exome. Second aim was to identify other mutations and not limit the search to SNVs.

By creating a custom database containing all these new mutations for MS spectra matching, 34 mutated peptides were identified, comprising seven out of the eight peptides identified in 2016 with the previous analysis (Bassani-Sternberg et al., 2016). For immunogenicity testing with autologous TILs 13 peptides were selected. A hint at immunogenicity of three new peptides was obtained, however it was not possible to isolate reactive T cells through sorting. One hypothesis could be that the T cells were too strongly activated and faced exhaustion instead of clonal expansion. The applied stimulation protocol remained constant throughout all experiments, however we speculated chosen peptide concentration (1µM) might be detrimental for the isolation of higher affinity TCRs.

The idea to search for alternative sources of neoantigens comes from the observation that the majority of cancer mutations lay in non-coding regions (Khurana et al., 2016) and that these can code for proteins which are then presented by the MHC complex (Laumont et al., 2016). It has been also proven that peptides deriving from non-coding regions are targeted by T cells (Kracht et al., 2017; Steven A. Rosenberg et al., 2002) and they can arise from different kinds of mutations such as indels, fusions, splice variants and other genetic variants (Bartel, Taubert, & Harris, 2002; Mertens, Antonescu, & Mitelman, 2016; Pellagatti et al., 2018; Turajlic et al., 2017; Y. Wang, Wu, Liu, & Jin, 2017).

For prioritization of the peptides to be tested, predicted MHC affinity and the presence of mutations in both RNA-seq and WES datasets were taken into consideration. Main drawback of using RNA sequencing data as a source for the identification of neoantigens was the lack of a perfectly suitable negative control, represented by healthy melanocytes, for the exclusion of false positives. On alternative approach could be the usage of thymic epithelial cells (Laumont et al., 2018), which express most genes, but is rarely available and may not be representative for our cohort. In addition, whole genome

sequencing data on a tissue of choice (e.g. PBMCs) may be used. In the present work, all peptides deriving from mutations found on transcriptome and not on the exome level were excluded for immunogenicity assessment due to limited numbers of TIL samples and the need for prioritization of the peptides. Although further validation of the performed analyses might be necessary, important parameters for ranking would be allele frequency with high read numbers and prediction analyses. Increase of sensitivity of immunopeptidomics analyses in the future may improve the detection of neoantigens by MS and broaden the candidate neoantigen repertoire.

1.40 TCRs

1.40.1 Comparison of the seven neoantigen-specific TCRs

Melanoma patient Mel15 case study offered the opportunity to perform an unprecedented in-depth characterization of seven neoantigen-specific TCRs. The characterization benefitted from the possibility to compare receptors with same origin, but different specificities and qualities. Through intensive in vitro and in vivo testing, we could learn plenty about the biological features of the TCRs.

TCR characterization, as well as, the evaluation of the patient's clinical history, extended our knowledge and contributed to corroborate other reports questioning the current consensus i.e. that effective adoptive T-cell therapy requires the transfer of T cells engineerd with high-avidity TCRs (Mackensen et al., 2006; C. Yee et al., 2002; Cassian Yee et al., 2000).

A direct comparison of all TCRs presented limitations. The most strinking one was the difference in transduction efficiency in primary T cells within the seven TCRs. This could not be overcome despite sequence modification and codon optimization of the native TCR chains. Retroviral transductions were performed always in parallel for all seven TCRs and led each time to slightly different percentages of transduced cells, although inter-TCR variability was always maintained.

Different transduction rates correlated with different surface expression levels of the transgenic TCRs. There are "dominant" TCRs like SYTL4-TIL1, SYTL4-PBC1 and KIF2C-PBC2, which are well expressed on the cell surface, and "subdominant" TCRs such as SYTL4-TIL2, SYTL4-PBC2 and KIF2C-PBC1, which appear to be less dense. A lower expression could be explained by competition with the endogenous TCR chains of transduced T cells, however, it was reported that difference in surface expression might represent an intrinsic quality of each TCR, depending on specific residues in the variable chains (Heemskerk et al., 2007; S. Thomas et al., 2019). This would be consistent with results from intracellular staining of transgenic beta chain, which showed no retaining of the TCRs, and with the fact that TCRs expression characteristics were replicated in different allogeneic donors.

In order to overcome different transduction rates, for functional experiments performed by Franziska Füchsl and reported in the scientific article about these TCRs, transduced T cells were enriched through

sorting, and effector cells were applied in equal numbers. In mouse experiments TCR-transgenic T cells were diluted with non-transduced T cells to reach a homogeneous number of effector cells for the different TCRs (E. Bräunlein et al., 2021).
Otherwise, differences in TCR transduction were regarded as a specific feature of the TCRs.

Another minor technical issue was presented by multimer staining of functional TCRs.
First experiments were performed with commercially available pentamers, which bound SYTL4-TIL1 and -PBC1 TCRs even when containing $SYTL4^{WT}$ peptide, which is contradictory to functional data. Multimer staining with tetramers produced by Prof. Dr. Dirk Busch was more specific, however all multimers failed in the detection of TCRs SYTL4-TIL2 and -PBC2. A possible explanation would be that the TCR avidity of these receptors was not high enough for the binding of multimers. TCR-affinity threshold required for staining with standard pMHC multimer protocols is in fact higher than that required for efficient T cell activation (Rius et al., 2018).

1.40.2 Functional discrepancies of neoantigen-specific TCRs in vitro and in vivo

Despite intense in vitro characterization of the seven neoantigen-specific TCRs, results of the mouse experiments came as a surprise (E. Bräunlein et al., 2021). In all in vitro assays a superiority of SYTL4-TCRs (except SYTL4-PBC2) was observed, in terms of IFN-γ secreted titers, functional avidity and cytotoxicity. In vivo experiment showed equal rejection potential for all TCRs (except SYTL4-TIL2), which significantly inhibited tumor growth, and even a better performance for KIF2C-PBC1 and SYTL4-PBC2. In order to allow a more direct comparison of TCR potentials, transduced cells were diluted to normalize transduction efficiencies and inject the same number of transgenic T cells. However, in the case of some TCRs (SYTL4-TIL2, KIF2C-PBC1 and NCAPG2-PBC1), transduction rate was so low, that less transgenic cells have been injected. For TCR SYTL4-TIL2 the amount of transgenic T cells injected was supposedly too low to trigger a response. For other TCRs, a relatively low initial number of transduced T cells still led to tumor control and rejection. In particular KIF2C-PBC1, injected in the lowest amount was the most powerful TCR, especially if compared to KIF2C-PBC2, which has the same target, is denser on T-cell surface and was injected in higher quantity (almost 6 times more). A second in vivo experiment was performed by Dr. Eva Bräunlein and Dario Gosmann with a higher number of transgenic neoantigen-specific TCR-T cells into a xonograft murine model bearing bilateral neoantigen expressing tumor. As control, T cells engineered with an unrelated TCR (Klar et al., 2014) were injected. Consistently to previous results, all neoantigen-specific TCRs showed significant tumor rejection potential compared to the control and prolonged survival of the mice. Inter-TCR differences were not significant, however KIF2C-TCRs were faster in mediating tumor shrinkage than SYTL4-TCRs. KIF2C-PBC1 was confirmed to be the most potent TCR, again despite the lower number of effector cells (E. Bräunlein et al., 2021).

Similar results were obtained Segal et al. in a non-Hodgkin B cell lymphoma mouse model and by Dougan et al. in a model of melanoma, where lower- and higher-affinity TCRs performed equally well in vivo, despite conflicting in vitro data (Dougan et al., 2013; G. Segal, Prato, Zehn, Mintern, & Villadangos, 2016). Possible hypotheses formulated by the authors are that in vivo conditions may improve cytotoxicity capacity of low-affinity clonotypes due to the cytokine microenvironment, the architecture of the lymphoid organs, and/or additional cell populations (G. Segal et al., 2016). This probably does not apply to our case, as both innate and adaptive immunity are heavily impaired in the adopted mouse model (E. Bräunlein et al., 2021).

Another interesting aspect is that higher TCR affinity can in some cases have a detrimental effect on T-cell activity, as it reduces the likelihood to undergo "serial triggering" and reach the activation threshold (Valitutti, Müller, Cella, Padovan, & Lanzavecchia, 1995). Furthermore, high-avidity interactions have the potential to evoke T cell apoptosis (Derby, Snyder, Tse, Alexander-Miller, & Berzofsky, 2001). This might explain why higher affinity TCRs are present at such low frequencies in the tumor and blood stream of Mel15 patient (E. Bräunlein et al., 2021; Oliveira et al., 2021) .
All these aspects might have been missed in in vitro experiments because of obvious technical and temporal reasons.

1.40.3 TCR-β deep sequencing and "orphan" receptors

TCR-β deep sequencing was performed on DNA extracted from the two metastases and sentinel lymph nodes (2014, 2016). Sequencing was also done on a lung biopsy (2013) and primary tumor (2008) in the attempt to have a picture of clones that expanded during the course of disease. Primary tumor and biopsy were very scarce material (100,000), therefore only few beta chains could be detected and frequencies are in a different range compared to other tissues. None of the investigated TCRs was found in the primary tumor, however KIF2C-PBC1 was found in the biopsy tissue. Despite this, two clonotypes were shared by primary tumor, biopsy and the two metastases, one of these being very abundant in M_{Int} (rank 7) and M_{Lung} (rank 17). Lung biopsy shares several clonotypes with the two metastases, three of them ranking among the first 4 most abundant in M_{Int} and one of them the most abundant in M_{Lung}. Shared clonotypes are certainly of great interest as they were localized in the tumor since the beginning of the disease and expand considerably in the metastases, implying that they might be tumor specific. Furthermore, some of the above mentioned clonotypes are also very abundant in peripheral blood. Clonotypes that expanded in blood between day 796 and 1120 during administration of Pembrolizumab might have been cancer reactive but the specificity could not be elucidated here.

Conclusion and future aspects

Within this work we succeeded in the identification a new neoantigen, through in silico affinity predictions and two TCRs specific to it, as well as, a comprehensive comparison of all receptors isolated from the same previously studied melanoma patient (Bassani-Sternberg et al., 2016).
Despite the limitations described above, an in-depth comparison of all analyzed TCRs and investigation of their functional features was feasible.
Collected data provided evidence that the TCRs with a lower functional avidity are at least as effective as higher avidity TCRs in preclinical models in vivo. The formers were also found at very high frequencies in the metastases and bloodstream of the patient. This prompted the hypothesis that T-cell clones carrying higher avidity TCRs might be more prone to exhaustion, which was indicated by subsequent experiments in vitro (E. Bräunlein et al., 2021).

In the future, efforts should be made to understand the interconnection between TCR affinity, avidity and epitope density. Besides, mechanisms compensating for lower avidity TCRs, resulting in an equal or better performance in vivo (e.g. “serial triggering”) should be further investigated. Ideal for this study would be to dispose of several TCRs with different avidities, but same specificity.

In conclusion, our work provided an unprecedented detailed characterization of neoantigen-specific TCRs, however more research and a multidisciplinary approach interfacing bioinformatics, biology and chemistry, will be needed to unravel the complexity of the TCR–pMHC interactions and contribute to the development of safer, more precise and effective adoptive T-cell cancer therapies.

References

Abramson, J. S., Palomba, M. L., Gordon, L. I., Lunning, M. A., Wang, M., Arnason, J., … Siddiqi, T. (2020). Lisocabtagene maraleucel for patients with relapsed or refractory large B-cell lymphomas (TRANSCEND NHL 001): a multicentre seamless design study. *The Lancet*, *396*(10254), 839–852. https://doi.org/10.1016/S0140-6736(20)31366-0

Ahmed, S., & Rai, K. R. (2003). Interferon in the treatment of hairy-cell leukemia. *Best Practice & Research Clinical Haematology*, *16*(1), 69–81. https://doi.org/10.1016/S1521-6926(02)00084-1

Allison, J. P., McIntyre, B. W., & Bloch, D. (1982). Tumor-specific antigen of murine T-lymphoma defined with monoclonal antibody. *Journal of Immunology (Baltimore, Md. : 1950)*, *129*(5), 2293–2300. Retrieved from http://www.ncbi.nlm.nih.gov/pubmed/6181166

Anagnostou, V., Smith, K. N., Forde, P. M., Niknafs, N., Bhattacharya, R., White, J., … Velculescu, V. E. (2017). Evolution of Neoantigen Landscape during Immune Checkpoint Blockade in Non–Small Cell Lung Cancer. *Cancer Discovery*, *7*(3), 264–276. https://doi.org/10.1158/2159-8290.CD-16-0828

Andreatta, M., & Nielsen, M. (2016). Gapped sequence alignment using artificial neural networks: application to the MHC class I system. *Bioinformatics*, *32*(4), 511–517. https://doi.org/10.1093/bioinformatics/btv639

Antoniou, A. N., Ford, S., Taurog, J. D., Butcher, G. W., & Powis, S. J. (2004). Formation of HLA-B27 Homodimers and Their Relationship to Assembly Kinetics. *Journal of Biological Chemistry*, *279*(10), 8895–8902. https://doi.org/10.1074/jbc.M311757200

Baitsch, L., Baumgaertner, P., Devêvre, E., Raghav, S. K., Legat, A., Barba, L., … Speiser, D. E. (2011). Exhaustion of tumor-specific CD8+ T cells in metastases from melanoma patients. *Journal of Clinical Investigation*, *121*(6), 2350–2360. https://doi.org/10.1172/JCI46102

Bajwa, R., Cheema, A., Khan, T., Amirpour, A., Paul, A., Chaughtai, S., … Hossain, M. A. (2019). Adverse Effects of Immune Checkpoint Inhibitors (Programmed Death-1 Inhibitors and Cytotoxic T-Lymphocyte-Associated Protein-4 Inhibitors): Results of a Retrospective Study. *Journal of Clinical Medicine Research*, *11*(4), 225–236. https://doi.org/10.14740/jocmr3750

Balachandran, V. P., Łuksza, M., Zhao, J. N., Makarov, V., Moral, J. A., Remark, R., … Leach, S. D. (2017). Identification of unique neoantigen qualities in long-term survivors of pancreatic cancer. *Nature*, *551*(7681), 512–516. https://doi.org/10.1038/nature24462

Bardhan, K., Anagnostou, T., & Boussiotis, V. A. (2016). The PD1:PD-L1/2 Pathway from Discovery to Clinical Implementation. *Frontiers in Immunology*, *7*. https://doi.org/10.3389/fimmu.2016.00550

Bartel, F., Taubert, H., & Harris, L. C. (2002). Alternative and aberrant splicing of MDM2 mRNA in human cancer. *Cancer Cell*, *2*(1), 9–15. https://doi.org/10.1016/S1535-6108(02)00091-0

Bassani-Sternberg, M., Bräunlein, E., Klar, R., Engleitner, T., Sinitcyn, P., Audehm, S., … Krackhardt, A. M. (2016). Direct identification of clinically relevant neoepitopes presented on native human melanoma tissue by mass spectrometry. *Nature Communications*, *7*(May). https://doi.org/10.1038/ncomms13404

Bassani-Sternberg, M., & Coukos, G. (2016). Mass spectrometry-based antigen discovery for cancer immunotherapy. *Current Opinion in Immunology*, *41*, 9–17. https://doi.org/10.1016/j.coi.2016.04.005

Benjamin, H., & Yiping, Y. (2018). New developments in immunotherapy for lymphoma. *Cancer Biology & Medicine*, *15*(3), 189. https://doi.org/10.20892/j.issn.2095-3941.2018.0037

Born, W., Yague, J., Palmer, E., Kappler, J., & Marrack, P. (1985). Rearrangement of T-cell receptor beta-chain genes during T-cell development. *Proceedings of the National Academy of Sciences*, *82*(9), 2925–2929. https://doi.org/10.1073/pnas.82.9.2925

Bräunlein, E., Lupoli, G., Füchsl, F., Abualrous, E. T., de Andrade Krätzig, N., Gosmann, D., … Krackhardt, A. M. (2021). Functional analysis of peripheral and intratumoral neoantigen-specific TCRs identified in a patient with melanoma. *Journal for ImmunoTherapy of Cancer*, *9*(9), e002754. https://doi.org/10.1136/jitc-2021-002754

Bräunlein, E. M. (2018). *Dissection of immune responses against naturally presented HLA ligands on native human melanoma identified by mass spectrometry*. Retrieved from http://nbn-resolving.de/urn/resolver.pl?urn:nbn:de:bvb:91-diss-20180514-1363150-1-3

Brunet, J.-F., Denizot, F., Luciani, M.-F., Roux-Dosseto, M., Suzan, M., Mattei, M.-G., & Golstein, P. (1987). A new member of the immunoglobulin superfamily—CTLA-4. *Nature*, *328*(6127), 267–270. https://doi.org/10.1038/328267a0

Burnet, M. (1957). Cancer: a biological approach. III. Viruses associated with neoplastic conditions. IV. Practical applications. *British Medical Journal*, *1*(5023), 841–847. https://doi.org/10.1136/bmj.1.5023.841

Burrows, S. R., Rossjohn, J., & McCluskey, J. (2006). Have we cut ourselves too short in mapping CTL epitopes? *Trends in Immunology*, *27*(1), 11–16. https://doi.org/10.1016/j.it.2005.11.001

Busch, D. H., Fräßle, S. P., Sommermeyer, D., Buchholz, V. R., & Riddell, S. R. (2016). Role of memory T cell subsets for adoptive immunotherapy. *Seminars in Immunology*, *28*(1), 28–34. https://doi.org/10.1016/j.smim.2016.02.001

Cafri, G., Yossef, R., Pasetto, A., Deniger, D. C., Lu, Y., Parkhurst, M., … Rosenberg, S. A. (2019). Memory T cells targeting oncogenic mutations detected in peripheral blood of epithelial cancer patients. *Nature Communications*, *10*(1), 449. https://doi.org/10.1038/s41467-019-08304-z

Chan, T. A., Yarchoan, M., Jaffee, E., Swanton, C., Quezada, S. A., Stenzinger, A., & Peters, S. (2019). Development of tumor mutation burden as an immunotherapy biomarker: utility for the oncology clinic. *Annals of Oncology*, *30*(1), 44–56. https://doi.org/10.1093/annonc/mdy495

Cibulskis, K., Lawrence, M. S., Carter, S. L., Sivachenko, A., Jaffe, D., Sougnez, C., … Getz, G. (2013). Sensitive detection of somatic point mutations in impure and heterogeneous cancer samples. *Nature Biotechnology*, *31*(3), 213–219. https://doi.org/10.1038/nbt.2514

Cmero, M., Yuan, K., Ong, C. S., Schröder, J., Corcoran, N. M., Papenfuss, T., … Macintyre, G. (2020). Inferring structural variant cancer cell fraction. *Nature Communications*, *11*(1), 730. https://doi.org/10.1038/s41467-020-14351-8

Cohen, C. J., Gartner, J. J., Horovitz-fried, M., Shamalov, K., Trebska-mcgowan, K., Bliskovsky, V. V, … Robbins, P. F. (2015). *Isolation of neoantigen-specific T cells from tumor and peripheral lymphocytes*. *125*(10), 3981–3991. https://doi.org/10.1172/JCI82416DS1.

Cohen, C. J., Zheng, Z., Bray, R., Zhao, Y., Sherman, L. A., Rosenberg, S. A., & Morgan, R. A. (2005). Recognition of Fresh Human Tumor by Human Peripheral Blood Lymphocytes Transduced with a Bicistronic Retroviral Vector Encoding a Murine Anti-p53 TCR. *The Journal of Immunology*, *175*(9), 5799–5808. https://doi.org/10.4049/jimmunol.175.9.5799

Coley, W. B. (1910). The Treatment of Inoperable Sarcoma by Bacterial Toxins (the Mixed Toxins of the Streptococcus erysipelas and the Bacillus prodigiosus). *Proceedings of the Royal Society of Medicine*, *3*(Surg Sect), 1–48. Retrieved from http://www.ncbi.nlm.nih.gov/pubmed/19974799

Coley, W. B. (1991). The treatment of malignant tumors by repeated inoculations of erysipelas. With a report of ten original cases. 1893. *Clinical Orthopaedics and Related Research*, (262), 3–11.

Retrieved from http://www.ncbi.nlm.nih.gov/pubmed/1984929

Couzin-Frankel, J. (2013). Cancer Immunotherapy. *Science*, *342*(6165), 1432–1433. https://doi.org/10.1126/science.342.6165.1432

Danaher, P., Warren, S., Lu, R., Samayoa, J., Sullivan, A., Pekker, I., … Cesano, A. (2018). Pan-cancer adaptive immune resistance as defined by the Tumor Inflammation Signature (TIS): results from The Cancer Genome Atlas (TCGA). *Journal for Immunotherapy of Cancer*, *6*(1), 63. https://doi.org/10.1186/s40425-018-0367-1

De Mattos-Arruda, L., Vazquez, M., Finotello, F., Lepore, R., Porta, E., Hundal, J., … Griffith, M. (2020). Neoantigen prediction and computational perspectives towards clinical benefit: recommendations from the ESMO Precision Medicine Working Group. *Annals of Oncology*, *31*(8), 978–990. https://doi.org/10.1016/j.annonc.2020.05.008

Derby, M. A., Snyder, J. T., Tse, R., Alexander-Miller, M. A., & Berzofsky, J. A. (2001). An abrupt and concordant initiation of apoptosis: antigen-dependent death of CD8+ CTL. *European Journal of Immunology*, *31*(10), 2951–2959. https://doi.org/10.1002/1521-4141(2001010)31:10<2951::aid-immu2951>3.0.co;2-q

Dougan, S. K., Dougan, M., Kim, J., Turner, J. A., Ogata, S., Cho, H.-I., … Ploegh, H. L. (2013). Transnuclear TRP1-Specific CD8 T Cells with High or Low Affinity TCRs Show Equivalent Antitumor Activity. *Cancer Immunology Research*, *1*(2), 99–111. https://doi.org/10.1158/2326-6066.CIR-13-0047

Duan, F., Duitama, J., Al Seesi, S., Ayres, C. M., Corcelli, S. A., Pawashe, A. P., … Srivastava, P. K. (2014). Genomic and bioinformatic profiling of mutational neoepitopes reveals new rules to predict anticancer immunogenicity. *Journal of Experimental Medicine*, *211*(11), 2231–2248. https://doi.org/10.1084/jem.20141308

Dudley, M. E. (2002). Cancer Regression and Autoimmunity in Patients After Clonal Repopulation with Antitumor Lymphocytes. *Science*, *298*(5594), 850–854. https://doi.org/10.1126/science.1076514

Engels, B., Noessner, E., Frankenberger, B., Blankenstein, T., Schendel, D. J., & Uckert, W. (2005). Redirecting human T lymphocytes toward renal cell carcinoma specificity by retroviral transfer of T cell receptor genes. *Human Gene Therapy*, *16*(7), 799–810. https://doi.org/10.1089/hum.2005.16.799

FDA Approves Second CAR T-cell Therapy. (2018). *Cancer Discovery*, *8*(1), 5–6. https://doi.org/10.1158/2159-8290.CD-NB2017-155

Ferrier, P., Krippl, B., Blackwell, T. K., Furley, A. J., Suh, H., Winoto, A., … Alt, F. W. (1990). Separate elements control DJ and VDJ rearrangement in a transgenic recombination substrate. *The EMBO Journal*, *9*(1), 117–125. https://doi.org/10.1002/j.1460-2075.1990.tb08087.x

Freeman, G. J., Long, A. J., Iwai, Y., Bourque, K., Chernova, T., Nishimura, H., … Honjo, T. (2000). Engagement of the Pd-1 Immunoinhibitory Receptor by a Novel B7 Family Member Leads to Negative Regulation of Lymphocyte Activation. *Journal of Experimental Medicine*, *192*(7), 1027–1034. https://doi.org/10.1084/jem.192.7.1027

Garcia-Garijo, A., Fajardo, C. A., & Gros, A. (2019). Determinants for Neoantigen Identification. *Frontiers in Immunology*, *10*(JUN), 1–19. https://doi.org/10.3389/fimmu.2019.01392

Ghorani, E., Rosenthal, R., McGranahan, N., Reading, J. L., Lynch, M., Peggs, K. S., … Quezada, S. A. (2018). Differential binding affinity of mutated peptides for MHC class I is a predictor of survival in advanced lung cancer and melanoma. *Annals of Oncology*, *29*(1), 271–279. https://doi.org/10.1093/annonc/mdx687

1296 Gillis, S., & Smith, K. A. (1977). Long term culture of tumour-specific cytotoxic T cells. *Nature*,
1297 *268*(5616), 154–156. https://doi.org/10.1038/268154a0

1298 Gros, A., Parkhurst, M. R., Tran, E., Pasetto, A., Robbins, P. F., Ilyas, S., … Rosenberg, S. A.
1299 (2016a). Prospective identification of neoantigen-specific lymphocytes in the peripheral blood of
1300 melanoma patients. *Nature Medicine*, *22*(4), 433–438. https://doi.org/10.1038/nm.4051

1301 Gros, A., Parkhurst, M. R., Tran, E., Pasetto, A., Robbins, P. F., Ilyas, S., … Rosenberg, S. A.
1302 (2016b). Prospective identification of neoantigen-specific lymphocytes in the peripheral blood of
1303 melanoma patients. *Nature Medicine*, *22*(4), 433–438. https://doi.org/10.1038/nm.4051

1304 Gros, A., Robbins, P. F., Yao, X., Li, Y. F., Turcotte, S., Tran, E., … Rosenberg, S. A. (2014). PD-1
1305 identifies the patient-specific CD8+ tumor-reactive repertoire infiltrating human tumors. *Journal*
1306 *of Clinical Investigation*, *124*(5), 2246–2259. https://doi.org/10.1172/JCI73639

1307 Gross, G., Waks, T., & Eshhar, Z. (1989). Expression of immunoglobulin-T-cell receptor chimeric
1308 molecules as functional receptors with antibody-type specificity. *Proceedings of the National*
1309 *Academy of Sciences of the United States of America*, *86*(24), 10024–10028.
1310 https://doi.org/10.1073/pnas.86.24.10024

1311 Gubin, M. M., Zhang, X., Schuster, H., Caron, E., Ward, J. P., Noguchi, T., … Schreiber, R. D.
1312 (2014). Checkpoint blockade cancer immunotherapy targets tumour-specific mutant antigens.
1313 *Nature*, *515*(7528), 577–581. https://doi.org/10.1038/nature13988

1314 Haen, S. P., & Löffler, M. W. (2020). Towards new horizons: characterization, classification and
1315 implications of the tumour antigenic repertoire. *Nature Reviews Clinical Oncology*, *17*(October),
1316 595–610. https://doi.org/10.1038/s41571-020-0387-x

1317 Heemskerk, M. H. M., Hagedoorn, R. S., van der Hoorn, M. A. W. G., van der Veken, L. T.,
1318 Hoogeboom, M., Kester, M. G. D., … Falkenburg, J. H. F. (2007). Efficiency of T-cell receptor
1319 expression in dual-specific T cells is controlled by the intrinsic qualities of the TCR chains
1320 within the TCR-CD3 complex. *Blood*, *109*(1), 235–243. https://doi.org/10.1182/blood-2006-03-
1321 013318

1322 Hodi, S. F., O'Day, S. J., McDermott, D. F., Weber, R. W., Sosman, J. A., Haanen, J. B., … Urba, W.
1323 J. (2010). Improved Survival with Ipilimumab in Patients with Metastatic Melanoma List of
1324 authors. *New England Journal of Medicine*, 711–723. https://doi.org/10.1056/NEJMoa1003466

1325 Hughes, M. S., Yu, Y. Y. L., Dudley, M. E., Zheng, Z., Robbins, P. F., Li, Y., … Morgan, R. A.
1326 (2005). Transfer of a TCR Gene Derived from a Patient with a Marked Antitumor Response
1327 Conveys Highly Active T-Cell Effector Functions. *Human Gene Therapy*, *16*(4), 457–472.
1328 https://doi.org/10.1089/hum.2005.16.457

1329 Hwang, S., Kim, E., Lee, I., & Marcotte, E. M. (2015). Systematic comparison of variant calling
1330 pipelines using gold standard personal exome variants. *Scientific Reports*, *5*(1), 17875.
1331 https://doi.org/10.1038/srep17875

1332 Irving, B. A., & Weiss, A. (1991). The cytoplasmic domain of the T cell receptor ζ chain is sufficient
1333 to couple to receptor-associated signal transduction pathways. *Cell*, *64*(5), 891–901.
1334 https://doi.org/10.1016/0092-8674(91)90314-O

1335 Ishida, Y., Agata, Y., Shibahara, K., & Honjo, T. (1992). Induced expression of PD-1, a novel member
1336 of the immunoglobulin gene superfamily, upon programmed cell death. *The EMBO Journal*,
1337 *11*(11), 3887–3895. https://doi.org/10.1002/j.1460-2075.1992.tb05481.x

1338 Jäger, E., Chen, Y.-T., Drijfhout, J. W., Karbach, J., Ringhoffer, M., Jäger, D., … Knuth, A. (1998).
1339 Simultaneous Humoral and Cellular Immune Response against Cancer–Testis Antigen NY-ESO-
1340 1: Definition of Human Histocompatibility Leukocyte Antigen (HLA)-A2–binding Peptide

Epitopes. *Journal of Experimental Medicine*, *187*(2), 265–270. https://doi.org/10.1084/jem.187.2.265

Jassim, A., Ollier, W., Payne, A., Biro, A., Oliver, R. T. D., & Festenstein, H. (1989). Analysis of HLA antigens on germ cells in human semen. *European Journal of Immunology*, *19*(7), 1215–1220. https://doi.org/10.1002/eji.1830190710

Jiang, X., Xu, J., Liu, M., Xing, H., Wang, Z., Huang, L., … Wu, S. (2019). Adoptive CD8+ T cell therapy against cancer:Challenges and opportunities. *Cancer Letters*, *462*, 23–32. https://doi.org/10.1016/j.canlet.2019.07.017

Johnson, L. A., Heemskerk, B., Powell, D. J., Cohen, C. J., Morgan, R. A., Dudley, M. E., … Rosenberg, S. A. (2006). Gene Transfer of Tumor-Reactive TCR Confers Both High Avidity and Tumor Reactivity to Nonreactive Peripheral Blood Mononuclear Cells and Tumor-Infiltrating Lymphocytes. *The Journal of Immunology*, *177*(9), 6548–6559. https://doi.org/10.4049/jimmunol.177.9.6548

June, C. H., Warshauer, J. T., & Bluestone, J. A. (2017). Is autoimmunity the Achilles' heel of cancer immunotherapy? *Nature Medicine*, *23*(5), 540–547. https://doi.org/10.1038/nm.4321

Jurtz, V. I., & Olsen, L. R. (2019). *Computational Methods for Identification of T Cell Neoepitopes in Tumors*. https://doi.org/10.1007/978-1-4939-8868-6_9

Kalaora, S., Barnea, E., Merhavi-Shoham, E., Qutob, N., Teer, J. K., Shimony, N., … Samuels, Y. (2016). Use of HLA peptidomics and whole exome sequencing to identify human immunogenic neo-antigens. *Oncotarget*, *7*(5), 5110–5117. https://doi.org/10.18632/oncotarget.6960

Kappler, J., Kubo, R., Haskins, K., Hannum, C., Marrack, P., Pigeon, M., … Trowbridge, I. (1983). The major histocompatibility complex-restricted antigen receptor on T cells in mouse and man: Identification of constant and variable peptides. *Cell*, *35*(1), 295–302. https://doi.org/10.1016/0092-8674(83)90232-5

Khurana, E., Fu, Y., Chakravarty, D., Demichelis, F., Rubin, M. A., & Gerstein, M. (2016). Role of non-coding sequence variants in cancer. *Nature Reviews Genetics*, *17*(2), 93–108. https://doi.org/10.1038/nrg.2015.17

Kim, S., Scheffler, K., Halpern, A. L., Bekritsky, M. A., Noh, E., Källberg, M., … Saunders, C. T. (2018). Strelka2: fast and accurate calling of germline and somatic variants. *Nature Methods*, *15*(8), 591–594. https://doi.org/10.1038/s41592-018-0051-x

Klar, R., Schober, S., Rami, M., Mall, S., Merl, J., Hauck, S. M., … Krackhardt, a M. (2014). Therapeutic targeting of naturally presented myeloperoxidase-derived HLA peptide ligands on myeloid leukemia cells by TCR-transgenic T cells. *Leukemia*, (October 2013), 1–12. https://doi.org/10.1038/leu.2014.131

Klebanoff, C. A., & Wolchok, J. D. (2018). Shared cancer neoantigens: Making private matters public. *Journal of Experimental Medicine*, *215*(1), 5–7. https://doi.org/10.1084/jem.20172188

Klein, L., Kyewski, B., Allen, P. M., & Hogquist, K. A. (2014). Positive and negative selection of the T cell repertoire: what thymocytes see (and don't see). *Nature Reviews Immunology*, *14*(6), 377–391. https://doi.org/10.1038/nri3667

Kracht, M. J. L., van Lummel, M., Nikolic, T., Joosten, A. M., Laban, S., van der Slik, A. R., … Roep, B. O. (2017). Autoimmunity against a defective ribosomal insulin gene product in type 1 diabetes. *Nature Medicine*, *23*(4), 501–507. https://doi.org/10.1038/nm.4289

Kuball, J., Dossett, M. L., Wolfl, M., Ho, W. Y., Voss, R.-H., Fowler, C., & Greenberg, P. D. (2007). Facilitating matched pairing and expression of TCR chains introduced into human T cells. *Blood*, *109*(6), 2331–2338. https://doi.org/10.1182/blood-2006-05-023069

Kuwana, Y., Asakura, Y., Utsunomiya, N., Nakanishi, M., Arata, Y., Itoh, S., … Kurosawa, Y. (1987). Expression of chimeric receptor composed of immunoglobulin-derived V resions and T-cell receptor-derived C regions. *Biochemical and Biophysical Research Communications*, *149*(3), 960–968. https://doi.org/10.1016/0006-291X(87)90502-X

Laumont, C. M., Daouda, T., Laverdure, J.-P., Bonneil, É., Caron-Lizotte, O., Hardy, M.-P., … Perreault, C. (2016). Global proteogenomic analysis of human MHC class I-associated peptides derived from non-canonical reading frames. *Nature Communications*, *7*(1), 10238. https://doi.org/10.1038/ncomms10238

Laumont, C. M., Vincent, K., Hesnard, L., Audemard, É., Bonneil, É., Laverdure, J.-P., … Perreault, C. (2018). Noncoding regions are the main source of targetable tumor-specific antigens. *Science Translational Medicine*, *10*(470). https://doi.org/10.1126/scitranslmed.aau5516

Leach, D. R., Krummel, M. F., & Allison, J. P. (1996). Enhancement of Antitumor Immunity by CTLA-4 Blockade. *Science*, *271*(5256), 1734–1736. https://doi.org/10.1126/science.271.5256.1734

Linette, G. P., Becker-Hapak, M., Skidmore, Z. L., Baroja, M. L., Xu, C., Hundal, J., … Carreno, B. M. (2019). Immunological ignorance is an enabling feature of the oligo-clonal T cell response to melanoma neoantigens. *Proceedings of the National Academy of Sciences*, *116*(47), 23662–23670. https://doi.org/10.1073/pnas.1906026116

Linnemann, C., van Buuren, M. M., Bies, L., Verdegaal, E. M. E., Schotte, R., Calis, J. J. A., … Schumacher, T. N. M. (2015). High-throughput epitope discovery reveals frequent recognition of neo-antigens by CD4+ T cells in human melanoma. *Nature Medicine*, *21*(1), 81–85. https://doi.org/10.1038/nm.3773

Locke, F. L., Ghobadi, A., Jacobson, C. A., Miklos, D. B., Lekakis, L. J., Oluwole, O. O., … Neelapu, S. S. (2019). Long-term safety and activity of axicabtagene ciloleucel in refractory large B-cell lymphoma (ZUMA-1): a single-arm, multicentre, phase 1–2 trial. *The Lancet Oncology*, *20*(1), 31–42. https://doi.org/10.1016/S1470-2045(18)30864-7

Mackensen, A., Meidenbauer, N., Vogl, S., Laumer, M., Berger, J., & Andreesen, R. (2006). Phase I study of adoptive T-cell therapy using antigen-specific CD8+ T cells for the treatment of patients with metastatic melanoma. *Journal of Clinical Oncology : Official Journal of the American Society of Clinical Oncology*, *24*(31), 5060–5069. https://doi.org/10.1200/JCO.2006.07.1100

Martinuzzi, E., Afonso, G., Gagnerault, M., Naselli, G., Mittag, D., Boitard, C., … Mallone, R. (2011). acDCs enhance human antigen – specific T-cell responses. *Blood*, *118*(8), 2128–2137. https://doi.org/10.1182/blood-2010-12-326231.The

Matsumura, M., Fremont, D. H., Peterson, P. A., & Wilson, Ian A. (1992). Emerging Principles for the Recognition of Peptide Antigens by MHC Class I Molecules. *Science*, *257*(5072), 927–934. https://doi.org/10.1126/science.1323878

Matsushita, H., Vesely, M. D., Koboldt, D. C., Rickert, C. G., Uppaluri, R., Magrini, V. J., … Schreiber, R. D. (2012). Cancer exome analysis reveals a T-cell-dependent mechanism of cancer immunoediting. *Nature*, *482*(7385), 400–404. https://doi.org/10.1038/nature10755

Maude, S. L., Laetsch, T. W., Buechner, J., Rives, S., Boyer, M., Bittencourt, H., … Grupp, S. A. (2018). Tisagenlecleucel in Children and Young Adults with B-Cell Lymphoblastic Leukemia. *New England Journal of Medicine*, *378*(5), 439–448. https://doi.org/10.1056/NEJMoa1709866

McDonald, K.-A., Kawaguchi, T., Qi, Q., Peng, X., Asaoka, M., Young, J., … Takabe, K. (2019). Tumor Heterogeneity Correlates with Less Immune Response and Worse Survival in Breast Cancer Patients. *Annals of Surgical Oncology*, *26*(7), 2191–2199. https://doi.org/10.1245/s10434-019-07338-3

1432 Mcgranahan, N., Furness, A. J. S., Rosenthal, R., Ramskov, S., Lyngaa, R., Saini, K., … Karl, S.
1433 (2016). *Clonal neoantigens elicit T cell immunoreactivity and sensitivity to immune checkpoint*
1434 *blockade*. *490*(March), 1–11.

1435 McGranahan, N., Furness, A. J. S., Rosenthal, R., Ramskov, S., Lyngaa, R., Saini, S. K., … Swanton,
1436 C. (2016a). Clonal neoantigens elicit T cell immunoreactivity and sensitivity to immune
1437 checkpoint blockade. *Science*, *351*(6280), 1463–1469. https://doi.org/10.1126/science.aaf1490

1438 McGranahan, N., Furness, A. J. S., Rosenthal, R., Ramskov, S., Lyngaa, R., Saini, S. K., … Swanton,
1439 C. (2016b). Clonal neoantigens elicit T cell immunoreactivity and sensitivity to immune
1440 checkpoint blockade. *Science*, *351*(6280), 1463–1469. https://doi.org/10.1126/science.aaf1490

1441 McGranahan, Nicholas, & Swanton, C. (2017). Clonal Heterogeneity and Tumor Evolution: Past,
1442 Present, and the Future. *Cell*, *168*(4), 613–628. https://doi.org/10.1016/j.cell.2017.01.018

1443 McGranahan, Nicholas, & Swanton, C. (2019). Neoantigen quality, not quantity. *Science*
1444 *Translational Medicine*, *11*(506). https://doi.org/10.1126/scitranslmed.aax7918

1445 Mertens, F., Antonescu, C. R., & Mitelman, F. (2016). Gene fusions in soft tissue tumors: Recurrent
1446 and overlapping pathogenetic themes. *Genes, Chromosomes and Cancer*, *55*(4), 291–310.
1447 https://doi.org/10.1002/gcc.22335

1448 Mezzanzanica, D., Canevari, S., Mazzoni, A., Figini, M., Colnaghi, M. I., Waks, T., … Eshhar, Z.
1449 (n.d.). Transfer of chimeric receptor gene made of variable regions of tumor-specific antibody
1450 confers anticarbohydrate specificity on T cells. *Cancer Gene Therapy*, *5*(6), 401–407. Retrieved
1451 from http://www.ncbi.nlm.nih.gov/pubmed/9917095

1452 Miao, D., Margolis, C. A., Vokes, N. I., Liu, D., Taylor-Weiner, A., Wankowicz, S. M., … Van Allen,
1453 E. M. (2018). Genomic correlates of response to immune checkpoint blockade in microsatellite-
1454 stable solid tumors. *Nature Genetics*, *50*(9), 1271–1281. https://doi.org/10.1038/s41588-018-
1455 0200-2

1456 Migden, M. R., Khushalani, N. I., Chang, A. L. S., Lewis, K. D., Schmults, C. D., Hernandez-Aya, L.,
1457 … Rischin, D. (2020). Cemiplimab in locally advanced cutaneous squamous cell carcinoma:
1458 results from an open-label, phase 2, single-arm trial. *The Lancet Oncology*, *21*(2), 294–305.
1459 https://doi.org/10.1016/S1470-2045(19)30728-4

1460 Morales, A., Eidinger, D., & Bruce, A. W. (1976). Intracavitary Bacillus Calmette-guerin in the
1461 Treatment of Superficial Bladder Tumors. *Journal of Urology*, *116*(2), 180–182.
1462 https://doi.org/10.1016/S0022-5347(17)58737-6

1463 Morgan, D., Ruscetti, F., & Gallo, R. (1976). Selective in vitro growth of T lymphocytes from normal
1464 human bone marrows. *Science*, *193*(4257), 1007–1008. https://doi.org/10.1126/science.181845

1465 Morgan, R. A., Dudley, M. E., Wunderlich, J. R., Hughes, M. S., Yang, J. C., Sherry, R. M., …
1466 Rosenberg, S. A. (2006). Cancer Regression in Patients After Transfer of Genetically Engineered
1467 Lymphocytes. *Science*, *314*(5796), 126–129. https://doi.org/10.1126/science.1129003

1468 Munn, D. H., & Bronte, V. (2017). *HHS Public Access*. 1–6.
1469 https://doi.org/10.1016/j.coi.2015.10.009.Immune

1470 Munshi, N. C., Anderson, L. D., Shah, N., Madduri, D., Berdeja, J., Lonial, S., … San-Miguel, J.
1471 (2021). Idecabtagene Vicleucel in Relapsed and Refractory Multiple Myeloma. *New England*
1472 *Journal of Medicine*, *384*(8), 705–716. https://doi.org/10.1056/NEJMoa2024850

1473 Murciano-Goroff, Y. R., Warner, A. B., & Wolchok, J. D. (2020). The future of cancer
1474 immunotherapy: microenvironment-targeting combinations. *Cell Research*, *30*(6), 507–519.
1475 https://doi.org/10.1038/s41422-020-0337-2

Nakamura, T., Shirouzu, T., Nakata, K., Yoshimura, N., & Ushigome, H. (2019). The Role of Major Histocompatibility Complex in Organ Transplantation- Donor Specific Anti-Major Histocompatibility Complex Antibodies Analysis Goes to the Next Stage -. *International Journal of Molecular Sciences*, *20*(18), 4544. https://doi.org/10.3390/ijms20184544

Nishimura, H. (2001). Autoimmune Dilated Cardiomyopathy in PD-1 Receptor-Deficient Mice. *Science*, *291*(5502), 319–322. https://doi.org/10.1126/science.291.5502.319

O'Rawe, J., Jiang, T., Sun, G., Wu, Y., Wang, W., Hu, J., … Lyon, G. J. (2013). Low concordance of multiple variant-calling pipelines: practical implications for exome and genome sequencing. *Genome Medicine*, *5*(3), 28. https://doi.org/10.1186/gm432

Ogasawara, K., Dodds, M., Mack, T., Lymp, J., Dell'Aringa, J., & Smith, J. (2021). Population Cellular Kinetics of Lisocabtagene Maraleucel, an Autologous CD19-Directed Chimeric Antigen Receptor T-Cell Product, in Patients with Relapsed/Refractory Large B-Cell Lymphoma. *Clinical Pharmacokinetics*. https://doi.org/10.1007/s40262-021-01039-5

Oliveira, G., Stromhaug, K., Klaeger, S., Kula, T., Frederick, D. T., Le, P. M., … Wu, C. J. (2021). Phenotype, specificity and avidity of antitumour CD8+ T cells in melanoma. *Nature*, *596*(7870), 119–125. https://doi.org/10.1038/s41586-021-03704-y

Pardoll, D. M. (2012). The blockade of immune checkpoints in cancer immunotherapy. *Nature Publishing Group*, *12*(4), 252–264. https://doi.org/10.1038/nrc3239

Parkhurst, M. R., Yang, J. C., Langan, R. C., Dudley, M. E., Nathan, D.-A. N., Feldman, S. A., … Rosenberg, S. A. (2011). T Cells Targeting Carcinoembryonic Antigen Can Mediate Regression of Metastatic Colorectal Cancer but Induce Severe Transient Colitis. *Molecular Therapy*, *19*(3), 620–626. https://doi.org/10.1038/mt.2010.272

Pellagatti, A., Armstrong, R. N., Steeples, V., Sharma, E., Repapi, E., Singh, S., … Boultwood, J. (2018). Impact of spliceosome mutations on RNA splicing in myelodysplasia: dysregulated genes/pathways and clinical associations. *Blood*, *132*(12), 1225–1240. https://doi.org/10.1182/blood-2018-04-843771

Rathe, S. K., Popescu, F. E., Johnson, J. E., Watson, A. L., Marko, T. A., Moriarity, B. S., … Largaespada, D. A. (2019). Identification of candidate neoantigens produced by fusion transcripts in human osteosarcomas. *Scientific Reports*, *9*(1), 358. https://doi.org/10.1038/s41598-018-36840-z

Renkvist, N., Castelli, C., Robbins, P. F., & Parmiani, G. (2001). A listing of human tumor antigens recognized by T cells. *Cancer Immunology, Immunotherapy : CII*, *50*(1), 3–15. https://doi.org/10.1007/s002620000169

Restifo, N. P., Smyth, M. J., & Snyder, A. (2016). Acquired resistance to immunotherapy and future challenges. *Nature Reviews Cancer*, *16*(2), 121–126. https://doi.org/10.1038/nrc.2016.2

Reuben, A., Spencer, C. N., Prieto, P. A., Gopalakrishnan, V., Reddy, S. M., Miller, J. P., … Wargo, J. A. (2017). Genomic and immune heterogeneity are associated with differential responses to therapy in melanoma. *Npj Genomic Medicine*, *2*(1), 10. https://doi.org/10.1038/s41525-017-0013-8

Ribas, A., & Wolchok, J. D. (2018). Cancer immunotherapy using checkpoint blockade. *Science*, *359*(6382), 1350–1355. https://doi.org/10.1126/science.aar4060

Richters, M. M., Xia, H., Campbell, K. M., Gillanders, W. E., Griffith, O. L., & Griffith, M. (2019). Best practices for bioinformatic characterization of neoantigens for clinical utility. *Genome Medicine*, *11*(1), 56. https://doi.org/10.1186/s13073-019-0666-2

Riley, R. S., June, C. H., Langer, R., & Mitchell, M. J. (2019). Delivery technologies for cancer

immunotherapy. *Nature Reviews Drug Discovery*, *18*(3), 175–196. https://doi.org/10.1038/s41573-018-0006-z

Rius, C., Attaf, M., Tungatt, K., Bianchi, V., Legut, M., Bovay, A., … Sewell, A. K. (2018). Peptide–MHC Class I Tetramers Can Fail To Detect Relevant Functional T Cell Clonotypes and Underestimate Antigen-Reactive T Cell Populations. *The Journal of Immunology*, *200*(7), 2263–2279. https://doi.org/10.4049/jimmunol.1700242

Rizvi, N. A., Hellmann, M. D., Snyder, A., Kvistborg, P., Makarov, V., Havel, J. J., … Chan, T. A. (2015). Mutational landscape determines sensitivity to PD-1 blockade in non-small cell lung cancer. *Science*, *348*(6230), 124–128. https://doi.org/10.1126/science.aaa1348

Robbins, P. F., Lu, Y., El-gamil, M., Li, Y. F., Gross, C., Lin, J. C., … Rosenberg, S. A. (2013). Mining Exomic Sequencing Data to Identify Mutaded Antigens Recognized by Adoptively Transferred Tumor-reactive cells. *Nature Medicine*, *19*(6), 747–752. https://doi.org/10.1038/nm.3161.Mining

Rooney, M. S., Shukla, S. A., Wu, C. J., Getz, G., & Hacohen, N. (2015). Molecular and Genetic Properties of Tumors Associated with Local Immune Cytolytic Activity. *Cell*, *160*(1–2), 48–61. https://doi.org/10.1016/j.cell.2014.12.033

Rosenberg, S. A., Yang, J. C., Sherry, R. M., Kammula, U. S., Hughes, M. S., Phan, G. Q., … Dudley, M. E. (2011). Durable Complete Responses in Heavily Pretreated Patients with Metastatic Melanoma Using T-Cell Transfer Immunotherapy. *Clinical Cancer Research*, *17*(13), 4550–4557. https://doi.org/10.1158/1078-0432.CCR-11-0116

Rosenberg, S. A., Yannelli, J. R., Yang, J. C., Topalian, S. L., Schwartzentruber, D. J., Weber, J. S., … White, D. E. (1994). Treatment of Patients With Metastatic Melanoma With Autologous Tumor-Infiltrating Lymphocytes and Interleukin 2. *JNCI Journal of the National Cancer Institute*, *86*(15), 1159–1166. https://doi.org/10.1093/jnci/86.15.1159

Rosenberg, Steven A., Lotze, M. T., Muul, L. M., Leitman, S., Chang, A. E., Ettinghausen, S. E., … Reichert, C. M. (1985). Observations on the Systemic Administration of Autologous Lymphokine-Activated Killer Cells and Recombinant Interleukin-2 to Patients with Metastatic Cancer. *New England Journal of Medicine*, *313*(23), 1485–1492. https://doi.org/10.1056/NEJM198512053132327

Rosenberg, Steven A., Packard, B. S., Aebersold, P. M., Solomon, D., Topalian, S. L., Toy, S. T., … White, D. E. (1988). Use of Tumor-Infiltrating Lymphocytes and Interleukin-2 in the Immunotherapy of Patients with Metastatic Melanoma. *New England Journal of Medicine*, *319*(25), 1676–1680. https://doi.org/10.1056/NEJM198812223192527

Rosenberg, Steven A., Tong-On, P., Li, Y., Riley, J. P., El-Gamil, M., Parkhurst, M. R., & Robbins, P. F. (2002). Identification of BING-4 Cancer Antigen Translated From an Alternative Open Reading Frame of a Gene in the Extended MHC Class II Region Using Lymphocytes From a Patient With a Durable Complete Regression Following Immunotherapy. *The Journal of Immunology*, *168*(5), 2402–2407. https://doi.org/10.4049/jimmunol.168.5.2402

Rosenberg, Steven A, & Restifo, N. P. (2015). *Adoptive cell transfer as personalized immunotherapy for human cancer*.

Rosenthal, R., Cadieux, E. L., Salgado, R., Bakir, M. Al, Moore, D. A., Hiley, C. T., … Swanton, C. (2019). Neoantigen-directed immune escape in lung cancer evolution. *Nature*, *567*(7749), 479–485. https://doi.org/10.1038/s41586-019-1032-7

Rossig, C., Kailayangiri, S., Jamitzky, S., & Altvater, B. (2018). Carbohydrate Targets for CAR T Cells in Solid Childhood Cancers. *Frontiers in Oncology*, *8*. https://doi.org/10.3389/fonc.2018.00513

Roszkowski, J. J., Lyons, G. E., Kast, W. M., Yee, C., Van Besien, K., & Nishimura, M. I. (2005). Simultaneous Generation of CD8 + and CD4 + Melanoma-Reactive T Cells by Retroviral-Mediated Transfer of a Single T-Cell Receptor. *Cancer Research*, *65*(4), 1570–1576. https://doi.org/10.1158/0008-5472.CAN-04-2076

Sadelain, M., Brentjens, R., & Rivière, I. (2013). The basic principles of chimeric antigen receptor design. *Cancer Discovery*, *3*(4), 388–398. https://doi.org/10.1158/2159-8290.CD-12-0548

Samstein, R. M., Lee, C.-H., Shoushtari, A. N., Hellmann, M. D., Shen, R., Janjigian, Y. Y., … Morris, L. G. T. (2019). Tumor mutational load predicts survival after immunotherapy across multiple cancer types. *Nature Genetics*, *51*(2), 202–206. https://doi.org/10.1038/s41588-018-0312-8

Scholten, K. B. J., Kramer, D., Kueter, E. W. M., Graf, M., Schoedl, T., Meijer, C. J. L. M., … Hooijberg, E. (2006). Codon modification of T cell receptors allows enhanced functional expression in transgenic human T cells. *Clinical Immunology*, *119*(2), 135–145. https://doi.org/10.1016/j.clim.2005.12.009

Schumacher, T. N., & Schreiber, R. D. (2015). Neoantigens in cancer immunotherapy. *Science*, *348*(6230), 69–74. https://doi.org/10.1126/science.aaa4971

Schumacher, Ton N., & Schreiber, R. D. (2015). Neoantigens in cancer immunotherapy. *Science*, *348*(6230), 69–74. https://doi.org/10.1126/science.aaa4971

Segal, G., Prato, S., Zehn, D., Mintern, J. D., & Villadangos, J. A. (2016). Target Density, Not Affinity or Avidity of Antigen Recognition, Determines Adoptive T Cell Therapy Outcomes in a Mouse Lymphoma Model. *The Journal of Immunology*, *196*(9), 3935–3942. https://doi.org/10.4049/jimmunol.1502187

Segal, N. H., Parsons, D. W., Peggs, K. S., Velculescu, V., Kinzler, K. W., Vogelstein, B., & Allison, J. P. (2008). Epitope Landscape in Breast and Colorectal Cancer. *Cancer Research*, *68*(3), 889–892. https://doi.org/10.1158/0008-5472.CAN-07-3095

Smart, A. C., Margolis, C. A., Pimentel, H., He, M. X., Miao, D., Adeegbe, D., … Van Allen, E. M. (2018). Intron retention is a source of neoepitopes in cancer. *Nature Biotechnology*, *36*(11), 1056–1058. https://doi.org/10.1038/nbt.4239

Smith, C. C., Selitsky, S. R., Chai, S., Armistead, P. M., Vincent, B. G., & Serody, J. S. (2019). Alternative tumour-specific antigens. *Nature Reviews. Cancer*, *19*(8), 465–478. https://doi.org/10.1038/s41568-019-0162-4

Snyder, A., Makarov, V., Merghoub, T., Yuan, J., Zaretsky, J. M., Desrichard, A., … Chan, T. A. (2014). Genetic Basis for Clinical Response to CTLA-4 Blockade in Melanoma. *New England Journal of Medicine*, *371*(23), 2189–2199. https://doi.org/10.1056/NEJMoa1406498

Spranger, S., Luke, J. J., Bao, R., Zha, Y., Hernandez, K. M., Li, Y., … Gajewski, T. F. (2016). Density of immunogenic antigens does not explain the presence or absence of the T-cell–inflamed tumor microenvironment in melanoma. *Proceedings of the National Academy of Sciences*, *113*(48), E7759–E7768. https://doi.org/10.1073/pnas.1609376113

Strønen, E., Toebes, M., Kelderman, S., Buuren, M. M. Van, Yang, W., Rooij, N. Van, … Schumacher, T. N. (2016). Targeting of cancer neoantigens with donor-derived T cell receptor repertoires. *Science*, *2288*(May), 1–11. https://doi.org/10.1126/science.aaf2288

Thomas, L. (1982). On immunosurveillance in human cancer. *The Yale Journal of Biology and Medicine*, *55*(3–4), 329–333. Retrieved from http://www.ncbi.nlm.nih.gov/pubmed/6758376

Thomas, S., Mohammed, F., Reijmers, R. M., Woolston, A., Stauss, T., Kennedy, A., … Stauss, H. J. (2019). Framework engineering to produce dominant T cell receptors with enhanced antigen-

specific function. *Nature Communications*, *10*(1), 4451. https://doi.org/10.1038/s41467-019-12441-w

Topalian, S. L., Drake, C. G., & Pardoll, D. M. (2015). Immune checkpoint blockade: A common denominator approach to cancer therapy. *Cancer Cell*, *27*(4), 450–461. https://doi.org/10.1016/j.ccell.2015.03.001

Topalian, S. L., Hodi, F. S., Brahmer, J. R., Gettinger, S. N., Smith, D. C., McDermott, D. F., … Sznol, M. (2019). Five-Year Survival and Correlates Among Patients With Advanced Melanoma, Renal Cell Carcinoma, or Non–Small Cell Lung Cancer Treated With Nivolumab. *JAMA Oncology*, *5*(10), 1411–1420. https://doi.org/10.1001/jamaoncol.2019.2187

Tran, E., Turcotte, S., Gros, A., Robbins, P. F., Lu, Y.-C., Dudley, M. E., … Rosenberg, S. A. (2014). Cancer Immunotherapy Based on Mutation-Specific CD4+ T Cells in a Patient with Epithelial Cancer. *Science*, *344*(6184), 641–645. https://doi.org/10.1126/science.1251102

Tran, Eric, Ahmadzadeh, M., Lu, Y.-C., Gros, A., Turcotte, S., Robbins, P. F., … Rosenberg, S. A. (2015). Immunogenicity of somatic mutations in human gastrointestinal cancers. *Science*, *350*(6266), 1387–1390. https://doi.org/10.1126/science.aad1253

Tran, Eric, Robbins, P. F., Lu, Y.-C., Prickett, T. D., Gartner, J. J., Jia, L., … Rosenberg, S. A. (2016). T-Cell Transfer Therapy Targeting Mutant KRAS in Cancer. *New England Journal of Medicine*, *375*(23), 2255–2262. https://doi.org/10.1056/NEJMoa1609279

Traversari, C., van der Bruggen, P., Luescher, I. F., Lurquin, C., Chomez, P., Van Pel, A., … Boon, T. (1992). A nonapeptide encoded by human gene MAGE-1 is recognized on HLA-A1 by cytolytic T lymphocytes directed against tumor antigen MZ2-E. *Journal of Experimental Medicine*, *176*(5), 1453–1457. https://doi.org/10.1084/jem.176.5.1453

Trolle, T., McMurtrey, C. P., Sidney, J., Bardet, W., Osborn, S. C., Kaever, T., … Peters, B. (2016). The Length Distribution of Class I–Restricted T Cell Epitopes Is Determined by Both Peptide Supply and MHC Allele–Specific Binding Preference. *The Journal of Immunology*, *196*(4), 1480–1487. https://doi.org/10.4049/jimmunol.1501721

Turajlic, S., Litchfield, K., Xu, H., Rosenthal, R., McGranahan, N., Reading, J. L., … Swanton, C. (2017). Insertion-and-deletion-derived tumour-specific neoantigens and the immunogenic phenotype: a pan-cancer analysis. *The Lancet Oncology*, *18*(8), 1009–1021. https://doi.org/10.1016/S1470-2045(17)30516-8

Tyanova, S., Temu, T., & Cox, J. (2016). The MaxQuant computational platform for mass spectrometry-based shotgun proteomics. *Nature Protocols*, *11*(12), 2301–2319. https://doi.org/10.1038/nprot.2016.136

US Food and Drug Administration Approved Products-KYMRIAH (Tisagenlecleucel). (2017). Retrieved from https://www.fda.gov/vaccines-blood-biologics/cellular-gene-therapy-products/kymriah-tisagenlecleucel

Vairy, S., Lopes Garcia, J., Teira, P., & Bittencourt, H. (2018). CTL019 (tisagenlecleucel): CAR-T therapy for relapsed and refractory B-cell acute lymphoblastic leukemia. *Drug Design, Development and Therapy*, *Volume 12*, 3885–3898. https://doi.org/10.2147/DDDT.S138765

Valitutti, S., Müller, S., Cella, M., Padovan, E., & Lanzavecchia, A. (1995). Serial triggering of many T-cell receptors by a few peptide–MHC complexes. *Nature*, *375*(6527), 148–151. https://doi.org/10.1038/375148a0

Van Allen, E. M., Miao, D., Schilling, B., Shukla, S. A., Blank, C., Zimmer, L., … Garraway, L. A. (2015). Genomic correlates of response to CTLA-4 blockade in metastatic melanoma. *Science*, *350*(6257), 207–211. https://doi.org/10.1126/science.aad0095

Van Rooij, N., Van Buuren, M. M., Philips, D., Velds, A., Toebes, M., Heemskerk, B., … Schumacher, T. N. (2013). Tumor exome analysis reveals neoantigen-specific T-cell reactivity in an ipilimumab-responsive melanoma. *Journal of Clinical Oncology*, *31*(32). https://doi.org/10.1200/JCO.2012.47.7521

Verdegaal, E. M. E., de Miranda, N. F. C. C., Visser, M., Harryvan, T., van Buuren, M. M., Andersen, R. S., … van der Burg, S. H. (2016). Neoantigen landscape dynamics during human melanoma–T cell interactions. *Nature*. https://doi.org/10.1038/nature18945

Wang, M., Jain, P., Chi, T. L., Chen, S. E., Heimberger, A., Weathers, S.-P., … Rossi, J. M. (2020). Management of a patient with mantle cell lymphoma who developed severe neurotoxicity after chimeric antigen receptor T-cell therapy in ZUMA-2. *Journal for ImmunoTherapy of Cancer*, *8*(2), e001114. https://doi.org/10.1136/jitc-2020-001114

Wang, Y., Wu, N., Liu, D., & Jin, Y. (2017). Recurrent Fusion Genes in Leukemia: An Attractive Target for Diagnosis and Treatment. *Current Genomics*, *18*(5). https://doi.org/10.2174/1389202918666170329110349

Waterhouse, P., Penninger, J. M., Timms, E., Wakeham, A., Shahinian, A., Lee, K. P., … Mak, T. W. (1995). Lymphoproliferative Disorders with Early Lethality in Mice Deficient in Ctla-4. *Science*, *270*(5238), 985–988. https://doi.org/10.1126/science.270.5238.985

Wells, D. K., van Buuren, M. M., Dang, K. K., Hubbard-Lucey, V. M., Sheehan, K. C. F., Campbell, K. M., … Huang, Z. (2020). Key Parameters of Tumor Epitope Immunogenicity Revealed Through a Consortium Approach Improve Neoantigen Prediction. *Cell*, *183*(3), 818-834.e13. https://doi.org/10.1016/j.cell.2020.09.015

Wilhelm, M., Zolg, D. P., Graber, M., Gessulat, S., Schmidt, T., Schnatbaum, K., … Kuster, B. (2021). Deep learning boosts sensitivity of mass spectrometry-based immunopeptidomics. *Nature Communications*, *12*(1). https://doi.org/10.1038/s41467-021-23713-9

Wolf, Y., Bartok, O., Patkar, S., Eli, G. B., Cohen, S., Litchfield, K., … Samuels, Y. (2019). UVB-Induced Tumor Heterogeneity Diminishes Immune Response in Melanoma. *Cell*, *179*(1), 219-235.e21. https://doi.org/10.1016/j.cell.2019.08.032

Xu, C. (2018). A review of somatic single nucleotide variant calling algorithms for next-generation sequencing data. *Computational and Structural Biotechnology Journal*, *16*, 15–24. https://doi.org/10.1016/j.csbj.2018.01.003

Yang, Y., Jacoby, E., & Fry, T. J. (2015). Challenges and opportunities of allogeneic donor-derived CAR T cells. *Current Opinion in Hematology*, *22*(6), 509–515. https://doi.org/10.1097/MOH.0000000000000181

Yee, C., Thompson, J. A., Byrd, D., Riddell, S. R., Roche, P., Celis, E., & Greenberg, P. D. (2002). Adoptive T cell therapy using antigen-specific CD8 + T cell clones for the treatment of patients with metastatic melanoma: In vivo persistence, migration, and antitumor effect of transferred T cells. *Proceedings of the National Academy of Sciences*, *99*(25), 16168–16173. https://doi.org/10.1073/pnas.242600099

Yee, Cassian, Thompson, J. A., Roche, P., Byrd, D. R., Lee, P. P., Piepkorn, M., … Greenberg, P. D. (2000). Melanocyte Destruction after Antigen-Specific Immunotherapy of Melanoma. *Journal of Experimental Medicine*, *192*(11), 1637–1644. https://doi.org/10.1084/jem.192.11.1637

Zacharakis, N., Chinnasamy, H., Black, M., Xu, H., Lu, Y., Zheng, Z., … Feldman, S. A. (2018). Immune recognition of somatic mutations leading to complete durable regression in metastatic breast cancer. *Nature Medicine*, *24*(6), 724–730. https://doi.org/10.1038/s41591-018-0040-8

Zhang, J., Caruso, F. P., Sa, J. K., Justesen, S., Nam, D.-H., Sims, P., … Iavarone, A. (2019). The

combination of neoantigen quality and T lymphocyte infiltrates identifies glioblastomas with the longest survival. *Communications Biology*, *2*(1), 135. https://doi.org/10.1038/s42003-019-0369-7

Zhao, L., & Cao, Y. J. (2019). Engineered T Cell Therapy for Cancer in the Clinic. *Frontiers in Immunology*, *10*. https://doi.org/10.3389/fimmu.2019.02250

Zhao, Q., Jiang, Y., Xiang, S., Kaboli, P. J., Shen, J., Zhao, Y., … Xiao, Z. (2021). Engineered TCR-T Cell Immunotherapy in Anticancer Precision Medicine: Pros and Cons. *Frontiers in Immunology*, *12*. https://doi.org/10.3389/fimmu.2021.658753

Zhao, Y., Zheng, Z., Robbins, P. F., Khong, H. T., Rosenberg, S. A., & Morgan, R. A. (2005). Primary Human Lymphocytes Transduced with NY-ESO-1 Antigen-Specific TCR Genes Recognize and Kill Diverse Human Tumor Cell Lines. *The Journal of Immunology*, *174*(7), 4415–4423. https://doi.org/10.4049/jimmunol.174.7.4415

Appendix

1.41 TCR sequences: native chains and optimized constructs

1.41.1 Native chains

Nucleotide sequence	TCR	
ATGGGCACCAGTCTCCTATGCTGGGTGGTCCTGGGTTTCCTAGGGACAGATCACACAGGTGCTGGAGTCTCCCAGT CTCCCAGGTACAAAGTCACAAAGAGGGGACAGGATGTAGCTCTCAGGTGTGATCCAATTTCGGGTCATGTATCCCT TTATTGGTACCGACAGGCCCTGGGGCAGGGCCCAGAGTTTCTGACTTACTTCAATTATGAAGCCCAACAAGACAAA TCAGGGCTGCCCAATGATCGGTTCTCTGCAGAGAGGCCTGAGGGATCCATCTCCACTCTGACGATCCAGCGCACAG AGCAGCGGGACTCGGCCATGTATCGCTGTGCCAGCAGCCTCACTAGGATGGGAGACCGTGGGGAGTTCTTCGGGC CAGGGACACGGCTCACCGTGCTAGAGGATCTGAGAAATGTGACTCCACCCAAGGTCTCCTTGTTTGAGCCATCAAA AGCAGAGATTGCAAACAAACAAAAGGCTACCCTCGTGTGCTTGGCCAGGGGCTTCTTCCCTGACCACGTGGAGCTG AGCTGGTGGGTGAATGGCAAGGAGGTCCACAGTGGGGTCTCCACGGACCCTCAGGCCTACAAGGAGAGCAATTAT AGCTACTGCCTGAGCAGCCGCCTGAGGGTCTCTGCTACCTTCTGGCACAATCCTCGAAACCACTTCCGCTGCCAAGT GCAGTTCCATGGGCTTTCAGAGGAGGACAAGTGGCCAGAGGGCTCACCCAAACCTGTCACACAGAACATCAGTGC AGAGGCCTGGGGCCGAGCAGACTGTGGAATCACTTCAGCATCCTATCATCAGGGGGTTCTGTCTGCAACCATCCTC TATGAGATCCTACTGGGGAAGGCCACCCTATATGCTGTGCTGGTCAGTGGCCTGGTGCTGATGGCCATGGTCAAGA AAAAAAATTCC	Beta chain (TRB7-6)	KIF2C-PBC1nc
ATGTCACTTTCTAGCCTGCTGAAGGTGGTCACAGCTTCACTGTGGCTAGGACCTGGCATTGCCCAGAAGATAACTCA AACCCAACCAGGAATGTTCGTGCAGGAAAAGGAGGCTGTGACTCTGGACTGCACATATGACACCAGTGATCAAAG TTATGGTCTATTCTGGTACAAGCAGCCCAGCAGTGGGGAAATGATTTTTCTTATTTATCAGGGGTCTTATGACGAGC AAAATGCAACAGAAGGTCGCTACTCATTGAATTTCCAGAAGGCAAGAAAATCCGCCAACCTTGTCATCTCCGCTTCA CAACTGGGGGACTCAGCAATGTATTTCTGTGCAATGAGAGAACAGAATAACAATGCCAGACTCATGTTTGGAGATG GAACTCAGCTGGTGGTGAAGCCCAACATCCAGAACCCAGAACCTGCTGTGTACCAGTTAAAAGATCCTCGGTCTCA GGACAGCACCCTCTGCCTGTTCACCGACTTTGACTCCCAAATCAATGTGCCGAAAACCATGGAATCTGGAACGTTCA TCACTGACAAAACCGTGCTGGACATGAAAGCTATGGATTCCAAGAGCAATGGGGCCATTGCCTGGAGCAACCAGA CAAGCTTCACCTGCCAAGATATCTTCAAAGAGACCAACGCCACCTACCCCAGTTCAGACGTTCCCTGTGATGCCACG TTGACTGAGAAAAGCTTTGAAACAGATATGAACCTAAACTTTCAAAACCTGTCAGTTATGGGACTCCGAATCCTCCT GCTGAAAGTAGCCGGATTTAACCTGCTCATGACGCTGAGGCTGTGGTCCAGTTGA	Alpha chain (TRA14/DV4)	
ATGGGCACAAGGTTGTTCTTCTATGTGGCCCTTTGTCTCCTGTGGACAGGACACATGGATGCTGGAATCACCCAGA GCCCAAGACACAAGGTCACAGAGACAGGAACACCAGTGACTCTGAGATGTCACCAGACTGAGAACCACCGCTATA TGTACTGGTATCGACAAGACCCGGGGCATGGGCTGAGGCTGATCCATTACTCATATGGTGTTAAAGATACTGACAA AGGAGAAGTCTCAGATGGCTATAGTGTCTCTAGATCAAAGACAGAGGATTTCCTCCTCACTCTGGAGTCCGCTACC AGCTCCCAGACATCTGTGTACTTCTGTGCCATCAGTGATACTTCAGGGGGCTTGTGGACAGATACGCAGTATTTTGG CCCAGGCACCCGGCTGACAGTGCTCGAGGATCTGAGAAATGTGACTCCACCCAAGGTCTCCTTGTTTGAGCCATCA AAAGCAGAGATTGCAAACAAACAAAAGGCTACCCTCGTGTGCTTGGCCAGGGGCTTCTTCCCTGACCACGTGGAGC TGAGCTGGTGGGTGAATGGCAAGGAGGTCCACAGTGGGGTCTCCACGGACCCTCAGGCCTACAAGGAGAGCAATT	Beta chain (TRB10-3)	KIF2C-PBC2nc

ATAGCTACTGCCTGAGCAGCCGCCTGAGGGTCTCTGCTACCTTCTGGCACAATCCTCGAAACCACTTCCGCTGCCAA GTGCAGTTCCATGGGCTTTCAGAGGAGGACAAGTGGCCAGAGGGCTCACCCAAACCTGTCACACAGAACATCAGT GCAGAGGCCTGGGGCCGAGCAGACTGTGGAATCACTTCAGCATCCTATCATCAGGGGGTTCTGTCTGCAACCATCC TCTATGAGATCCTACTGGGGAAGGCCACCCTATATGCTGTGCTGGTCAGTGGCCTGGTGCTGATGGCCATGGTCAA GAAAAAAAATTCC		
ATGAAATCCTTGAGAGTTTTACTAGTGATCCTGTGGCTTCAGTTGAGCTGGGTTTGGAGCCAACAGAAGGAGGTGG AGCAGAATTCTGGACCCCTCAGTGTTCCAGAGGGAGCCATTGCCTCTCTCAACTGCACTTACAGTGACCGAGGTTCC CAGTCCTTCTTCTGGTACAGACAATATTCTGGGAAAAGCCCTGAGTTGATAATGTTCATATACTCCAATGGTGACAA AGAAGATGGAAGGTTTACAGCACAGCTCAATAAAGCCAGCCAGTATGTTTCTCTGCTCATCAGAGACTCCCAGCCC AGTGATTCAGCCACCTACCTCTGTGCCGTGAAGGAACGGGCATCAGGAGGAAGCTACATACCTACATTTGGAAGA GGAACCAGCCTTATTGTTCATCCGTACATCCAGAACCCAGAACCTGCTGTGTACCAGTTAAAAGATCCTCGGTCTCA GGACAGCACCCTCTGCCTGTTCACCGACTTTGACTCCCAAATCAATGTGCCGAAAACCATGGAATCTGGAACGTTCA TCACTGACAAAACCGTGCTGGACATGAAAGCTATGGATTCCAAGAGCAATGGGGCCATTGCCTGGAGCAACCAGA CAAGCTTCACCTGCCAAGATATCTTCAAAGAGACCAACGCCACCTACCCCAGTTCAGACGTTCCCTGTGATGCCACG TTGACTGAGAAAAGCTTTGAAACAGATATGAACCTAAACTTTCAAAACCTGTCAGTTATGGGACTCCGAATCCTCCT GCTGAAAGTAGCCGGATTTAACCTGCTCATGACGCTGAGGCTGTGGTCCAGTTGA	Alpha chain (TRA12-2)	

Variable chain
Constant chain

1717

1718 1.41.2 Codon optimized and murinized TCR constructs

Nucleotide sequence	TCR
ATGGGTACTTCCTTGCTGTGCTGGGTGGTTCTCGGGTTCCTTGGCACTGATCACACAGGGGCGGGTGTAAGTCAATCAC CGCGATACAAGGTGACGAAAAGGGGGCAAGATGTCGCCCTCCGGTGCGACCCTATATCTGGACATGTCAGCTTGTATT GGTACCGGCAAGCGCTTGGACAAGGACCCGAGTTCTTGACTTACTTCAACTACGAGGCTCAACAGGACAAATCAGGGC TGCCTAATGACCGGTTCTCCGCAGAAAGACCGGAGGGTAGTATATCCACCCTCACGATCCAAAGGACAGAGCAAAGAG ACTCCGCAATGTACCGATGTGCTTCAAGCCTCACCCGCATGGGGGATCGAGGTGAGTTCTTTGGACCTGGGACCCGATT GACTGTACTTGAAGACCTCAGGAACGTGACGCCTCCGAAGGTGTCCCTGTTTGAACCGTCAAAAGCTGAAATCGCAAAC AAGCAAAAAGCGACGCTGGTCTGCCTCGCACGAGGATTCTTTCCTGATCATGTAGAGCTGAGCTGGTGGGTGAATGGT AAGGAGGTACACAGTGGGGTG**TGC**ACGGATCCACAGGCGTACAAAGAAAGTAATTACTCCTATTGCCTCAGCTCACGA CTTCGGGTGTCCGCTACTTTCTGGCATAACCCCCGAAATCACTTCCGATGTCAGGTGCAATTTCACGGACTGTCCGAAGA AGACAAGTGGCCGGAAGGGAGTCCAAAACCCGTTACACAAAATATATCAGCAGAAGCGTGGGGCAGAGCGGACTGTG GTATAACGTCAGCCAGCTACCATCAAGGTGTGCTCAGCGCTACCATATTGTACGAAATCCTTCTCGGTAAGGCTACGCTC TACGCAGTACTCGTGAGCGGCCTTGTACTTATGGCAATGGTCAAAAAAAAAAAATTCCGGAAGCGGCGCCACGAACTTCT CTCTGTTAAAGCAAGCAGGAGACGTGGAAGAAAACCCCGGTCCCATGTCCCTTAGTAGTCTTCTGAAAGTAGTGACAGC TAGTCTTTGGCTCGGCCCTGGTATCGCCCAAAAGATTACACAAACTCAGCCGGGCATGTTTGTACAAGAAAAGGAGGCC GTCACCCTCGACTGTACTTATGATACATCAGATCAGAGCTACGGGCTGTTTTGGTACAAGCAACCCTCCAGTGGTGAAAT GATTTTTCTTATCTATCAGGGCAGCTATGATGAACAAAACGCGACAGAGGGTCGGTATAGCCTGAACTTTCAGAAAGCG CGCAAGTCCGCGAACTTGGTAATAAGTGCTTCTCAACTGGGTGATAGCGCCATGTACTTCTGTGCTATGCGAGAGCAAA ACAATAATGCAAGATTGATGTTTGGGGATGGTACGCAGCTTGTAGTTAAGCCCAATATCCAGAACCCTGAACCGGCCGT CTACCAGCTCAAGGACCCTCGATCTCAGGACTCCACACTTTGCTTGTTCACCGACTTCGACAGCCAAATCAACGTGCCCA AGACAATGGAGAGTGGGACGTTCATCACTGACAAA**TGC**GTTCTCGACATGAAAGCAATGGATAGCAAAAGTAACGGG GCGATAGCTTGGTCAAACCAAACATCCTTTACTTGCCAGGATATTTTTAAAGAAACCAACGCAACTTATCCAAGTTCAGA TGTCCCCTGTGATGCCACCCTGACGGAGAAGTCTTTTGAGACTGACATGAATTTGAATTTCCAAAACCTCTCCGTAATGG GTCTTAGAATCTTGTTGCTGAAGGTTGCCGGATTCAATCTTCTGATGACATTGCGGCTGTGGTCATCTTGA	KIF2C-PBC1om.c
ATGGGGACGAGACTGTTCTTCTACGTCGCTCTCTGCCTTCTCTGGACCGGGCACATGGACGCTGGCATCACCCAAAGCC CACGGCACAAAGTTACGGAAACCGGGACTCCTGTGACCCTGAGATGCCACCAAACAGAGAATCACAGGTACATGTATT GGTATCGACAGGACCCAGGCCACGGGTTGAGGTTGATACACTACAGTTATGGGGTTAAGGACACGGACAAGGGTGAG GTATCTGACGGATACTCAGTTAGCAGGAGTAAGACTGAGGATTTTCTGCTCACACTTGAAAGCGCGACGAGTTCTCAAA CTTCAGTGTATTTCTGTGCCATAAGTGATACGTCCGGAGGGCTTTGGACCGATACTCAGTACTTTGGACCCGGAACCAG ACTCACAGTATTGGAGGATTTGAGAAATGTAACTCCACCAAAAGTCAGTCTCTTCGAGCCGTCCAAAGCTGAAATTGCT AACAAGCAAAAGGCGACCCTCGTTTGTTTGGCCCGAGGATTCTTTCCAGATCATGTTGAGCTGTCTTGGTGGGTGAATG GAAAGGAAGTACATAGCGGCGTG**TGC**ACCGACCCACAGGCATACAAAGAGTCAAATTACAGTTATTGCTTGAGTTCAA GACTCAGGGTATCTGCGACATTCTGGCACAATCCGCGCAATCATTTCCGATGTCAGGTGCAATTTCATGGCCTCAGCGA GGAAGACAAGTGGCCTGAAGGCAGTCCGAAACCAGTCACACAGAACATAAGCGCCGAGGCGTGGGGGCGGGCGGAC TGCGGGATCACATCTGCCTCTTACCATCAAGGTGTCCTTTCTGCGACTATACTTTATGAGATCCTGCTTGGGAAAGCAAC GCTGTACGCGGTGTTGGTTAGTGGCCTCGTGTTGATGGCGATGGTGAAAAAAAAGAATAGCGGAAGCGGCGCCACGA ACTTCTCTCTGTTAAAGCAAGCAGGAGACGTGGAAGAAAACCCCGGTCCCATGAAGAGTCTTAGAGTTCTCCTTGTCAT	KIF2C-PBC2om.c

ACTTTGGCTCCAACTTAGCTGGGTCTGGTCTCAGCAAAAAGAGGTAGAACAGAACTCCGGGCCACTTAGCGTACCGGA
GGGAGCCATAGCATCTCTCAACTGTACGTACAGTGATAGGGGAAGCCAAAGTTTTTTTTGGTATCGGCAGTACTCTGGT
AAAAGTCCCGAACTGATTATGTTTATATACTCAAATGGTGATAAAGAAGATGGGCGCTTCACCGCGCAGCTTAATAAGG
CTTCTCAGTATGTGTCCCTGTTGATAAGGGATTCACAGCCTAGTGATTCTGCGACCTACCTTTGTGCAGTAAAGGAGCGC
GCTAGTGGGGGGAGCTACATTCCTACTTTCGGCAGAGGAACTTCCCTTATTGTGCATCCTTACATTCAGAACCCTGAACC
AGCAGTCTATCAACTTAAAGATCCGCGCAGCCAAGACTCAACTCTGTGCCTTTTTACGGATTTTGATAGTCAGATAAACG
TACCTAAAACTATGGAGTCCGGAACCTTTATAACTGACAAG**TGT**GTATTGGATATGAAAGCCATGGACAGCAAGTCAAA
TGGCGCGATAGCTTGGTCAAATCAGACCAGTTTCACTTGTCAGGACATTTTCAAGGAGACAAATGCGACGTACCCGTCT
AGTGACGTACCCTGTGACGCGACTCTGACTGAGAAGTCCTTTGAAACCGATATGAACCTCAACTTTCAAAACCTGAGTGT
GATGGGTCTGCGAATACTCCTTCTTAAGGTGGCGGGCTTCAATCTGCTGATGACATTGAGACTCTGGTCATCCTGA

Variable native beta chain
Murine constant beta chain (mTrbc2)
P2A element
Variable native alpha chain
Murine constant alpha chain (mTrac)
TGC: cysteines

1.42 Affinity ranking of Mel15 predicted nonamers for HLA-A03:01 and B27:05

HLA-A0301

	Peptide	nM	n. aff rank (original list)
1	KIFNFYPRK	6,8	3
2	KMKNFFFTK	7,4	4
3	RMLRRRAQK	8,7	6
4	TLYSPRGEK	9,2	9
5	AMYQRAKLK	9,5	11
6	SLLTPPSTK	9,6	12
7	RLMFFRPIK	9,8	13
8	SLYLKIHLK	11	14
9	KIYAAGTFY	11,2	16
10	YLFFIQGYK	12,5	21
11	TTYSPIGEK	14,5	24
12	RLYKLILWR	14,7	25
13	KTYPCKIFY	16,6	28
14	SLQPRGSFK	18,2	33
15	KVINLSPFK	18,6	37
16	CLFFGIPWK	19,2	39
17	KQFSAMALK	21,4	44
18	**RLFLGLAIK**	**21,6**	**45**
19	KLKLPIIMK	23,3	54
20	LLINRGFSK	25,2	62
21	RLKCPFYGK	26,1	70
22	KVMTDPSRK	28,7	84
23	RIAGKALKK	31,5	97
24	**KLILWRGLK**	**32,6**	**103**
25	KLYQCNECK	32,7	104
26	LGYASHLMK	36,3	122
27	TSLKFFFNK	37,8	139
28	ASYLFQQNK	39,4	147
29	ILVLRPSAK	43,4	158
30	RIIAKYAPK	43,8	160
31	WLFGTFFCK	44,8	163
32	ALFFFMTHR	45,8	168
33	CLRCGKGFK	46	169
34	KMNDAATFY	46,2	172
35	ATMFLKTTK	49,1	183
36	YLRKLLIRK	49,5	185
37	MAFNFARVK	50,2	189
38	TSSWPKYFK	50,5	191
39	IMSFLRQRK	51,2	198

40	QLYSDIIPK	52	204
41	QSYTYIIEK	52,6	208
42	MQMDGQMAK	53,3	212
43	RSYYRGAAR	54,4	217
44	SSYFFDMDK	54,9	220
45	ALQARHGKK	57	231
46	LTFMRSQTK	59,1	240
47	AAYYGVLDK	59,4	244
48	RSIHRLIIK	59,8	247
49	LLLNEMAKK	60,1	248
50	GVLPRWVAK	61,4	252
51	HTQGPLLKK	63,9	262
52	KSSSSVCWK	64,4	263
53	KAIRRSLKK	64,4	263
54	RSLKKYVEK	65,5	272
55	HVFWKATPY	70	288
56	KLSKIIFHR	71	294
57	KAMQTVYLK	73,8	306
58	GTYRCRGFY	73,8	306
59	RQSKTHILK	74	310
60	RSYGYLYRY	74,6	312
61	LLHLLRSPK	76,1	320
62	NIFANTLGK	76,4	324
63	TVHTRLKYK	77,6	328
64	RSRRFSSLY	77,7	329
65	ALRKPQLFH	79,5	335
66	LSITVSSLK	80,4	339
67	KLCVTSCTK	83,3	350
68	WLNSTHALK	83,9	353
69	QTYGHFLSR	85,3	357
70	SMKELYVRK	87	365
71	SSLNQNMNK	88,8	369
72	SLFGICQIK	91,8	383
73	KSYYLFNLR	91,9	384
74	FILKAFFKK	93,2	386
75	TVLQGTQFK	94,4	390
76	CLSKSIKTK	94,7	392
77	LSMAQRGSK	101	420
78	KTACKLKMK	106	441
79	LLLHFQSLR	110,7	460
80	AVRMAQCLK	111,5	462
81	RQSLSSILK	112,9	466
82	MSFLKNNPK	115,1	474
83	SIISLTGPK	116,6	480
84	RSMSELVEK	117,4	482
85	KVDLHFIKK	118,4	489
86	ITTYEMLLK	118,4	489
87	HQYHSKIDK	119,5	494
88	YVWDTQTLK	123,2	504
89	TAVFLTLYK	132	538
90	RGRKSPLLK	132,1	539
91	KSYFSPKGY	132,6	540
92	LSAAGTTVK	132,8	541
93	FIYSLKNEK	133	542
94	MLYIGIVEY	135,1	556
95	HQWSYSFIK	136,2	559
96	CSLLQGMAK	136,9	562
97	VTESKHLFK	136,9	562
98	KLRRIIAKY	137,7	567
99	NLMEVFYPK	140,4	581
100	LLQPASMFY	141,1	584
101	LAYNYLQEK	145,8	598
102	EMAPPTPPK	151,4	610

103	TLKPGTCVK	152,5	612
104	ATWETVYNK	152,6	613
105	TMRTRHSTR	152,9	614
106	KVAVAGLDK	156,9	631
107	RVFRSVQKY	158,9	636
108	AIQEPSPRK	159,6	641
109	RSGKAHITK	161,3	644
110	QLARVPSLY	163,2	653
111	TAFFGVTIK	163,9	655
112	HSVTCACLK	166,8	663
113	ASRSIVLFY	169,5	668
114	AARMSVLKK	169,8	671
115	ISSTSSWPK	170,8	677
116	MQMDERMAK	178	697
117	STKPLLASK	179,9	706
118	ASYSSPPGY	179,9	706
119	TILKNTRPK	183,4	715
120	YQYDKPLGK	183,9	718
121	TLNNGKSLY	184,6	722
122	VTQTFGIKK	184,6	722
123	AVSTALQPK	186,1	736
124	TSVQILFFK	188,7	748
125	HLRSYGYLY	194,8	766
126	KGYAKIKEK	205,4	798
127	PVFTPSVKK	206,8	801
128	HLFKVFRIR	207,7	803
129	KMHKFEDIK	211,7	820
130	ASVLHNLRK	216	833
131	SQYFVKQEK	219,1	847
132	FLLLNEMAK	221,3	856
133	RGREKLIYK	225,2	866
134	QFYHLLSSK	226,5	871
135	FLAPLGHKK	226,5	871
136	KASRRPRRK	233,8	894
137	KLLDTIWNR	235,1	899
138	KLLNLVELY	236,3	901
139	RVAIDILIK	238,3	907
140	ISLLVVGNK	239,7	911
141	LLAQKGIYY	241,2	918
142	GVRGVGACK	241,8	921
143	RFFFLLCSK	244	926
144	QLMVFYEGK	244,1	927
145	TVAMMCTRK	245,3	931
146	KSRDPRVFR	246,4	933
147	SFFNVNLSK	246,6	935
148	RLRPCSGER	249,7	945
149	RQYMEKIIK	251,1	952
150	KIYTGEKPY	257	966
151	KIYTGEKPY	257	966
152	GGYIFSTQK	264,5	982
153	LLIRKNQPK	275,5	1009
154	QQFLNLMKK	276,6	1011
155	KTFSTCAFH	277,4	1015
156	STHALKTCK	279,7	1020
157	KLGSSTAAR	296,7	1077
158	STTDCLNYK	299,7	1087
159	CVALNGSVK	302,5	1099
160	GVAVVLIEK	305,6	1112
161	IGYLELFLK	305,8	1114
162	YVKTSEFLK	306,2	1118
163	RQMAFNFAR	312,7	1142
164	TVAIVCTRK	317,1	1149
165	TLQVFVLDK	317,2	1150

166	LLLVENCLK	322,6	1162
167	YVRKVAELK	327,5	1175
168	KLQRDLSFR	328	1176
169	KMQKCNFKY	328,8	1179
170	LIKEYNYLK	341,2	1216
171	KVCIDVFKK	342,8	1226
172	SLKKYVEKK	345,9	1240
173	NVFRKEQFK	353,4	1261
174	TSTLPASPK	355,7	1267
175	AMFPYSGQH	358,7	1277
176	GLQSANTKK	364,2	1293
177	IDYYFSPQK	366,1	1301
178	LIGPLFICK	368,2	1307
179	TIPSDFIFK	370,9	1315
180	SMSELVEKK	372,6	1318
181	ALKPHACLR	384,5	1353
182	SSEARFFSK	393,4	1374
183	KDWFGALHK	400,1	1392
184	QEYSGTLRK	403,6	1406
185	SISPGPKGK	407,6	1415
186	TAYDLEIMK	410,7	1427
187	SLFRVSERR	413,9	1438
188	FLAFLLSLR	422	1448
189	SVEAATVLK	428,6	1462
190	CTWQDLSSK	431,3	1472
191	RFFMPDLSK	432	1474
192	MINELVEKK	437,4	1489
193	LLQRPPEGK	444,7	1503
194	SLILFLSFR	446,7	1512
195	STEKKFFWK	455,9	1533
196	KTFNTCISH	456	1534
197	LLEVPPSTK	459,2	1540
198	RSDRLMFFR	462,9	1554
199	TSNLTKIKK	471,4	1568
200	KLKEDSRKK	471,6	1569
201	FLRRMTVMR	474,5	1577
202	FLRRMTVMR	474,5	1577
203	LLSDCDLKK	476	1579
204	SLGSMSQYY	483,7	1593
205	GTRILTRVK	492,1	1615

1721

HLA-B2705

	Peptide	**nM**	**n. aff rank (original list)**
1	RRFSSLYSF	11,5	4
2	RRLLILGRI	11,5	4
3	FRMFLTQGF	15	9
4	ARWTAFFGV	17,1	14
5	GRWALHSAF	17,5	16
6	**GRIAFFLKY**	**18,4**	**17**
7	KRFLHRQPL	20,2	19
8	ARFAVNLRL	20,7	21
9	WRNSFLLRY	24	27
10	YRIYDIPPK	24	27
11	ARLFLGLAI	25,7	33
12	YRHLFKVFR	26,6	36
13	FRFFTRKSL	26,9	37
14	RRHCRSYNR	27,6	39
15	KRRLLILGR	28	40
16	FRQSLYLKI	29,2	45
17	RRTQRYFMK	29,3	46

18	FRICPIFVF	32,3	50
19	KRTNVGILK	33,3	52
20	LRILRIKLR	35,6	55
21	KRHEVPVPL	36,8	57
22	HRYFFFVAM	37,5	61
23	FRFFATPAL	38,3	65
24	LRFSIIEEF	45,9	97
25	SRVILFSPL	46	99
26	YRATVIQVF	46,2	100
27	WRYHFESFF	46,3	101
28	RRKQIVGGK	46,7	102
29	RQMAFNFAR	49	110
30	FRFDGVTFM	49	110
31	YRIVLWEVM	51,7	120
32	RRGRKSPLL	53,2	123
33	WRVHTGEKL	55,2	133
34	KRTMIQSPF	55,7	138
35	YRGAARALL	62,3	151
36	LRKRYFSGL	62,7	153
37	GRVGIILTV	65,3	159
38	FRTFPGIRK	70,4	167
39	KRGAKGFGF	73	176
40	RRLAWVRNW	73,8	178
41	FRCQCPVGF	74,1	179
42	HRFYVMREK	74,3	180
43	FRLRKRKNM	80,4	200
44	MRVLYLLFL	80,8	202
45	LRALFLAFL	81,1	204
46	IRYLFQEAF	89,8	228
47	MRAKLRPSM	92,7	239
48	RRYDQRKER	102,7	257
49	KRYLGDLTL	104,5	264
50	KRIQMNAAL	104,8	269
51	KRTLGIHQR	105,3	271
52	KRNYHIFYR	105,3	271
53	FRIRFDILV	105,8	273
54	KRYFSGLIY	109,1	285
55	LRSRRFSSL	111,9	296
56	VRMAQCLKV	113,6	304
57	KRMASCRCI	119	327
58	ARALLVYDI	124,5	338
59	MRFHGVSVL	128,2	343
60	LQARLFLGL	131,7	350
61	RKLFVLILK	134,6	357
62	LRIEGVTTL	139,3	368
63	GQLNLLVPF	139,5	369
64	GRINVTTAV	143,8	376
65	ARLFPNFTM	145,7	382
66	VRVRAGGGI	151,5	392
67	FRYAFLLES	153,8	399
68	RRAALKTFN	167,5	434
69	YRSDRLMFF	168,5	437
70	QRLPLTGGK	169	438
71	GRLPLSEKK	178,4	458
72	GRKSPLLKK	180,8	466
73	LRVGRKALY	185,3	474
74	LRIKLRSLA	186,1	477
75	RQLWDRTRL	186,3	479
76	KRKNMSKLM	186,8	482
77	YRGAAEALL	187,4	484
78	RRLQEELNK	190,8	492
79	YRCRGFYPH	203,5	521
80	IRKWRKTHL	213,8	541

81	TRFTRQTLV	214,9	545
82	HQWSYSFIK	215,3	547
83	YRLQDYGGR	216,6	552
84	LRKPQLFHY	220,8	556
85	YRLYKLILW	222,9	560
86	KQFSAMALK	232,3	582
87	RRVYSISSS	234,2	587
88	KRVRAIWIW	237	596
89	RRPQLKELI	242,1	610
90	RRRQRKESF	247,7	633
91	WRTQTGCVF	249,3	642
92	HRGKLVAAI	262,6	669
93	HRDLLRYVK	263,7	671
94	LRGNSGFVL	265,2	677
95	SRFLSQLDK	265,8	678
96	RRYKKVIPE	270,1	687
97	QRYFMKANR	273,1	697
98	KQLARVPSL	274,5	700
99	ERISHGFSM	278,9	710
100	QRVHLREKV	279,2	712
101	GRTGAGKSF	281,6	719
102	RKMPLPFGV	282,4	721
103	YKWKSPFGL	285	732
104	ARQDLGLSY	285,5	733
105	QRVLRIEEF	287,8	741
106	DRLMFFRPI	288,1	743
107	VRQVVFKSK	290,6	749
108	GRCAAMRAK	293,1	753
109	TRWDDMEKL	302	773
110	SRKNIIFFT	302,4	775
111	LRVPRGGGF	304,6	781
112	FRSSKSVAK	307,8	787
113	CRACGYDFL	311,3	801
114	CRSYNRRAL	314	804
115	FRGPHFTFF	319,7	813
116	RRPRRKEGI	324,8	818
117	LRLQTGGSV	329,5	832
118	VRTGYGYVY	331,4	837
119	VRTGYGYVY	331,4	837
120	VRKSSAVLK	339,1	852
121	RKWRKTHLT	347,6	877
122	LRQVLGETF	348,6	880
123	LRLAVKFFS	352,5	889
124	ARTLYEVFL	354,4	894
125	LRIGAISQA	354,5	895
126	GQHVRISRL	355,1	896
127	TRKLFVLIL	355,3	897
128	VRVTDAPSL	359,9	918
129	QRAKLKTCK	368,1	947
130	GRLSLGYYC	369	951
131	YREEKILPK	375,6	966
132	KRMQHQFQQ	378,9	974
133	MQLCFGHHF	413,8	1057
134	LRYNSRENR	419,2	1078
135	FRSVQKYHV	423	1084
136	HRSLSRCPI	424,1	1086
137	TRLEVQQWY	428,3	1096
138	RRIIAKYAP	434,2	1115
139	TRALAQYLV	442,1	1132
140	TRAFDQLRI	442,3	1133
141	VRYPVIFNA	445	1141
142	KRVVTSLLT	449,8	1154
143	LRHAKFIIT	461,8	1176

144	GQIMFLTRM	472,2	1203
145	QRSKFFFLA	487,2	1237
146	TRILTRVKV	497,6	1261

1722

1723

1724 ## 1.43 Peptides identified with Immunopeptidomics 2018

1725 Table 44 Mutated peptides identified with Immunopeptidomics 2018 pipeline

Gene	Sequence	a.a. Alt	HLA allele predicted affinity (nM); % rank; binding level	MaxQuant database	MS score	FDR	Biotype Ensembl
AKAP6[1]	KLKLP**I**IMK	M1482I	HLA-A03:01; 23.3; 0.100; SB	MInt exome	87.26	1%	Protein coding
CASR	FIN**K**EKILW	E525K	HLA-B35:03; 26497.6; 3.000; --	MInt exome	81.3	5%	Protein coding
CDH8	ETKK**F**YTLK	S350F	HLA-A68:01; 10.3; 0.100; SB	MInt exome	89.14	5%	Nonsense mediated decay
CLEC4F	PQEVD**F**VAM	S24F	HLA-B35:03; 26497.6; 3.000; --	MInt exome	85.27	5%	Protein coding
CTNNA2	EKGD**L**LNIAIDK	P361L	HLA-A03:01; 543.4; 1400; WB	MInt exome	51.84	5%	Protein coding
DDX21	**F**VPPTAISHF	S517F	HLA-B35:03; 27320.9; 3.000; --	MInt exome/RNA	79.12	5%	Protein coding
FN1	QAD**K**EDSRE	R232K	HLA-B35:03; 44775.5; 31.000; --	MInt RNA	51.45	5%	Protein coding
FSIP2	**I**EKVIKIID	M6319I	HLA-B35:03; 46657.8; 55.000; --	MInt exome	50.81	5%	Protein coding
H3F3C[1]	RIKQ**T**ARK	T4I	HLA-A03:01; 1614.0; 3.000; --	MInt exome	101.72	1%	Protein coding
HLA-J	RR**K**SSVTHF	K83R	HLA-B27:05; 48.2; 0.200; SB	MInt RNA	69.63	5%	Processed transcript
ITGA6	D**A**AFLSLTQR	G308A	HLA-A68:01; 16.9; 0.250; SB	MInt RNA	67.03	5%	Protein coding
MAP2K1	KRLEA**L**LTQK	F53L	HLA-A03:01; 181.7; 0.700; WB	MInt RNA/ MLung exome	141.25	5%	Protein coding
MAP2K1	RKRLEA**L**LTQK	F53L	HLA-B27:05; 701.7; 1700; WB	MInt RNA	71.03	5%	Protein coding
MAP3K9[1]	ASWVVPIDI**K**	E403K	HLA-A03:01; 401.0; 1.200; WB	MInt exome	91.07	5%	Protein coding
NCAPG2[1]	K**L**ILWRGLK	P333L	HLA-A03:01; 32.6; 0.15; SB	MInt exome/RNA	100.39	1%	Protein coding
NUP153	ET**L**KPGTCVKR	P706L	HLA-A68:01; 730.0; 3.000; --	MInt exome/RNA	180.67	5%	Protein coding
OPN5	TVRKSSAVL**K**	E348K	HLA-A03:01; 53.4; 0.250; SB	MInt exome	59.25	5%	Protein coding
PID1	GI**N**SGPLVNTK	D30N	HLA-A03:01; 1129.7; 2.500; --	MInt exome	85.67	5%	Protein coding
POU2F1	LMSNSTLA**I**I	T598I	HLA-A03:01; 8194.1; 7.500; --	MInt exome	87.32	5%	Protein coding
PPFIBP1	IPDST**V**ETL	A79V	HLA-B35:03; 3929.5; 0.150; SB	MInt RNA	100.07	5%	Protein coding
PTPN2	IGLEEEKLI	T326I	HLA-B35:03; 35172.0; 6.500; --	MInt RNA	51.34	5%	Protein coding
PTPN2P1	RI**V**EKELVK	M17V	HLA-A03:01; 363.0; 1100; WB	MInt RNA	54.44	5%	Processed pseudogene

RBPMS[1]	R**L**FKGYEGS LIK	P46L	HLA-A03:01; 29.3; 0.150	MInt exome	119.69	1%	Protein coding
REC8	TSSPP**S**SSP	P32S	HLA-A68:01; 16843.5; 15.000; --	MInt RNA	60.36	5%	Retained intron
RPS23P2	KAHLGT**T**P K	A26T	HLA-A03:01; 194.9; 0.700; WB	MInt exome	49.53	5%	Processed pseudogene
RRBP1	EGA**P**NQGK K	Q456P	HLA-A68:01; 2087.1; 4.500; --	MInt RNA	70.53	5%	Protein coding
SEC23A[1]	**L**PIQYEPVL	P52L	HLA-B35:03; 436.3; 0.015	MInt exome	107.32	1%	Protein coding
SLC4A2	GAAEDDPL **W**R	R662W	HLA-A68:01; 1108.1; 3500; --	MInt exome	91.04	5%	Protein coding
STON2	DVFHNSRVI LFS	N462S	HLA-B35:03; 38536.3; 10.000; --	MLung exome	54.47	5%	Retained intron
SYTL4[1]	GRIAF**F**LKY	S363F	HLA-B27:05; 18.43; 0.6; SB	MInt exome	107.59	1%	Protein coding
THUMPD1 P1	KAFLKD**I**KK	M103I	HLA-A03:01; 384.1; 1100; WB	MInt exome	60.48	5%	Processed pseudogene
TIGD6	NASG**I**EKM R	T221I	HLA-A68:01; 17.5; 0.250; SB	MInt RNA	64.76	5%	Protein coding
TP53BP2	SSEDILRD**V**	A494V	HLA-B27:05; 29929.1; 39.000; --	MInt exome/RNA	63.31	5%	Protein coding
VIMP	AAVEPDV**A** VKR	V52A	HLA-A68:01; 2360.9; 4.500; --	MInt RNA	138.4	5%	Protein coding

[1] Peptides described in Bassani-Sternberg et al., 2016

1726

1.44 List of figures

Figure 1. Illustration from (Jiang et al., 2019) 15
Figure 2. Clinical course of disease of patient Mel15. 62
Figure 3. IFN-γELISpot for immunogenicity assessment of in-silico predicted peptides. 63
Figure 4. PBMC-derived neoantigen reactivity over time. 64
Figure 5. Enrichment of KIF2C reactive T cells. 64
Figure 6. T-cell clone reactivity against KIF2C^{P13L}. 65
Figure 7. TCR variable chain repertoire PCR on cDNA from T cell clone 3D5. 65
Figure 8. Temporal-spatial monitoring of neoantigen-specific TCR β-chain frequencies using deep sequencing of TCRb chains. 67
Figure 9. Venn diagram from variable TCR-β chain overlap in metastases, biopsy and primary tumor. 68
Figure 10. Isolation of CD8$^+$ T cells from healthy-donors' derived PBMC. 69
Figure 11. Expression of TCR alpha and beta native chains in CD8$^+$ T cells. 69
Figure 12. Functional analysis of CD8$^+$ T cells transduced with native TCR chains. 71
Figure 13. Surface expression of transduced neoantigen-specific TCRs on human CD8$^+$ T cells. 71
Figure 14. Expression of transduced SYTL4^{S363F}-specific TCRs on the surface of CD8$^+$ T cells assessed by multimer staining. 73
Figure 15. Expression of transduced KIF2C^{P13L} and NCAPG2^{P333L}-specific TCRs on the surface of CD8$^+$ T cells assessed by multimer staining. 74
Figure 16. Surface and intracellular staining of TCRs KIF2C-PBC1 and KIF2C-PBC2. 75
Figure 17. Surface expression of codon-optimized KIF2C-TCRs. 76
Figure 18. Functionality of CD8$^+$ T cells transduced with optimized TCRs. 77
Figure 19. Functional characterization of neoantigen-specific TCR. 79
Figure 20. Cross-reactivity assessment of neoantigen-specific transgenic TCRs. 81
Figure 21. Standard Europium release assay for the assessment of TCR mediated cytolysis. 83
Figure 22. TCR-transgenic CD8$^+$ T cells mediate killing and detaching of target cells expressing tumor neoantigens. 85
Figure 23. Assessment of TCR transduction rates for standardization of effector T cell injection. 86
Figure 24. In vitro functional assessment of injected TCR-transgenic T cells. 87
Figure 25. In vivo performance of T cells transgenic for neoantigen-specific TCRs. 88
Figure 26. Growth kinetics of tumor xenografts for single mice. 89
Figure 27. TIL stimulation with mutated peptides identified through Immunopeptidomics 2018. 90
Figure 28. CD137 expression on TILs after stimulation with mutated pepitdes identified through Immunopeptidomics 2018. 91

1.45 List of tables

Table 1. List of FDA approved checkpoint inhibitors adapted from (Riley, June, Langer, & Mitchell, 2019) 14
Table 2. List of FDA approved CAR-T cell treatments 16
Table 3. Clinical Trials with TCR-T cells (L. Zhao & Cao, 2019; Q. Zhao et al., 2021 and ClinicalTrials.gov). 19
Table 4. Technical Equipment 25
Table 5. Consumables 26
Table 6. Mel15 primary samples 27
Table 7. DNA vector plasmids 27
Table 8. Cell lines 28
Table 9. Cell lines produced by retroviral transduction 29
Table 10. Lymphoblastoid cell lines (LCLs) 29
Table 11. Reagents and chemicals 29
Table 12. Kits 31
Table 13. Composition of buffers and solutions 32
Table 14. Composition of media 32

Table 15. Cytokines and TLR ligands 32
Table 16. Peptides used for immunogenicity assessment and T cell stimulation 33
Table 17. Peptides for alanine/threonine scanning 34
Table 18. Fluorescently labeled antibodies used for flow cytometry 35
Table 19. Multimers 35
Table 20. Primers for sequencing 36
Table 21. Primer for S1 downgrading 36
Table 22. Primers for TCR alpha and beta chain repertoire 36
Table 23. Primers for molecular cloning 37
Table 24. Software tools 38
Table 25. Web-based tools 38
Table 26. Arrangement of peptide pools for immunogenicity assessment. Table adapted from (E. Bräunlein et al., 2021) 42
Table 27. Tested peptides identified with immunopeptidomic 2018 pipeline 46
Table 28. Reagent amounts for RNA extraction 49
Table 29. Reaction mix for TCR alpha and beta repertoire 50
Table 30. Thermal profile of TCR repertoire PCR 50
Table 31. Digestion mix 51
Table 32. Ligation mix 52
Table 33. Reaction mix for standard PCR using KOD polymerase 52
Table 34. Thermal profile PCR with KOD polymerase 53
Table 35. Composition of sub-pools for HLA-A03:01 and B27:05 predicted ligands 55
Table 36. Combination of sub-pools within peptide pools 55
Table 37. Antibody mixes for CD8+ T cell isolation assessment 58
Table 38. Experiment set-up to assess in vivo anti-tumor potential of TCRs 60
Table 39. Sequence details of alpha and beta chains isolated from KIF2C^{P13L} reactive T-cell clones. 66
Table 40. Productive frequencies (%) of neoantigen-specific TCR β-chains in tumor and blood samples. 68
Table 41. Number of human proteins potentially targeted transgenic TCRs according to recognition motif (E. Bräunlein et al., 2021). 81
Table 42. HLA alleles expressed by LCL cell lines (E. Bräunlein et al., 2021). 82
Table 43. Number of TCR-T cells injected per mouse based on transduction efficiency and mice per group. 87
Table 44 Mutated peptides identified with Immunopeptidomics 2018 pipeline 120

1.46 Abbreviations

µl	Microliter
µM	Micromolar
ADCC	Antibody-dependent cell-mediated cytotoxicity
AEC	3-Amino-9-ethylcarbazole
AKAP6	A-kinase anchoring protein 6
AML	Acute myeloid leukemia
ACK	Ammonium-Chloride-Potassium
APC	Allophycocyanin
BATDA	bis(acetoxymethyl) 2,2':6',2''-terpyridine-6,6''-dicarboxylate
BSA	Bovine serum albumine
CAR	Chimeric antigen receptor
CD	Cluster of Differentiation
CDC	Complement-dependent cytotoxicity
CDR3	Complementary-determining region 3
c_{END}	Endconcentration
CML	Chronic myeloid leukemia
CMV	cytomegalovirus
c_{STOCK}	Stock concentration
CTLA-4	Cytotoxic T-lymphocyte associated protein 4
c_{WORK}	Concentration of working dilution
DC	Dendritic cell
DEPC	Diethyl pyrocarbonate
DMEM	Dulbecco's Modified Eagle Medium
DMF	Dimethylformamide
DMSO	Dimethyl sulfoxide
DNA	Deoxyribonucleic acid
dNTP	Deoxynucleotide triphosphates
DsRed	Discosoma sp. red fluorescent protein
EBV	Epstein-Barr virus
EC50	Half maximal effective concentration
EDTA	Ethylenediaminetetraacetic acid
EF	Endotoxin-free
EGFR	Epidermal growth factor receptor
ELISA	Enzyme-linked immunosorbent assay
ELIspot	Enzyme-linked immunospot
FACS	Fluorescence activated cell sorting
FCS	Fetal calf serum
FFPE	Formalin fixed paraffin embedded
FITC	Fluorescein isothiocyanate
GFP	Green fluorescent protein
GM-CSF	Granulocyte-macrophage colony-stimulating factor
GvHD	Graft-versus-Host disease
h	Hour
HD	Healthy donor
HEPES	4-(2-hydroxyethyl) -1-piperazineethanesulfonic acid
HIV	human immunodeficiency virus
HLA	Human leukocyte antigen
HPV	human papilloma virus
HRP	Horseradish peroxidase
HS	Human serum
IFN	Interferon

IL	Interleukin
KIF2C	Kinesin Family Member 2C
LB	Lysogeny broth
LC	Liquid chromatography
LCL	Lymphoblastoid cell line
mAb	Monoclonal antibody
MDS	Myelodysplastic syndromes
mg	Minigene
MHC	Major histocompatiblity complex
min	Minute
Mio	Million
ml	Milliliter
mM	Millimolar
MS	Mass spectrometry
nc	Native TCR chains
NCAPG2	Non-SMC condensin II complex subunit G2
NGS	Next-gene-sequencing
NEAA	Non-essential amio acids
NHSCC	Head and Neck Squamous Cell Carcinoma
nM	Nanomolar
NPC	Nasopharyngeal Cancer
NSCLC	Non-small-cell lung cancer
o.n.	Over night
P2A	Peptide 2A
PBMC	Peripheral blood mononuclear cells
PBS	Phosphate-Buffered Saline
PCR	Polymerase chain reaction
PCR	Polymerase chain reaction
PD-1	Programmed cell death 1
PDL-1	Programmed cell death ligand 1
PE	Phycoerythrin
PFA	Paraformaldehyde
PI	Propidium Iodide
Poly-I:C	Polyinosinic-polycytidylic acid
rh	Recombinant human
RNA	Ribonucleic acid
RNA-seq	RNA sequencing
RPMI 1640	Roswell Park Memorial Institute 1640
RT	Room temperature
s	Second
SYTL4	Synaptotagmin like 4
TAA	Tumor-associated antigen
TAE	Tris-acetate-EDTA
TCR	T-cell receptor
TIL	Tumor-infiltrating lymphocytes
TRAC	T cell receptor alpha constant
TRBC	T cell receptor beta constant
TSA	Tumor-specific antigen
U	Unit
UV	Ultraviolet
VEGF	Vascular endothelial growth factor
V_{END}	Endvolume
WES	Whole exome sequencing

Acknowledgements

I thank Prof. Dr. Angela Krakchardt for offering me the chance to work in her laboratory on this attractive and stimulating project and for being an exceptional scientist. Thanks to her supervision I could learn so much and pursue great achievements for my future career.

I would like to thank Prof. Dr. Florian Bassermann for the possibility to work in the IIIrd Medical Department and for providing laboratory rooms and equipment.

I thank my former second supervisor Prof. Dr. Antes, who sadly prematurely left us, for our fruitful multidisciplinary collaboration on the exciting topic of protein modelling.

I would like to thank Prof. Dr. Feige, who promptly took over the role of second supervisor of my thesis.

A very special acknowledgment goes to my mentor and current cooperation partner Prof. Dr. Ulrike Protzer, who who has been behind every important step of my career since the end of my Master studies. Thanks to her hospitality I could work in the vibrant environment of her laboratory, connect to wonderful people and discover the beautiful city of Munich. Prof. Protzer has opened many doors for me professionally and for this I will always be grateful.

A warm thank you to Dr. Eva Bräunlein for her guidance throughout my whole time in the lab and for her efforts during the drafting of our publication.

I thank Dario Gosmann for being a wonderful colleague and confidant and for always giving me a good laugh.

I would like to thank all my former colleagues, Celina, Henrique, Anja, Stefan, Sabine, Theresa, Kristine, Christina and Philipp for the nice time we had together.

I thank my partner Paul for always being on my side and motivating me to be the best version of myself.

I want to thank the friends I made in Munich, Davide, Lisa, Francesco and Valeria for being my new family abroad.

I thank my friend Sara for being a constant in my life, no matters how many kilometers are between us.

In the end, I would like to thank my family for all the love and support and also for annoying and pushing me to move forward, because you want the best for me.